INFORMATION TO USERS

This manuscript has been reproduced from the microfilm master. UMI films the text directly from the original or copy submitted. Thus, some thesis and dissertation copies are in typewriter face, while others may be from any type of computer printer.

The quality of this reproduction is dependent upon the quality of the copy submitted. Broken or indistinct print, colored or poor quality illustrations and photographs, print bleedthrough, substandard margins, and improper alignment can adversely affect reproduction.

In the unlikely event that the author did not send UMI a complete manuscript and there are missing pages, these will be noted. Also, if unauthorized copyright material had to be removed, a note will indicate the deletion.

Oversize materials (e.g., maps, drawings, charts) are reproduced by sectioning the original, beginning at the upper left-hand corner and continuing from left to right in equal sections with small overlaps. Each original is also photographed in one exposure and is included in reduced form at the back of the book.

Photographs included in the original manuscript have been reproduced xerographically in this copy. Higher quality 6" x 9" black and white photographic prints are available for any photographs or illustrations appearing in this copy for an additional charge. Contact UMI directly to order.

UMI

A Bell & Howell Information Company
300 North Zeeb Road, Ann Arbor MI 48106-1346 USA
313/761-4700 800/521-0600

Université d'Ottawa · University of Ottawa

An Experimental Study on the Cyclic Behaviour of Riveted Stiffened Seat Angle Connection with Concrete Encasement

by

Marc A. Bisson

Thesis submitted to the School of Graduate Studies
in partial fulfilment of the requirements for the
Master of Applied Science Degree in Civil Engineering
under the auspices of the
Ottawa-Carleton Institute for Civil Engineering

June 1997

Department of Civil Engineering, University of Ottawa
Ottawa, Canada, 1997

Abstract

Many older buildings have been constructed using what are considered today as semi-rigid or flexible types of connections. A concrete encasement was typically added to columns in the past for the sole purpose of fire protection. The behaviour of semi-rigid connections under cyclic loading and the contribution to seismic resistance of the concrete encasement is a concern. An experimental investigation was undertaken to determine the effect of concrete encasement on cyclic behaviour of a typical riveted stiffened seat angle connection, and the improvement in behaviour when retrofitted with a proposed method. Existing connections were tested and hysteretic moment-rotation curves were obtained. Models previously developed by other researchers were verified and practical recommendations are presented.

To my family

Acknowledgments

My sincere thanks go to my supervisor, Dr. Michel Bruneau, for all his help, insight and patience throughout this work. I am also grateful to Dr. M. Saatcioglu and Dr. N.J. Gardner for their assistance. I would also like to thank Mr. Alain Bilodeau of the Construction Materials Section, Mineral Sciences Laboratories, CANMET, Energy, Mines and Resources Canada for his help in obtaining mix designs incorporating slag. The technicians at the University of Ottawa, Dept. of Civil Engineering machine shop and Structures laboratory are also greatly acknowledged for their help in building the test set-up.

My deepest thanks go to my family for their endless support throughout my life and studies.

Table of contents

CHAPTER 3

CHAPTER 4

CHAPTER 5

CHAPTER 6

List of Tables

List of Figures

Notations

C_r	factored compressive resistance of a member, kN
d_1,.d_4	measured displacements by LVDTs, mm
F_u	tensile strength of steel, MPa
F_v	shear strength of steel, MPa
F_y	yield strength of steel, Mpa
h	depth of beam, mm
h_1,.h_4	distance between column face and LVDTs, mm
M	applied moment, kN.m
T_r	factored tensile resistance of a member, kN
θ	average connection rotation, radian
θ_r	connection rotation on right side, radian
θ_l	connection rotation on left side, radian

CHAPTER 1

Introduction

1.1 General

For most of the early half of this century, lateral load resisting systems were not explicitly designed in buildings since resistance to wind or earthquake was not required by the building codes of that era. As a result, many older buildings were constructed using what are considered today as semi-rigid or flexible types of connections. These connections are adequate to resist gravity loads, but they are generally considered unable to resist moments as they allow large rotations to develop.

As earthquakes caused a large number of fatalities and severely damaged many buildings, the importance of implementing seismic design requirements in codes and effective lateral load resisting systems in building frames was recognized, and these requirements became more rigorous with time. However, the older buildings incorporating the connections mentioned above still make up a large part of our infrastructure, and the subject of their seismic adequacy must be addressed.

To date, when confronted with structural evaluations of frames containing these older semi-rigid or flexible connections, practising engineers have conservatively neglected their potential contribution to lateral load resistance. As a result of such an assumption, major and sometimes intrusive seismic retrofitting is deemed required in such buildings in order to upgrade their resistance to lateral loads. This can be very costly and frequently disrupts the normal use and occupancy of the building.

The lack of knowledge on the behaviour of these types of connections in steel frames is certainly responsible for such extreme solutions. If it could be shown that these connections can in fact develop, in a ductile manner, some inherent moment resisting capability, and since they are present in every beam-to-column connection of every frame in these old buildings, their contribution to lateral load resistance could add up to be significant, therefore minimizing the magnitude of the required retrofitting or even avoiding retrofitting altogether in less active seismic zones.

Recent studies have shown that some connections, traditionally considered to be flexible and unable to develop any moment resistance, can actually be considered as semi-rigid connections. Therefore, these connections thought to be flexible can inherently resist some moment while developing a certain rotation. Riveted stiffened seat angle connections, once commonly used in buildings, is one such type of connection that can be classified as semi-rigid. Today, there exists little literature on the cyclic behaviour of these types of connections. Furthermore, the contribution to seismic resistance of the concrete encasement, typically added to columns in the past for the sole purpose of fire protection is still not totally clear.

1.2 Knowledge on connection behaviour

Because beam-to-column connections suffer large inelastic excursions during a severe earthquake, it is essential to understand the cyclic behaviour of these riveted stiffened seat angle connections encased in concrete. Although recent experimental and analytical studies have been completed on the behaviour of semi-rigid beam-to-column connections, few have explored the cyclic characteristics of these joints, especially considering the quality of the building materials used at the time of construction.

1.3 Objectives of this Research

It is the objective of the research presented in this thesis to provide:
i) Additional experimental results on the cyclic behaviour of riveted stiffened seat angle connections, as well as an understanding of the contribution to the total resistance provided by the existing concrete encasement;
ii) A new retrofit strategy to improve the seismic resistance of this specific type of construction and an experimental validation of that strategy;
iii) Based on knowledge obtained from the test results, other possible effective retrofit alternatives can be suggested.

1.4 Scope of Work

In this experimental study, two tests were performed on two identical beam column specimens taken from an existing building, with the following distinction: the first test was performed on a specimen to determine the behaviour characteristics of the original connection, while the second test was conducted on a retrofitted specimen. Two connections are simultaneously tested in each specimen and the test set-up is such that two sets of data are collected for each test (i.e. one for each connection).

A comparison will be made between the test results and the predicted capacities using simple models, and this will be used as a basis for applying the results to similar connections with elements of different sizes.

1.5 Outline of the Thesis

Chapter 2 outlines the existing literature on the behaviour and modelling of semi-rigid connections. Descriptions of the specimens and the test set-up, predictions of the connections capacity as well as the experimental procedure are included in Chapter 3. Chapter 4 contains

the experimental test results and observations. Chapter 5 then expands on these results and compares them with the predicted capacities. Conclusions and recommendations are then drawn from these experimental results and presented in Chapter 6.

CHAPTER 2

Literature Review

2.1 General

There exist many types of connections that fall into the category of semi-rigid. For example, web clip angle, as well as top and seat-angle connections with or without stiffeners are within this classification. However, as mentioned in the previous chapter, engineers generally treat these types of connections as perfectly flexible when conducting an analysis on frames, assuming that their true behaviour is nearly flexible.

Early investigations into the behaviour of semi-rigid connections focused mainly on obtaining their monotonic response. These early investigations showed that semi-rigid connections can in fact develop a considerable moment resistance, and further demonstrated that lighter beams could be used if this end restraint was taken into consideration.

Recently, as earthquake design requirements have become more predominant and the important role ductile connections fulfill in steel frames is better understood, the need to further investigate the cyclic behaviour of semi-rigid connections became apparent. Experimental and analytical models were developed in order to anticipate the cyclic M-θ relationship of different types of connections into the inelastic range. Since this has been a fairly recent research effort, there still exists very little literature on this topic. A brief summary of the available experimental and analytical information follows.

2.2 Experimental Investigations

Experimental data is essential for understanding the behaviour of connections, but also for the development of reliable analytical models that can allow engineers to easily and adequately evaluate the performance of a broad variety of connections.

2.2.1 Monotonic Tests of Bare Steel Connections

Investigations into the behaviour of riveted connections began when Wilson and Moore (1917) tested a series of 12 full scale beam-to-column connections. Later, Young and Jackson (1934) tested riveted assemblies subjected to monotonic loading as well as limited reversed loading. Both of these experiments focused mainly on determining the effects of wind loads on the connections. Rathbun (1936) investigated the behaviour of riveted top and seat angle, with and without web angles, and T-stub connections. At approximately the same time, Batho et al. (1936, 1938) tested riveted and bolted assemblies as well as bare steel and concrete encased specimens. M-θ curves for monotonic loading and unloading were obtained for different types of connections: top and seat angles, top and seat T-stubs, and top and seat T-stubs with double web angles. They typically found that, from the early stages of loading, the M-θ curves for these connections were non-linear. For the top and seat angles type of connection of interest here, it was determined that large rotations could be sustained without any significant loss in shear capacity. They also found that the most important factor affecting connection rigidity was the thickness of the seat angle.

Hechtman and Johnston (1947) tested forty-seven steel riveted connections. The focus of this investigation was mainly on top and seat angle connections (34 specimens), but also included several other types of joints. From these experiments, slippage between the connecting elements was found to be a significant source of rotation in the assembly.

Lewitt et al. (1969) investigated the behaviour of semi-rigid joints by applying monotonic

tension and compression to angles and observing their response. Using these experimental results, a failure mode for the angle was determined and a model was developed to express its load deformation characteristics using an exponential function.

Other experimental investigations were undertaken to further understand the monotonic behaviour of semi-rigid connections (e.g. Munse et al. 1959; Maxwell et al. 1981; Marley 1982). The data derived from these tests was used by other researchers to develop experimentally based monotonic models. Some of the principles developed in these models (summarized in section 2.3) can be applied to this study.

2.2.2 Monotonic Tests of Encased Steel Connections

Tests on steel connections encased in concrete were apparently first undertaken by Batho and Lash (1936). In this study, thirteen (13) bolted top and seat angle connections encased in concrete were tested to failure. The researchers determined that the strength and stiffness of the specimens were enhanced until the concrete in tension cracked. They concluded that the improved behaviour of the specimens depended on the arrangement and amount of reinforcement in the concrete encasement. One specimen tested, which is relevant to this study, had no reinforcement. The initial stiffness of the unreinforced specimen was increased due to the confining effect of the concrete, which results in a higher yielding moment. However, once cracks formed in the concrete encasement, the curve became approximately parallel to the bare steel specimen. Generally, the concrete encasement was found to reduce the amount of bending in the angle legs, and also prevented the vertical angle legs from separating from the column, thus decreasing the rotation of the beam.

Batho (1938) tested another series of bolted concrete encased connections. The concrete encasement had an average compressive strength of 4980 psi (34 MPa) and all specimens in this investigation were reinforced with bars and stirrups. The experiments confirmed the earlier findings that the strength and stiffness of the specimens were increased until cracks

formed in the concrete encasement.

2.2.3 Cyclic Tests

It is interesting that in the Young and Jackson (1934) tests mentioned earlier, where small load reversals were applied to riveted steel connections to investigate rigidity under wind loading, a significant pinching was observed in the M-θ curve even at small magnitude of rotations.

Other cyclic tests on semi-rigid connections were conducted only much later when Radziminsky et al. (1986) tested connections of double web angles with top and seat angles subjected to low amplitude cyclic loading. Astaneh et al. (1989a) tested bolted and welded double web angle connections until failure under large cyclic rotations. One of the conclusions reached by the researchers was that connections incorporating A325 bolts tightened as specified in the AISC Manual showed ductile behaviour and performed well, but pinching was observed for all specimens and cracks formed in the angles when rotations were larger than 0.025 radians. An experimental investigation was also conducted by Astaneh et al. (1989b) by implementing the same connections in frames subjected to shake table excitations. Later, Bernuzzi et al. (1992) tested a series of bolted semi-rigid connections to failure under cyclic loading. The connection types tested were the top and seat angles, flush end plates, and extended end plates. Of interest here, slippage was found to substantially affect the performance of top and seat angles connection, causing pinching in the M-θ curve.

Roeder et al. (1994) tested a total of twenty-three specimens under monotonic and cyclic loading. The specimens were constructed to simulate the existing elements of a building located in San Francisco. The experiments included bare and concrete encased specimens and included T-stub with and without web angles, as well as clip angles (or top and seat angle) with web angles. The original concrete used for encasement in the prototype building was designed to have a 17 MPa (2500 psi) 28 day compressive resistance. The authors assumed

that the concrete strength in the columns of that building would have increased well beyond this value over time and therefore designed the encasement concrete for their specimens to have a 24 MPa (3500 psi) 28 day compressive strength. A light mesh (6"x6"-10/10) of welded wire fabric was also used as reinforcement in the concrete encasement. It is important to note that the specimens used in this study were all built from new materials. Some of the riveted connection assemblies were constructed using a specially developed in-laboratory riveting capability, while in other specimens, rivets were simulated by using mild steel bolts fitted tightly in their holes and over tightened. The results obtained from this investigation generally showed pinched and deteriorating M-θ curves from the onset of loading until failure. The failure mode observed for many specimens with top and seat angle connections was the shear failure of the rivets connecting the angle leg to the beam flange. The concrete encasement was reported to increase the joint stiffness by as much as 200% to 300% for the clip angle connections, while an increase of only 10% to 30% was reported for the T-stub connections. A rehabilitation technique for an encased connection was also tested. Angles were placed in each corner of the joint and clamped together with threaded rods. Although the maximum resistance of the connection had increased by approximately 25%, the M-θ curve still showed severe pinching.

Bruneau and Sarraf (1996) were able to salvage test specimens from an existing building scheduled for demolition. The connections were riveted stiffened seat angle and encased in concrete. For this experimental investigation, the encasement was removed from the specimens. Since the connections and members being tested were constructed using materials and procedures of the early 1900's, they offered an excellent insight into the behaviour of these typical existing connections. Specimens were tested by applying cyclic loading until failure. The results from a test on a specimen with these connections showed severe pinching in the M-θ curve, which indicates poor energy dissipation as shown in Fig. 2.1. The experiment ended with the shear failure of one of the rivets connecting the angle leg to the beam flange. Models were developed for both the top angle and the stiffened seat angle and will be reviewed in section 2.3. Two other specimens were retrofitted using strategies

designed to enhance energy dissipation during cyclic loading. The retrofits were successful, but required the removal of the concrete encasement.

2.3 Experimentally-Based Models

Using experimental data as a basis, many attempts have been made to develop M-θ curves that closely agree with the observed monotonic behaviour of semi-rigid connections.

2.3.1 Linear Models

Rathbun (1936), Monforton et al. (1963) and Lightfoot et al. (1974) developed single stiffness linear models that use the initial stiffness throughout the entire range of loading. Tarpy et al. (1981) and Lui et al. (1983) developed bi-linear and piecewise linear models.

2.3.2 Polynomial Model

The polynomial model proposed by Fry and Morris (1976) uses curve fitting constants as well as a standardization parameter that is based on the connection type and geometry. Although this model can be used for different types of connections with a fair amount of accuracy, at some values of moment, the stiffness may become negative.

2.3.3 B-Spine Model

The B-spline curve-fitting method proposed by Jones et al. (1982) to fit experimental data models the experimentally obtained M-θ relationship very well, but a large number of data points are required for calibration of the model.

2.3.4 Power and Exponential Models

The idea of using power models was introduced by Beaufoy et al. (1948). Later, this concept was generalized by Richard et al. (1980) to include single plate and double angle connections. Colson et al. (1983) and Kishi and Chen (1990) developed similar three parameter power models, which utilized the initial stiffness, ultimate moment capacity and a shape parameter. Ang and Morris (1984) introduced a four parameter power model .

A multi parameter exponential model was developed by Lui and Chen (1986), which utilized a strain hardening parameter. Because this model could not adequately represent sharp changes in the M-θ curve, it was later refined by Kishi and Chen (1986). A four parameter exponential model was then introduced by Yee et al. (1986). This model incorporates three analytically determined parameters (plastic moment, initial elastic stiffness, and strain hardening stiffness), and one curve fitting parameter. Later, a three parameter exponential model was developed by Wu and Chen (1990).

2.3.5 Data Bases

There exists compilations of experimental test data for several types of connections. These data are summarized in the data base and include details of the joint assemblies tested. The available data are included in the Goverdhan (1983), Nethercot (1985a, 1985b), and Kishi and Chen (1986) data bases.

The models described in the above sections only represent the monotonic behaviour of semi-rigid connections. Further, the use of models developed by using curve fitting techniques to experimental data can only be applied to similar connections with different sizes of elements if it can be reasonably proven to be appropriate.

2.4 Physical Analytical Models

Lewitt et al. (1966) studied double angles under axial loading. The model developed by Lewitt predicted the monotonic M-θ curve for double angle web connections taking into consideration the tensile load deformation characteristics of the angles, and the centre of rotation of the entire beam-column connection.

Youssef-Agha et al. (1989) developed an analytical model to predict the behaviour of top and seat angle connections. The monotonic non-linear M-θ relationship is obtained and then simplified to a bi-linear form, which has initial stiffness and strain hardening stiffness as the key parameters. Column flange deformations are considered, while the model for the angle under tensile load ignores bolt slippage and represents bolt elongation by a spring with linear stiffness. The M-θ relationship and angle model adopted are shown in Fig. 2.2. The extension of this model to cyclic loading was attempted by comparing experimental results from other researchers on one and two story frames subjected to low intensity seismic load (Marly, 1981; Stelmack, 1983; Stelmack et al., 1986) with those produced from a computer program incorporating the model. The comparison between the analytical and test results showed reasonable agreement.

De Stephano et al. (1994) developed a mechanical model for the cyclic response of double web angle connections. In this model, the column and beam web are represented by rigid bars and considered undeformable. The angles are divided into strips at the mid point in between two adjacent bolts, and then represented by non-linear springs, as shown in Fig. 2.3. Each strip is represented by a beam model which incorporates a simple bi-linear stress strain law with kinematic hardening as well as a gap element to account for the alternating contact of the column flange with the top and bottom of the angles when subjected to cyclic loads. This model was extended to capture the behaviour of top and seat angle connections by De Luca (1995). Comparison of the model with test results shows that the characteristic pinching is not represented by the model, although the strength is well predicted (Fig. 2.4).

Following a series of laboratory tests described earlier, Roeder et al. (1994) suggested an analytical model to predict the ultimate resistance of a top and seat angle connection. The model developed considers the formation of two plastic hinges in the angle legs as well as prying action and tensile yielding of the connectors, as shown in Fig. 2.5. Roeder et al. also suggested a model for encased top and seat angle connections. The failure mechanism of the steel elements remains the same, but a compressive force due to concrete encasement is added while the contribution from the steel mesh in the encasement is ignored. The magnitude of the concrete compressive force is evaluated using standard ultimate strength design rectangular stress block as shown in Fig. 2.6.

The physical models developed by Bruneau and Sarraf (1996) are directly relevant to this study since they specifically model the behaviour of the type of top and stiffened seat angle connections considered in this thesis. A plastic mechanism has been formulated to provide a realistic model for these instances where a wide top angle (which is also the case for the specimens experimentally tested by the author of this thesis) is used and the simple assumption of yield lines parallel to the longitudinal axis of the angle has been replaced by a more complex yield line pattern. The minimum load (P) required to cause the failure mechanism is obtained by applying the virtual displacement shown in Fig. 2.7, and using the principle of virtual work. Another similar model has been developed for the riveted stiffened seat angle connection. This model, also based on a wide angle, develops the same hinging mechanism in the seat angle as described above and then forms a hinge in the stiffener angles at the level of the second row of fasteners, as shown in Fig. 2.8. The sum of these loads must be applied to the stiffened seat in order to develop the mechanism. These models adequately estimated the resistance of the specimens tested by Sarraf and Bruneau. They are therefore chosen to predict the capacity of the specimens tested in this study.

CHAPTER 3

Experimental Approach

3.1 General Description of Specimens

For this experimental study, the specimens used were salvaged from an existing 86 year old building scheduled for demolition. The structure in question, built in 1910 and demolished in 1992, was the Daly Building located in downtown Ottawa at the corner of Rideau and Sussex streets. Therefore the specimens used in this study were not built specifically for this purpose with materials of current standards and quality, but incorporate the material properties of the aged as-is materials as well as the construction procedures typical of that era.

The structure was a seven story office building with 5 bays in the East-West direction and 8 bays in the North-South direction, each bay with an approximate span of 20 feet. The southern half of the building resisted loads by means of steel frames spanning in the East-West direction, while concrete space frames comprised the load resisting system in the North-South direction.

The specimens obtained were flame cut from the existing frames at beam and column locations, as far as possible from the connecting elements, in order to preserve the connections. The specimens were then placed on the deck of a flatbed truck and transported to the laboratory, where they were stored in a dry environment for a few years before testing commenced.

Both specimens tested were of the top and stiffened seat angle connection type and were identical in the size and arrangement of connecting elements, column configuration as well as

the amount of concrete encasement provided strictly for fire protection purposes. The typical beam-to-column connection details are shown in Fig. 3.1

3.2 Preliminary Tests

The physical properties of the existing steel and rivets are necessary to accurately predict the behaviour of the specimens. The strength of the concrete encasement, although originally provided for fire protection, is also necessary in order to assess the contribution of the concrete to the total resistance of the connection.

3.2.1 Existing Steel Properties

Since the specimens considered in this test program were of the same origin and obtained simultaneously to those test by Bruneau and Sarraf (1996), the material values reported in that document for tensile and weldability tests, as well as tensile and shear tests on existing rivets are used here. These tests confirmed the weldability of the steel and showed an average yield point, F_y of 225 MPa, and an average tensile strength, F_u of 400 MPa. The stress strain relationships obtained for the base metal are shown in Fig. 3.2. The stress-strain diagram obtained from the rivet tensile test is shown in Fig. 3.3 where a yield point of 258 MPa, and a tensile strength of 483 MPa are observed. Since the rivet shear tests proved inconclusive, the ultimate shear stress of 0.75 F_u as reported in existing literature (Kulak et al. 1987) was used.

3.2.2 Existing Concrete Properties

In order to evaluate the strength of the existing concrete, large sections of concrete were removed from different areas of one of the existing specimens and three 100 mm cubes were cut from these sections with a diamond tipped saw. The cubes were then subjected to a compressive test. The three cubes averaged a compressive resistance of 8.3 MPa, which corresponds to a strength of 6.6 MPa when converted to the strength for a standard 150mm x

305mm cylinder based on commonly accepted relationships between values obtained from these two different standard specimen sizes (Neville, 1995). The low concrete strength obtained was expected since the quality of concrete encasing the specimens was observed to be very poor (i.e. some concrete was removable by hand and most of the aggregates were porous and lightweight). It is noteworthy that the strength of the concrete used for fire proofing purposes for the columns of the Daly Building, when tested 86 years after being poured, was much lower than values considered by Roeder et al. (1994).

The ability to duplicate this concrete strength was important because large sections of the existing concrete cover were removed in order to install strain gages to monitor the connection behaviour during the test. The removed concrete had to be replaced with a material having similar strength characteristics. Concrete mix designs of 7 MPa using normal Portland cement are no longer used in current construction practices.

However, an alternative solution was found using results from a study by Malhotra (1986) that investigated the mechanical properties of concrete having various mix designs incorporating from 0 to 100% of ground granulated blast-furnace slag used as a replacement for normal Portland cement. This study showed that with a water/cement+slag ratio as high as 0.70, and using 50% to 75% slag as replacement for cement, 7-day compressive strength of 6 to 8 MPa could be obtained with a corresponding 28 day strength between 13 and 16 MPa. Furthermore, when replacing 100% of the cement with slag and lowering the water/slag ratio in the range of 0.45 to 0.55, 7-day compressive strength results were between 6 and 7 MPa, with 28-day strength between 10 and 11 MPa.

Using these mix designs as a guide, two trial mix designs were made in an attempt to duplicate these results. Both mixes incorporated 100 % slag as replacement for cement, while the water/slag ratios were varied. Because slag is used only in small quantities in current concrete mix designs, batching plants tend to store only an amount necessary for its immediate needs, therefore slag is more difficult to obtain in small quantities as required for this project. The

slag was obtained from Francon Lafarge's Bearbrook road batching plant located in Blackburn Hamlet, Ontario. The slag used in the trial mixes and the mix for the first specimen were obtained from one shipment, while the slag used in the mix for the second specimen was obtained from a different shipment. Table 3.1 indicates the proportions of materials used in both mixes. As indicated in this table, the initial water/slag ratio of the chosen mix was adjusted to ensure workability when placing the concrete in the forms.

Table 3.2 lists the 14 and 42 day compressive test results obtained from both batches and compares these with the results obtained from the cubes extracted from the existing column. These test intervals (14 and 42 days) were chosen because they were believed to reflect the most realistic time intervals between the pouring of the concrete encasement and the actual testing of the specimens. Table 3.2 clearly shows that mix A better approximated the strength characteristics of the existing concrete.

3.3 Preparation of the Specimens

3.3.1 General

Applying a point load on the beam at a distance from the column face induces a moment at the connection. The magnitude of the point load required to generate a desired moment at the connection is a function of the length of cantilever. The length of cantilever was chosen in order to minimize the loading that would be required from the testing equipment, as well as to avoid any undesirable beam behavior, namely lateral torsional buckling. The length of beams that remained on the specimens after their removal from the existing building frame (called "stub-beams" hereafter) were too short to fulfill the requirements described above. Two extension arms were available for use from a previous study that incorporated a similar test set-up. These extensions arms were still not long enough, therefore additional extensions were fashioned from identical structural shapes that were removed from the same building. Fig. 3.4 shows the column with its attached stub beams and the additional extensions. Both

of these extension arms were designed and connected in such a manner as to be removed and reused for testing other specimens. Some bolted and some welded splices were used for that purpose, depending on the expected magnitude of moments and shears at the splice.

Since slippage at the bolted beam splices was a concern, all bolted splices were designed as slip critical connections according to CAN/CSA-S16.1-M89 (Limit States Design of Steel Structures), clause 13.12, and the splicing plates were designed to resist the maximum moment and shear expected at each location during the tests. This required a large number of high strength bolts at each splice. In order to further reduce the amount of bolts, the splices were designed to behave in double shear. An attempt was made to design a bolted splice at the extension arm connection nearest to the column face, but the number of bolts that would have been necessary there was still too large to accomodate the required splice plates; therefore this splice location was welded. These welds, being close to the area of highest moment of these specimens would be highly strained. Therefore for safety and expediency, the beam web and flanges of the extension arms were joined to the stub-beams with single bevel complete penetration welds.

The moment capacities of the connections were calculated for different failure modes for both specimens using the results from the preliminary tests described earlier, and using ultimate resistance models (Sarraf and Bruneau, 1996) or Limit States Design principles for structural steel (Canadian Institute of Steel Construction, 1992) and omitting the performance factor ϕ (details are available in Appendix A). The contribution of the concrete was ignored, assuming that it would crack early in the test given its relatively low strength. These estimates provide some perspective on the accuracy of engineering models available at the time of testing to estimate the ultimate resistance of this type of connection. The moment capacities corresponding to various limit states are summarized in Tables 3.3 and 3.4. Unfortunately, because of the concrete cover present on the specimens, it was impossible to visually observe the onset of many of the limit states, although some pertinent information was obtained later by analysing the strain gage data.

3.3.2 Specimen 1

This specimen was used to study the cylic behaviour of the existing connection in its as-is condition. No modifications were made to this specimen, other than the removal of some of the existing concrete in order to install strain gages on the connecting elements and replacement of the removed material using the equivalent mix described in section 3.2. The instrumentation used for this specimen is shown in Fig. 3.5, and the details of this instrumentation are discussed in section 3.5.

3.3.3 Specimen 2

Some guidelines exist for the retrofitting of existing bare steel structures (FEMA, 1992), but most of the proposed retrofit strategies would be very intrusive to the normal occupation for the type of buildings considered here. Some of the strategies currently used, and proven to be effective, include the implementation of shear walls, braced frames or base isolation into the existing structural system. Although these solutions are currently being implemented in retrofit projects, they are most often very costly and, as mentioned above, disruptive to the normal use of the building because new structural elements often need to be introduced in order to adapt to the new load paths. Some of the literature suggests retrofitting techniques that are less intrusive and directly applicable to the connections (Sarraf and Bruneau, 1996). Although the solutions offered are proven to be effective, they are again only applicable to bare steel connections, meaning that removal of the concrete cover would be required in order to proceed with any of the suggested techniques.

For the particular type of construction being investigated, a steel frame with a concrete encasement strictly for fire protection, the removal of the concrete is considerered to add unnecessarily to both the quantity of work needed and the intrusiveness of that work. There was therefore a need for a new retrofit strategy that does not require the removal of any of the existing concrete to expose the existing steel connection.

The retrofit strategy proposed here consists of a steel band wrapped around the column concrete to transfer loads to the column and a "fuse-plate" as an energy dissipator connecting the beam flange to the steel band, as shown in Fig. 3.6. Testing of specimen 2 permits to investigate the improvement in cyclic behaviour using the proposed scheme when compared to the performance of the original connection.

In order to obtain maximum energy dissipation from the new connecting elements, certain design criteria had to be observed, as well as some other constraints arising from the fact that this retrofit would have to be performed on existing buildings. Some of these criteria are outlined in the following:

a) The steel-band/fuse-plate assembly must be of such dimensions as to avoid contact with other structural elements in the vicinity (i.e. joists supported by beams, floor elements immediately above the beam, etc.).

b) The energy dissipators must be designed to allow a reasonable amount of story drift, without causing excessive drifts since large P-Δ effects could have a negative impact on global frame stability.

c) Under applied moments, this connection detail would cause tension in one of the fuse-plates and compression in the other. In order to maximize the energy absorption of such a system, the compression member must be designed with a slenderness ratio as low as possible. Therefore, the fuse-plates must be designed with a compression to tension ratio (Cr/Tr) as close as possible to 1.0.

d) The fuse-plate must be designed to yield and dissipate energy in an optimum manner. If the fuse-plate is designed to resist a large load level, undesired failure mechanisms may form elsewhere in the structural system (i.e. plastic hinges may form in the beams or columns). If designed to yield at too small of a load, it will be subjected to excessive ductility demands

at the expected drifts, and fail to provide a sizeable energy dissipation.

Taking the above mentioned criteria into consideration, the fuse-plates were designed to yield at a moment of 200 KN•m which was a significant improvement over the original connection ultimate resistance, comparable in magnitude to the resistance of other proposed retrofit techniques for similar connection configurations (Sarraf and Bruneau, 1996), yet without overwhelming the capacity of the beams or column. Rounded edges were provided at both ends of the fuse section to avoid large stress concentrations in these areas. Design calculations for the steel-band/fuse-plate assembly, as well as the required welds, are found in Appendix B. The steel-bands were designed to remain elastic.

For ease of installation, and to minimize the amount of field welding required, the steel-band/fuse-plate assembly was conceived such that two halves of the assembly could be first welded in-shop. The two pieces can then be transported to the site and joined together with complete penetration welds. The end of the fuse-plates were welded to the beams, using standard SMAW (sheet metal arc welding) with E70 electrodes. Welding was chosen to minimize the length of plate required, but a bolted connection could just as easily have been designed. Note that if this bolted option is considered, the bolts should be designed as slip critical and care must be taken to avoid any net area tensile yielding in the vicinity of the bolts.

Once the steel-band/fuse-plate assembly was in place and connected to the beams, grout was poured behind the steel-band to ensure uniform contact with the column face. The grout used was of a quick setting type with a 28 day compressive resistance of 30 MPa. For most construction applications, the grout should be a non-shrink type, but in this case the testing was performed within a short period of time from placing the grout.

Additional strain gages were installed to the fuse-plates in order to observe their cyclic behaviour. The instrumentation for this specimen is shown in Fig. 3.7, while the details of this retrofit are shown in Fig. 3.8.

3.4 Set-up Description

Instead of building a vertical reaction frame, it was found more advantageous to use the existing laboratory strong floor, with a 915mm thickness, to support the set-up and transfer the loads. A horizontal test set-up was therefore designed for this experimental investigation. It is shown in Fig. 3.9.

In that set-up, the load applied on the column by an actuator is balanced by reaction forces on pinned supports at the ends of the extension beams. This is an indirect way of obtaining the same behaviour as if point loads were applied by actuators to the beam ends. Large floor bolts were used to provide true pinned supports in this test setup. These pins were inserted through the beam webs by flame cutting a hole in the extension arms and welding another piece of steel machined with a smooth slotted hole to accommodate the floor bolt. This slotted hole was provided in order to avoid the development of axial forces in the beam when the length of beam changes during rigid body rotation about one of the connecting elements at the column face. Also, to ensure that these supports acted in a hinged manner, and to protect the bolt threads, threaded rings were machined to fit inside of the beam web slotted hole. Large nuts were placed both above and below the web; one to support the weight of the beam and to keep the beam in horizontal alignment, and the other to prevent uplifting and provide lateral support. A bracing system was then provided to rigidly support the bolt from the floor to the underside of the specimen.

The column was connected to an MTS actuator with a dynamic force rating of 960.8 KN in tension and 1460.0 KN in compression. To allow free movement from the applied actuator load, the column was laid on lightly oiled steel plates, then on round HSS sections and then on more oiled steel plates laid on the laboratory strong floor in order to minimize any frictional resistance from the rolling round HSS sections. The possibility of any adverse column behaviour, such as buckling or lifting of the specimen, was eliminated by the short length of column between the actuator and the connecting elements as well as the mass of concrete

provided for encasement on the column. Great care was taken to ensure that the specimen and actuator were horizontally aligned, and both ends of the MTS actuator are swivelled which minimizes the effect of any eccentricity in the horizontal application of the forces.

The reaction buttress for the actuator was built by anchoring both ends of a channel through its web to the floor using 70mm diameter bolts and welding an HP section in the centre at the bottom of the channel. The actuator was then bolted to a thick plate itself welded to the HP section. The other end of the actuator was bolted to another thick plate which was bolted to two large angles, each having two triangular stiffener plates welded to both legs to prevent flexural yielding of the outstanding leg. These two angles were then bolted to two plates welded to the flanges of the specimen's column.

It is noteworthy that for the testing of the first specimen, which was left in its as-is condition as described in section 3.3.2, four large diameter bolts were used to anchor the test set-up to the laboratory floor, two of which were used to connect the beam ends of the specimen in a pinned condition. For testing of the second specimen, the same set-up configuration was initially used but later modified to instead use six large diameter bolts to anchor the test set-up. For reasons described later, the beam end reaction supports had to be modified to withstand higher loads, and thus two more bolts were required for the anchorage to the floor. This slightly modified set-up is not shown in Fig. 3.9.

3.5 Instrumentation

In order to monitor the progress of the experiments and also to determine the behaviour of the various connecting elements, several instruments were used to collect experimental data on applied loads, connection rotations and strains at strategic locations.

3.5.1 Measuring Strains

Stress levels at points of interest in the connecting elements were determined by installing Micro-Measurements strain gages model EP-08-250BG-120 with a strain range of 4% and an accuracy of 3.8×10^{-6} mm/mm. The number of strain gages used, as well as their positions, varied in specimens 1 and 2 as shown in Figs. 3.5 and 3.7 respectively.

3.5.2 Measuring Connection Rotations

Connection rotations were measured in order to determine the moment-rotation relationship for each experiment. Since the beam-column connections were identical on either side of the column for both specimens, rotations for each side were measured independently. Two methods of determining rotations were devised, as redundancy in experimental investigations is always desirable.

For the first method, four Linear Voltage Displacement Transducers (LVDTs) are used; two installed on each side of the column. The LVDTs were placed as far as possible from each other in order to obtain good accuracy, but not too far so as to stay within the travel range of the instruments, and bolted to angles clamped to the beams (Figs. 3.5 and 3.7). For specimen 1, the points of contact for the LVDTs on the column were square pieces of plexiglass bolted to angles which were epoxied to the columns. This type of contact point was chosen because of the severe concrete deterioration anticipated in these areas. For specimen 2, the points of contact were epoxied directly to the column face. The distances between the two LVDTs were measured and did not change throughout the course of the experiment. Knowing these distances and the displacements recorded by the LVDTs, the following equations were applied to transform the measured displacements recorded by LVDTs (d_1 to d_4) and the fixed linear

distances (h, and h_1 to h_4) into rotations for each side of the column:

$$\theta_R = \frac{(d_1 - d_2)}{(h + h_1 + h_2)} \tag{3.1}$$

$$\theta_L = \frac{(d_3 - d_4)}{(h + h_3 + h_4)} \tag{3.2}$$

The distances and LVDT displacements referred to above are shown in Figs. 3.5 and 3.7.

For the second method, MTS Temposonics were used on either side of the column to record beam deflections at a distance l_i from the column face under known loading. The Temposonics consist of two pieces; a metal bar connected to a sensor and a magnet with a hole in the centre. The displacements are recorded by the Temposonics when changes in the magnetic field generated by the magnet are detected by the sensor. The magnet was bolted to a swivel to maintain the alignment with the metal rod when the beam deflected and rotated under the applied load. The swivel was then bolted underneath the beam to angles that had been clamped to the beam far enough from the column face to prevent any damage to the instruments from falling debris. The metal rod was inserted though the centre of the magnet to it's mid point and then bolted to angles which were fixed through the floor.

However, note that the displacements recorded at these locations by the Temposonics include an elastic deformation of the beam that must be removed in order to obtain the true rotation of the connection. The distance from the column face to each Temposonic was measured and the rotations are determined by geometry using the following equations:

$$\theta_R = \frac{(\Delta_{elastic} - d_5)}{(2745 - l - l_1)} \tag{3.3}$$

$$\theta_L = \frac{(\Delta_{elastic} - d_6)}{(2745 - l - l_2)} \tag{3.4}$$

The displacements and distances referred to are shown in Fig. 3.10, where a "stick" representation of the test set-up is used for clarity. As a third method to obtain the same information, the connection rotation can also be determined using the same principles outlined above and using the displacement of the actuator.

3.6 Control and Recording Measurements

In order to collect the experimental data, a Scimetric Instruments Model 200 data acquisition system was used in parallel with the MTS data recording equipment. The Scimetric system recorded applied load, LVDT and Temposonic displacements as well as strain data every 5 seconds, while the MTS system recorded load and actuator displacements and Temposonic displacements every time the position of the specimen changed by more than 0.5mm.

The loading rate and magnitude was controlled by the MTS Testar controller system. This system also allowed the simultaneous plotting of recorded data to observe the development of the load displacement relationship in order to have an idea of the moment rotation relationship and to control the flow of the experiment.

CHAPTER 4

Experimental Results

Because of the type of equipment used for testing (MTS actuator and Testar control system) the progress of the experiments were very closely monitored and controlled. A large number of cycles of loading were applied to each specimen (28 to 45) and a large number of data points were collected (4000 to 20500). The data obtained from both data acquisition systems were plotted separately in order to compare the values obtained from a time-based system (Scimetric) and a displacement-based system (MTS). The plots showed that both datasets correlated well with each other, but the data obtained from the MTS system had better resolution. For this reason, the data collected by the MTS system is used to present the experimental results in the following sections, however the additional test data collected is provided in Appendix C.

The most significant results presented in the following sections are the moment rotation relationships of the connections. It is therefore important to understand how the values of moments and rotations are acquired.

The moments were calculated by two different methods. The first method used the measured load applied by the MTS actuator, recorded by the MTS system, and multiplied one half of this value by the lever arm measured from the hinge support to the column face. The second method used the strains measured on the top and bottom beam flanges near the column face, recorded by the Scimetric system, converted into applied moment at the connection using simple mechanics of materials relationships. The results obtained by both methods generally showed good correlation, but once again the data collected by the MTS system was of better quality and was chosen to present the experimental results.

As described in section 3.5.2, two methods were also devised for determining beam rotations. However, in the first experiment, the LVDTs installed at the column faces eventually went out of range and had to be removed before the specimen reached failure in order to avoid damaging the instruments. Therefore the last few hysteretic loops of that first test program are not included in the recorded dataset for these instruments. When comparing the results of the rotations calculated from the LVDTs with those calculated using the actuator displacement, the correlation is very good as shown in Fig. 4.1. The slightly larger rotations measured by the actuator was found to be due to deformations of the pin-supports and some slip in the reaction buttress. Nonetheless, to present the entire range of test results as an average for both connections, the data from the actuator displacement was used to calculate the connection rotations for the first experiment.

During testing of the second specimen, problems developed with the Scimetric data acquisition system and only sporadic values were recorded for the LVDTs. The values of rotations obtained from the LVDTs were compared with the values calculated using the Temposonic measuring beam deflections. Once again, a good correlation was observed between the two results, as shown in Fig. 4.2, but it is important to note that the data collected by the LVDTs is not continuous and that several loops of data are missing. The data recorded by the Temposonics was chosen to present the results of the second test.

One observation made when comparing the two datasets was that the Temposonics seemed to consistently record a certain amount of slip in the test set-up at each loads reversal, such a slip is not present in the data recorded by the LVDTs. The slip can be seen in Fig. 4.3 which shows a comparison between the data collected by the LVDTs and one of the Temposonics. This slip was attributed once again to the movement of the reaction buttress, but more so to the modified pin-supports, which incorporated more bolted parts. Therefore, being simply a consequence of slack in the experimental set-up due to cycling of the loads, it was felt necessary to correct the data accordingly. A computer program, included in Appendix D, was developed to remove the slip element from the recorded data. A comparison of the recorded

and corrected data is shown in Fig. 4.4 for a typical Temposonic reading, prior to conversion of the recorded displacement values into rotations.

4.1 Experiment 1

The final M-θ relationship obtained for the connection is shown in Fig. 4.5. This specimen was subjected to twenty eight (28) cycles of loading. The hysteretic loops are visibly severely pinched, even in the early stages of the experiment. The maximum positive moment reached (M^+_{max}) was 59 kN•m corresponding to a maximum positive rotation (θ^+_{max}) of 26.7×10^{-3} radian, while the maximum negative moment (M^-_{max}) was -100 kN•m and the maximum negative rotation (θ^-_{max}) was -43.1×10^{-3} radian. The experiment ended with the shear failure of the two rivets connecting the East beam to the stiffened seat angle.

The loading of the specimen was controlled as suggested by ATC-24 "Guidelines for Cyclic Seismic Testing of Components of Steel Structures". The applied force was chosen as the initial control parameter. The first three cycles were completed at $\frac{1}{2}F_y$, where F_y was based on an estimate of the connection resistance as described in section 3.3.1 and Appendix A. This corresponded to $M^+ = 24$ kN•m with $\theta^+ = 1.3 \times 10^{-3}$ radian in positive flexure, and $M^- = -36$ kN•m with $\theta^- = -3.6 \times 10^{-3}$ radian in negative flexure. Small hairline cracks were visible in the concrete surface at the North-East beam-column connection location during the second cycle in positive flexure. Slight pinching was observed in these initial M-θ loops.

For the next three cycles, load was applied up to $\frac{3}{4}F_y$, i.e. until $M^+ = 36$ kN•m with a corresponding $\theta^+ = 2.8 \times 10^{-3}$ radian, and $M^- = -70$ kN•m with $\theta^- = -8.1 \times 10^{-3}$ radian. Small cracks were observed running in the North-South direction at the level of the beam-column connection on both sides of the specimen, indicating the onset of the separation of the concrete from the specimen. Fig. 4.6 shows these cracks highlighted with a black felt tip marker. Pinching and non-linearity, especially during negative flexure, was observed in the M-θ curve. After the third cycle, the regulating parameter for the flow of the experiment was

changed to displacement-control.

In the next three cycles, the moment reached $M^+ = 45$ kN•m with a corresponding $\theta^+ = 4.2\text{x}10^{-3}$ radian, and $M^- = -76$ kN•m with $\theta^- = -11.2\text{x}10^{-3}$ radian. The same cracks observed in the previous set of cycles grew larger (approximately 2mm in negative flexure and less than 1mm in positive flexure). From this observation, and non-linearity observed in the negative region of the M-θ plot, the negative θ_y seemed to have been exceeded and was approximated at $-4.5\text{x}10^{-3}$ radian .

Before proceeding with the next set of cycles, the M-θ curve showed some softening on the negative side, while the positive region was still quite linear. Therefore, the positive displacement was increased until the same softening observed in the negative region of the M-θ curve was observed in the positive portion. Therefore, the displacement was increased until $M^+ = 48$ kN•m and $\theta^+ = 6.1\text{x}10^{-3}$ radian, while θ^- remained the same at $-11.2\text{x}10^{-3}$ radian. In the process, the M^- corresponding to that θ^- dropped slightly to -70 kN•m, further indication that $-\theta_y$ had been exceeded. The positive θ_y was approximated at $2.5\text{x}10^{-3}$ radian. At this amount of displacement, the cracks at the North and South connections were now of the same width; approximately 2mm each.

During the next three cycles, the displacements were considered to be in the range of $\pm 3.0\ \theta_y$. The positive moment reached $M^+ = 50$ kN•m at a positive rotation $\theta^+ = 8.3\text{x}10^{-3}$ radian, while the negative moment reached $M^- = -78$ kN•m at $\theta^- = -13.5\text{x}10^{-3}$ radian. At this load level, small cracks were noticed underneath the West beam on the stiffened seat angle side. The larger cracks observed in the previous cycles continued to widen and no longer closed when the loads reversed. Pinching in the M-θ curve continued, and even seemed to get more severe.

For the next two cycles, the displacements were increased to $\pm 3.5\ \theta_y$, and then to $\pm 4.0\ \theta_y$ for two additional cycles. Throughout these four cycles, the cracks kept getting wider and the

pinching of the M-θ curve kept getting more severe. The displacements were gradually increased in steps of θ_y and sets of two cycles were completed for each step.

During the two cycles at a displacement of approximately $\pm 7.0\Delta_y$, the positive moment reached $M^+ = 53$ kN•m and a positive rotation $\theta^+ = 18.9 \times 10^{-3}$ radian, while the negative moment reached $M^- = -95$ kN•m and the negative rotation $\theta^- = -31.8 \times 10^{-3}$ radian. The crack width was now very large, approximately 25mm on the North end, and the LVDTs were removed to prevent their damage.

In the following cycle, severe concrete damage was observed with large crack openings and large concrete sections on the verge of falling. Fig. 4.7 shows the deterioration of the specimen at this point. In the next cycle ($\pm 9.0\Delta_y$), load was applied until $M^+ = 59$ kN•m and a positive rotation $\theta^+ = 23.9 \times 10^{-3}$ radian, while the negative moment reached $M^- = -100$ kN•m and the negative rotation $\theta^- = -40.8 \times 10^{-3}$ radian. The crack opening varied between 18 to 30mm depending on the location, but was generally 30mm in the vicinity of the connecting elements. In the next cycle ($\pm 10.0\Delta_y$), the maximum positive moment was reached at $M^+_{max} = 59$ kN•m as well as the maximum positive rotation $\theta^+_{max} = 26.7 \times 10^{-3}$ radian, but failure occurred in negative flexure when the maximum negative moment, M^-_{max}, reached -100 kN•m and the maximum negative rotation, θ^-_{max}, -43.1×10^{-3} radian. The shear failure of the rivets connecting the East beam to the stiffened seat angle is shown in Figs. 4.8 and 4.9.

Since the presence of the concrete cover made it impossible to visually inspect the connecting elements during the experiment for signs of yielding and formation of plastic hinges, the concrete was removed after the test in order to inspect the damages. The top angles showed signs of large inelastic excursions. The backs of both angles were separated from the column face as shown in Figs. 4.10 and 4.11 and evidence of the formation of the hinge mechanism in the vertical leg of both of the top angles was also present (Figs. 4.12 and 4.13). The rivets of the vertical leg of the top angles showed signs of yielding and large elongations as shown in Fig. 4.14. The residual deformation of the seat angle and the stiffeners of the West side are

shown in Fig. 4.15, indicating large inelastic excursions suffered during the experiment.

4.2 Experiment 2

The M-θ relationship for the right and left side of the column are shown in Figs. 4.16 and 4.17 respectively. The M-θ relationship based on the average results of the connections on both sides of the column is shown in Fig. 4.18. Slight pinching is observed in the hysteretic loops once the specimen has undergone large rotations. A total of forty eight (48) cycles of loading were applied to the connection during this experiment (although 18 were in the elastic range for reasons described later). The connection developed a maximum positive moment (M^+_{max}) of 250 kN•m and a maximum positive rotation (θ^+_{max}) of 27.9×10^{-3} radian, while the maximum negative moment resisted (M^-_{max}) was -243 kN•m and the maximum negative rotation (θ^-_{max}) was -58.0×10^{-3} radian. The specimen reached failure when the North-East fuse-plate ruptured from excessive cyclic alternating plasticity due to repeated plastic buckling and tensile yielding. Fig. 4.19 describes the amount of buckling, or uplift from the beam flange, of the fuse-plates at different cycles.

Since the interaction between the existing connection and new steel member added as part of the retrofit was unknown and difficult to predict, the specimen was initially loaded in a similar fashion as in the first experiment (i.e. with smaller loads applied in the positive moment direction due to the weaker top angle). The loading conventions of ATC-24 were once again followed as much as possible. The first three cycles were completed at $\frac{1}{2}F_y$, the next three at $\frac{3}{4}F_y$ and then another three at 1.0 F_y, where F_y was that for the bare steel specimen and as estimated previously. During the last cycle at 1.0 F_y, the positive moment developed (M^+) was 35 kN•m and the positive rotation (θ^+) was 0.4×10^{-3} radian, while the negative moment developed (M^-) was -70 kN•m and the negative rotation (θ^-) was -1.4×10^{-3} radian. The following three cycles were completed at a force level of approximately 1.75 F_y where the positive moment was 77 kN•m and the positive rotation was 1.3×10^{-3} radian, while the

negative moment was -128 kN•m and the negative rotation was -2.8×10^{-3} radian. At this point the M-θ curve was still linear and the specimen showed no signs of yielding.

Symmetry was also observed in the behaviour of the M-θ curve for the positive and negative resisting elements and the positive applied load was increased to equal the negative load. During the next three cycles, this action proved to be appropriate because the symmetry remained between the positive and negative cycles. The anticipated value of F_y now considered as a control parameter was changed to the F_y of the steel-band/fuse-plate assembly. The loads were gradually increased over the next two sets of three cycles each, where specimen behaviour remained elastic.

During the 19th , 20th, and 21st cycles the value of F_y for the steel-band/fuse-plate assembly was reached, corresponding to an applied moment of M = 205 kN•m and a corresponding rotation of $\theta = 7.5 \times 10^{-3}$ radian. Evidence of yielding appeared as small cracks in the paint of the narrow part of the fuse plate (Fig. 4.20), and the moment-strain diagrams of gages 17 and 20 (Figs. 4.21 and 4.22 respectively) confirm the yielding of these plates. Non-linearity was observed in the M-θ curve and this approximately defined the yield point (θ_y).

In the first half of the next cycle, the positive applied moment was increased to 216 kN•m and attained a rotation of 8.5×10^{-3} radian. Both fuse-plates on the south side showed slight buckling at this load level, as indicated in Fig. 4.23. At this point, one of the floor bolts in the test set-up failed. More specifically, it is one of the assemblies specially designed to stiffen the floor bolts that acted as a pin-support at the end of the extension beam end that failed.

The experiment was halted and stronger supports were designed and constructed. After a delay for design, construction, and installation of the new floor bolt supports, the experiment resumed.

Since the fuse plates had just reached yielding and only one set of the plates had buckled when

the floor bolt support failed, the anticipated behaviour of the specimen during the re-test was still expected to be a good representation of the actual retrofit behaviour. Some residual deformation remained in the specimen after the previous test and the first few hysteretic loops obtained during re-test were not centred about the original axes of the M-θ graph, but after the first two sets of cycles in the elastic range, the hysteretic loops obtained under negative and positive applied loads of identical absolute magnitude seemed to shift their centre into a more concentric location about the axes, particularly as the other fuse-plates buckled and reached the same deformation as those plates which yielded in the previous test. The cycle count in the following descriptions begins at cycle 23, since the specimen was subjected to 22 complete cycles of loading prior to resuming this test.

As mentioned above, two sets of three cycles each were applied to the connections in the elastic range. These cycles were performed to determine if the behaviour of the specimen had changed in the elastic range. The M-θ curve indeed showed good linear behaviour during cycles 23 through to 28. During cycles 29 to 31, some non-linearity was observed in the M-θ loops, especially in the negative region, at an average moment of M = 165 kN•m and an average joint rotation of $\theta = 7.5 \times 10^{-3}$ radian, which is the yield displacement observed during the first part of the experiment. The fuse-plate in the North-East joint corner showed signs of slight buckling, the one in the North-West corner remained un-buckled, while both fuse-plates on the South side of the connection showed an equal amount of buckling when under compression.

After the next set of three cycles, the hysteretic loops seemed to have centred themselves about the original starting point, and the control of the experiment was changed to displacement control. The displacement was increased to what was considered to be approximately $\pm 1.5\theta_y$ for cycles 35 to 37, which produced a moment M = 230 kN•m and a rotation of $\theta = 11.1 \times 10^{-3}$ radian. During the first cycle at this load level, small vertical hairline cracks (in the North-South direction) formed in the concrete surface at the level of the existing connections (Fig. 4.24). The fuse plates continued to yield when subjected to tension,

buckle when subjected to compression, and they buckled further with each cycle. The North-East fuse plate buckled considerably during these three cycles, lifting up from the face of the beam by up to 20mm during the 37th cycle (Fig. 4.25), while the North-West plate showed very little buckling (lifting 2 to 3.5mm). The two fuse plates on the South side buckled by relatively the same amount, lifting at mid-length of approximately 13mm each.

The displacement was then further increased to approximately $\pm 2.0\theta_y$ for cycles 38 to 40, where M = 245 kN•m and a rotation of $\theta = 14.5 \times 10^{-3}$ radian were attained. During the 41st cycle, the displacement was increased to $\pm 2.5\theta_y$ and when this value was attained for the first time in positive bending, two sharp "snap-like" noises were heard and the applied moment dropped abruptly from 245 kN•m to 220 kN•m while the rotation increased from 17.9×10^{-3} to 19.5×10^{-3} radian. This no doubt indicated the shear failure of the two rivets connecting the top East beam flange to the outstanding leg of the top angle. These rivets were located at the North-East corner. During the following two cycles, the same displacement in the positive direction was achieved at a much lower moment (M = 190 kN•m). From this point in the experiment, the stiffness degradation observed in the rising segment of the M-θ curve was more pronounced; the same displacements and rotations were reached at a lower value of moment with each passing cycle. During these cycles, the East beam was sliding through the concrete encasement causing local spalling of the concrete near the North-East beam flange as shown in Fig. 4.26.

In the next set of three cycles, the displacement was increased to about $\pm 3.0\theta_y$. Further stiffness degradation was observed in the rising segment of the M-θ curve with each cycle. The North-East corner fuse-plate suffered large buckling deformations, which reached 51mm during the 46th cycle, while the North-West corner fuse-plate buckled between 5 to 7mm during these cycles. The South plates buckled between 20 to 40mm. The East beam slid further through the concrete as the fuse-plate suffered additional tensile elongation, as shown by the paint marks near the large tapered end of the fuse-plate in Fig. 4.27.

Two cycles were performed at a displacement of approximately $\pm 3.5\theta_y$. The North-East fuse-plate reached a maximum buckling deformation of 61mm (Fig. 4.28), while the South-West fuse-plate reached 49mm (Fig. 4.29). Then, the displacement was further increased to $\pm 4.5\theta_y$. During the first excursion in positive bending, the specimen reached failure when the North-East fuse-plate suffered a gross area tensile failure in the middle of the fuse-plate, where a plastic hinge had formed to allow buckling (Fig. 4.30). After inspection of the failed plate, the load was reversed in hope of creating a similar failure in negative flexure. The specimen was loaded until a rotation of $\theta = -58.4 \times 10^{-3}$ radian was reached at a moment of M = -226 kN•m but no such failure occurred, even at this very large deformation. It was felt that more cycles of alternating plasticity would have been necessary to produce another such failure, and since this was not possible anymore, the experiment was then ended.

CHAPTER 5

Comparison and Discussion of the Results

5.1 Comparison of Test Results with Predicted Capacities

5.1.1 Experiment 1

Table 5.1 compares the predicted failure capacities with the experimental values obtained under the application of positive moment. The maximum applied positive moment was 59 kN•m, therefore failure modes 3 to 8 were not observed experimentally. The presence of concrete encasement also hindered the possibility of observing failure modes 1 and 2 during the experiment, therefore the strain gage data is relied upon for determining the load levels corresponding to the different events. It is important to note that some failure modes could not be visually observed during the experiment, because of concrete encasement, or even detected through experimental data because of practical implications (i.e. for example, it was not possible to install a strain gage on the rivet shank to observe rivets yielding).

The onset of failure mode 1 was difficult to pinpoint for reasons described above, but experimental observations set this value at approximately 45 kN•m. At this point, significant cracking and separation of the concrete from the column was observed during testing, indicating the initial movement of the angle due to this failure mode. Further, strain gage data indicates that the first significant movement of the top leg occurred at this value, as indicated in Fig. 5.1. This value is in very good agreement with the predicted value calculated taking into account the effect of prying action of the top angle leg on the rivet.

Failure mode 2 was, once again, impossible to visually observe due to the concrete

encasement. Unfortunately, strain gage data is not available for gages 10 or 12 located on the anticipated yield lines because these gages failed early during the test. However, by referring to Fig. 4.5, the hinge mechanism in the top angle seems to start to form at a moment of approximately 50 kN•m. Since this value compares relatively well to the predicted value, the model proposed by Sarraf and Bruneau (1996) to evaluate the behaviour of a wide top angle seems suitable.

The comparison of the predicted failure modes with the experimental values obtained under the application of negative moment is made in Table 5.2. Since the applied moment was limited to 100 kN•m in negative flexure, failure modes 3 to 5 described in Table 3.4 were not observed.

The formation of the hinge mechanism in the stiffener angle, failure mode 1, can be observed from the experimental data at approximately 80 kN•m. Strain gage 2, which is located on the angle leg next to the column flange, indicates the formation of the plastic hinge as shown in Fig. 5.2. Therefore, the model used provides a good estimate of the capacity of a stiffened seat angle (76 kN•m predicted to 80 kN•m observed) . Note that the model of the stiffener angles developed by Sarraf and Bruneau (1996) does not consider a contribution to the resistance from the first row of fasteners, since these rivets connect the stiffener angles to the seat angle and not directly to the column; therefore the fasteners move along with the angle deformation and do not develop any tensile resistance.

The predicted value for failure mode 2 shows a difference of approximately 20% with the experimental value (123 compared to 100 kN•m). Since strain gage data shows that these angle legs are subjected to flexure, the shear/tension interaction could have reduced the shear capacity of the rivets. Also, the diametric shrinkage, common with the cooling of field driven rivets (Kulak et al., 1987), could have reduced the effective area used when calculating the shear resistance of the rivets. These combined effects could account for the difference obtained between the predicted and experimentally observed failure loads.

As a general observation, the behaviour of this specimen does not seem to be affected by the concrete encasement. A comparison of the results obtained in this experimental investigation with results from a similar test on an identical bare steel specimen (Fig. 5.3) indicate that, for connections similar to those considered here, the concrete encasement can be ignored when analysing the connection capacity. This can be attributed to the fact that columns in the Daly Building were encased in a weak unreinforced concrete, and this concrete cracked very early in the test. This contradicts findings by other investigators who have shown that a concrete encasement can enhance the performance of the bare connection, as discussed in Chapter 2. However, the type of encasement considered here was taken from an existing turn-of-the-century building, and is believed to be more representative of similar buildings built at the time in Eastern North America.

5.1.2 Experiment 2

During this experiment, the yielding of the fuse plates occurred when the applied moment was 208 kN•m. There is very good agreement between the experimental value and the predicted value of 192 kN•m, calculated as shown in Appendix B. The progression of this experiment indicates that the resistance provided by the existing connection does not provide any significant contribution to the overall specimen behaviour. The steel-band fuse-plate assembly provided as retrofit is much stiffer than the existing connection and consequently resist virtually all of the applied loads.

The concrete encasement was not found to provide any significant additional resistance to the connection, as was the case for specimen 1. However, the confinement provided by the steel-band allows the transfer of loads to the column by maintaining the integrity of the connection, even after the existing elements of the connection have failed. The steel-band assembly also prevents the concrete encasement from cracking or spalling until large rotations have been attained.

5.2 Hysteretic Response of the Connections

5.2.1 Specimen 1: Non-retrofitted

The M-θ relationship obtained from this experiment indicates poor energy dissipation since the hysteretic loops are severely pinched. The pinching seems to be typical of this type of connection as reported elsewhere (Sarraf and Bruneau, 1996; Roeder et al., 1994; Bernuzzi, 1992). The reasons for this pinching, which have been well documented by Sarraf and Bruneau and also observed in this study, are: slippage at rivet holes, rocking of top angles, and lack of integrity of stiffened seat angles. All these factors contribute to the pinching of the hysteretic loops and poor energy dissipation.

However, this type of connection can definitely resist a non-negligible moment that might be sufficient to provide the necessary seismic resistance in small to moderate seismic zones. This remains to be investigated.

5.2.2 Specimen 2: Steel-Band Fuse-Plate Retrofit

The retrofitted specimen shows good hysteretic behaviour, but the M-θ relationship for this connection shows some pinching at large joint rotations. This characteristic can be explained by the simultaneous buckling in compression and elongation in tension of the fuse-plates. Since these plates were designed with a C_r/T_r ratio very close to 1.0 (0.95), the tensile yielding and compressive buckling of the plates is practically simultaneous.

There is some stiffness degradation shown at large rotations by the steady decrease in slope of the rising segment in the M-θ curve for the retrofitted specimen. Once the plate has yielded in tension, it becomes slightly longer than its original dimension. When the load is reversed, buckling occurs earlier than in the previous cycle because the elongated plate no longer fits in the original position. As the loading progresses, buckling occurs earlier in each subsequent

cycle than in the previous one. As the buckled plate straightens, the tensile resistance can be developed anew, but this will occur at progressively larger drifts. Furthermore, under excessive yielding, the North-East and both South plates developed visible necking in the last few cycles of this test.

The effectiveness of the proposed seismic retrofit strategy can be seen by comparing the moment-curvature experimentally obtained for the two specimens. This is accomplished in Fig. 5.4, using the same scale for both axes. This clearly illustrates the enhanced seismic resistance and energy dissipation capability of the retrofitted specimen.

CHAPTER 6

Conclusions and Recommendations

6.1 Conclusions

The following conclusions can be drawn from the experimental results and analytical predictions obtained from this investigation:

- The type of semi-rigid connection studied here, namely riveted top and stiffened seat angles, can in fact develop a non-negligible moment resistance and sustain numerous cycles of loading without severe strength degradation. The resistance can be evaluated, taking into consideration the size and arrangement of the connecting elements, using the analytical models presented in this study.

- The existing connections can dissipate some hysteretic energy, but their hysteretic loops are severely pinched indicating a relatively poor energy dissipation.

- Unreinforced concrete encasement of the type commonly found in buildings built at the turn-of-the-century in Eastern North America does not improve connection strength or behaviour.

- The proposed steel-band fuse-plate retrofit strategy significantly improves the cyclic behaviour and hysteretic energy dissipation capacity of this type of connection, as demonstrated experimentally.

6.2 Recommendations

6.2.1 Existing Connections

When attempting to determine the effect of concrete encasement, the strength of the existing concrete must be determined as accurately as practically possible. Every effort should be made to assess the existing concrete strength as well as the arrangement of the reinforcing, if present. For the type of connection considered here, in Eastern North America, it is recommended that the effect of concrete encasement be neglected at this time, until further experimental evidence can demonstrate otherwise.

For that reason the experimental results show that the analytical models used in this study to predict the capacity of the existing connection, previously developed by other researchers, are reliable. Practising engineers may use these models to determine the capacity of riveted top and stiffened seat angle connections, as well as the capacity of connections incorporating similar elements.

6.2.2 Steel-Band Fuse-Plate Assembly

The steel-band fuse-plate retrofit strategy proved to be an effective mean of improving the connection strength and cyclic hysteretic behaviour. The installation of the required elements is unobtrusive; the removal of any of the existing elements is not required, and the work can be sequential, going from connection to connection, in an existing building, therefore minimizing any interruptions to its normal use and occupancy. The use of this retrofit strategy can likely be extended to other connection types or configurations.

The key parameters for the design of a steel-band fuse-plate assembly are as follows:

- The compression to tension resistance ratio (C_r/T_r) of the fuse-plate should be as close as possible to 1.0. Stiffeners may be used on the fuse-plate in order to achieve this ratio, if necessary.

- The moment capacity provided by the retrofit must be smaller than the moment which would cause a plastic hinge to form in the adjacent column.

In order to minimize on-site welding, most of the steel-band fuse-plate assembly can be welded in-shop, transported to the site and welded or bolted to the beams, and welded together around the columns.

The test set-up used in this experimental investigation is not intended to take into consideration column behaviour, as would be the case in an earthquake where columns are subjected to flexure and shear. However, experimental observations showed that the steel band did not separate from the column concrete face under the applied loads, and the behaviour would be satisfactory in the mode of testing described above, although this remains to be experimentally confirmed.

6.3 Further Research Required

Although recent research efforts have been made on the subject of semi-rigid connections, additional information is required to further existing knowledge on the cyclic behaviour of these types of connections. The following topics should be addressed:

- Further investigations on the effect of concrete encasement, with and without reinforcement, on the hysteretic behaviour of semi-rigid connections.

•Analytical hysteretic models to predict the M-θ cyclic relationship of this type of connection, taking into account the progressive stiffness degradation of the ascending segment. These would be used for non-linear inelastic computer analyses to investigate seismic behaviour of buildings having this type of structural elements.

•Further investigations on different types of retrofit strategies, such as using different energy dissipators to reduce the amount of pinching and stiffness degradation observed in this study at large rotations (i.e. use a fuse element that yields in a flexural or shear mode rather than tension and compression).

Further understanding the behaviour of these types of connections, and the development of simple analytical models which can be easily incorporated into computer programs, will lead to a more accurate representation of the contribution to lateral load resistance provided by these existing or retrofitted connections. This could save many buildings in low to moderate seismic zones built with these semi-rigid connections from otherwise undergoing large and expensive retrofitting projects.

References

Ang, K.M., and Morris, G.A. (1984). "Analysis of three-dimensional frame with flexible beam-column connections" *Can. J. Civ. Engrg.*, 11, 245-254.

Astaneh, A., et al. (1989a). "Cyclic behaviour of double angle connections" *J. Struct Div.*, ASCE, 115(5), 1101-1118.

Astaneh, A., et al. (1989b). "Experimental Studies of a Single Story Steel Structure with Fixed, Semi-Rigid and Flexible Connections" *Earthquake Engineering Research Centre*, Report No. UCB/EERC-89/15.

Batho, C. (1938). "The Effect of Concrete Encasement on the Behaviour of Beam and Stanchion Connections", *The Structural Engineer*, December 1938, 427-447.

Batho, C., and Lash, S. D. (1936). "Further Investigations on Beam and Stanchions Connections, Including Connections Encased in Concrete; Together with Laboratory Investigations on a Full-Scale Steel Frame", Final Report of the Steel Structures Research Committee, Department of Scientific and Industrial Research, His Majesty's Stationery Office, London, 1936, 276-363.

Beaufoy, L.A. and Mohorram (1948). "Derived moment-angle curves for web-cleat connections", Preliminary Publication, *Third Congress, International Association for Bridge and Structural Engineering.*

Bernuzzi, C., Zandonini, R., and Zanon, P. (1992). "Semi-Rigid Steel Connections Under Cyclic Loads", *Proceedings of the First World Conference on Constructional Seel Design*, Acapulco, Mexico, December 1992.

Bruneau, M., and Sarraf, M. (1996). "Cyclic Testing of Existing and Retrofitted Riveted Stiffened Seat Angle Connections", *J. Struct. Engrg.*, ASCE, 122(7), 762-775.

Canadian Institute of Steel Construction (1992). *Handbook of Steel Construction (CISC)*, Willowdale, Ont.

Colson, A., et al. (1983). "Connection incidence on the elastic behaviour of steel structures", *Euremech Colloquium*, 174.

DeLuca, A. (1995). "Behaviour and Modelling of Top and Seat and Top and Seat and Web Angle Connections", *Connections in Steel Structures III: Behaviour, Strength and Design*; Proceedings of the third International Workshop, Trento, Italy, 289-297.

De Stephano, M., et al. (1994). "Modelling of Cyclic Moment-Rotation Response of Double-Angle Connections", *J. Struct. Engrg.*, ASCE, 120(1), 212-223.

FEMA (Federal Emergency Management Agency) (1992). "NEHRP Handbook for seismic rehabilitation of existing buildings", *FEMA*-172/June 1992.

Fry, M.J., and Morris, G.A. (1976). "Analysis of flexibly connected steel frames", *Can. J. Civ. Engrg.*, 2(3), 280-291.

Goverdhan, A.V. (1983). "A Collection of Experimental Moment-Rotation Curves and Evaluation of Prediction Equations for Semi-Rigid Connections", *Master's Thesis*, Vanderbilt University, Nashville, TN.

Hetchman, R.A., et al. (1947). "Riveted semi-rigid beam-to-column building connections, progress report no. 1", AISC Research at Lehigh Univ., Bethlehem, Pa.

Jones, S.W., et al. (1982). "Columns with semirigid joints", *J. Struct. Engrg.*, ASCE, 108(2), 361-372.

Kishi, N., and Chen, W.F. (1990). "Moment-rotation relations of semirigid connections with angles", *J. Struct. Engrg.*, ASCE, 116(7), 1813-1834.

Kishi, N., and Chen, W.F. (1986). "Data base of steel beam-to-column connections", *Struct. Engrg. Report No. CE-STR-86-26*, School of Civ. Engrg., Purdue Univ., West Lafayette, Ind.

Kulak, et al. (1987). "Guide to Design Criteria for Bolted and Riveted Joints", Second Edition, John Wiley and Sons, New York, 28,29,30,33,115.

Lewitt, C.W., et al. (1966). "Restraint Characteristics of flexible riveted and bolted beam-to-column connections", *Dept. Civ. Engrg.*, Univ. of Illinois, Urbana, Ill.

Lightfoot, E., et al. (1974). "Elastic analysis of frameworks with elastic connections", *J. Struct. Engrg.*, ASCE, 100(ST6), 1297-1309.

Lui, E.M., Chen, W.F. (1983). "Strength of H-columns with small end restraints", *Journal of the Institution of Structural Engineers*, 61.B(1), 17-26.

Lui, E.M., et al. (1986). "Analysis and behaviour of flexibly jointed frames", *Engineering Structures*, Butterworth Publishers, Surrey, U.K., 8(2), 107-118.

Malhotra, V.M. (1986). "Mechanical Properties and Freezing and Thawing Durability of Concrete Incorporating a Ground Granulated Blast-Furnace Slag",

Marley, M.J., et al. (1982). "Analysis and test of flexibly-connected steel frames", *Report to AISC under Project 199*, AISC, Chicago, Ill.

Maxwell, S.M., et al. (1981). "A realistic approach to the performance and application of semi-rigid joints in steel structures", *Joints in Structural Steel Work*, J.H. Howlett, W.M. Jenkins and R. Stansby, eds., Pentech Press, 2.71-2.98.

Monforton, A.R., et al. (1963). "Matrix analysis of semi-rigidly connected frames", *J. Struct. Engrg.*, ASCE, 86(ST6), 14-42.

Munse, W.H., et al. (1959). "Behaviour of Rivetted and Bolted Beam-to-Column Connections", *Journal of the Structural Division*, ASCE, No. ST3, 29-51.

Nethercot, D.A. (1985a). "Utilization of Experimentally Obtained Connection Data in Assessing the Performance of Steel Frames", *Connection Flexibility and Steel Frames*, edited by W.F. Chen, New York, Structural Division, ASCE.

Nethercot, D.A. (1985b). "Steel Beam-to-Column Connections - A Review of Test Data", London, CIRIA.

Neville, A.M. (1995). Properties of Concrete, Longman Group Limited, England, 592-593.

Radziminski, J.B., and Azizinamini, A. (1986). "Low cyclic fatigue of semi-rigid steel beam-to-column connections", *Proceedings of the third U.S. National Conference on Earthquake Engineering*, 1285-1296.

Rathbun, J.C. (1936). "Elastic properties of riveted connections", *Trans. ASCE*, Paper No. 1933, Vol. 101, 524-563.

Richard, R.M., et al. (1980). "The analysis and design of single plate framing connections", *ASCE Engrg. J.*, 2nd Quarter, 38-52.

Roeder, C., et al. (1994). "Strength, Stiffness and Ductility of Older Steel Structures Under Seismic Loading", *Report No. SGEM 94-4*, Dept. Civ. Engrg, Univ. of Washington, Seattle, Washington.

Stelmack, T.W., et al. (1983). "Analytical and experimental response of flexibly connected steel frames", *Reported to AISI CEAE Dept.*, Univ. of Colorado, Boulder, Col.

Stelmack, T.W. (1986). "Analysis and tests of flexibly connected steel frames", *J. Struct. Engrg.*, ASCE, 112(7), 1573-1586.

Tarpy, T.S., et al. (1981). "Behaviour of semi-rigid beam-to-column end plate connections", Proceedings Conference, *Joints in Structural Steelwork*, J.H. Howlett, W.M. Jenkins and R. Stainsby, eds., Halsted Press, 2.3-2.5.

Wilson, W.M., and Moore, H.F. (1917). "Tests to determine the rigidity of riveted joints of steel structures", *Engineering Experiment Station, Bulletin No. 104*, Univ. of Illinois, Urbana, Ill.

Wu, F.S., and Chen, W.F. (1990). "A Design Model for Semi-Rigid Connections", *Engineering Structures*, 12(2), 88-97.

Yee, Y.L., and Melchers, R.E. (1986). "Moment-Rotation Curves for Bolted Connections", *J. Struct. Engrg*, ASCE, 112(ST3), 615-635.

Young, C.R., and Jackson, K.B. (1934). "The relative rigidity of welded and riveted connections", *Canadian Journal of Research*, vol. 11, 62-100.

Youssef-Agha, W., et al. (1989). "Seismic response of low-rise steel frames", *J. Struct. Engrg.*, ASCE, 115(3), 594-605.

Mix	w/s	Water	Slag	C.A.*	F.A.**
A	0.78	137	196	1133	756
B	0.60	145	263	1121	746

* C.A. = Coarse Aggregate (19mm)
**F.A. = Fine Aggregate
All quantities are in kilograms

Table 3.1 Mix design proportions

Mix	Sample	14 Days	42 Days
A	1	6.80	10.9
	2	6.61	12.2
	3	6.58	12.3
	Avg.	6.66	11.8
B	1	8.10	14.2
	2	8.83	12.4
	3	8.09	12.1
	Avg.	8.34	12.9

Cube	Cube Strength
A	9.50
B	8.85
C	7.44
Avg.	8.60
E.C.S.*	6.88

*Calculated Equivalent Cylinder Strength: E.C.S. = Avg. Cube Strength /1.25

Table 3.2 Comparison of cube strength with trial mixes at 14 and 42 days.

No.	Mode	Moment (kN•m)
1	Top rivets tensile yielding	40
2	Formation of hinge mechanism in top angle	62
3	Top rivets tensile failure	75
4	Rivets shear failure	123
5	Bearing failure at rivet holes in top angle	165
6	Angle leg net section yield	212
7	Angle leg gross section yield	247
8	Top angle leg gross section shear failure	263

Table 3.3 Positive moment capacities for various limit states of specimen 1

No.	Mode	Moment (kN•m)
1	Formation of hinge mechanism in seat angle stiffeners	76
2	Bottom rivets shear failure	123
3	Angle leg net section yield	216
4	Angle leg gross section yield	254
5	Stiffener angles gross section shear failure	362

Table 3.4 Negative moment capacities for various limit states of specimen 1 (based on models by Sarraf and Bruneau, 1996)

No.	Mode	Predicted Moment (kN•m)	Experimental Moment (kN•m)
1	Top rivets tensile yielding	40	45
2	Formation of hinge mechanism in top angle	62	50

Table 5.1 Comparison of the predicted and experimental positive moment capacities for specimen 1 (predicted capacities based on models by Sarraf and Bruneau, 1996).

No.	Mode	Predicted Moment (kN•m)	Experimental Moment (kN•m)
1	Formation of hinge mechanism in seat angle stiffeners	76	80
2	Bottom rivets shear failure	123	100

Table 5.2 Comparison of the predicted and experimental negative moment capacities for specimen 1 (predicted capacities based on models by Sarraf and Bruneau, 1996).

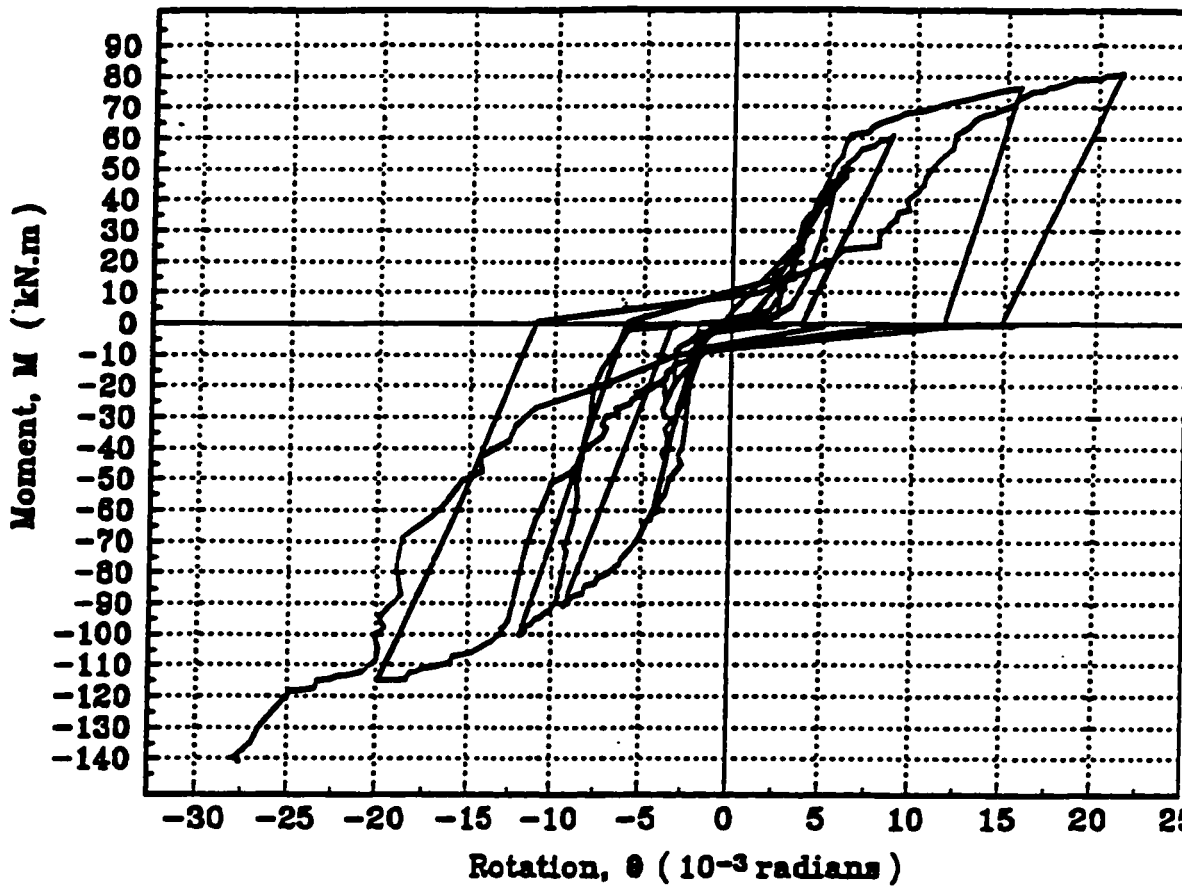

Figure 2.1 M-θ relationship based on average results for connection detail 1, specimen1 (Bruneau and Sarraf, 1996)

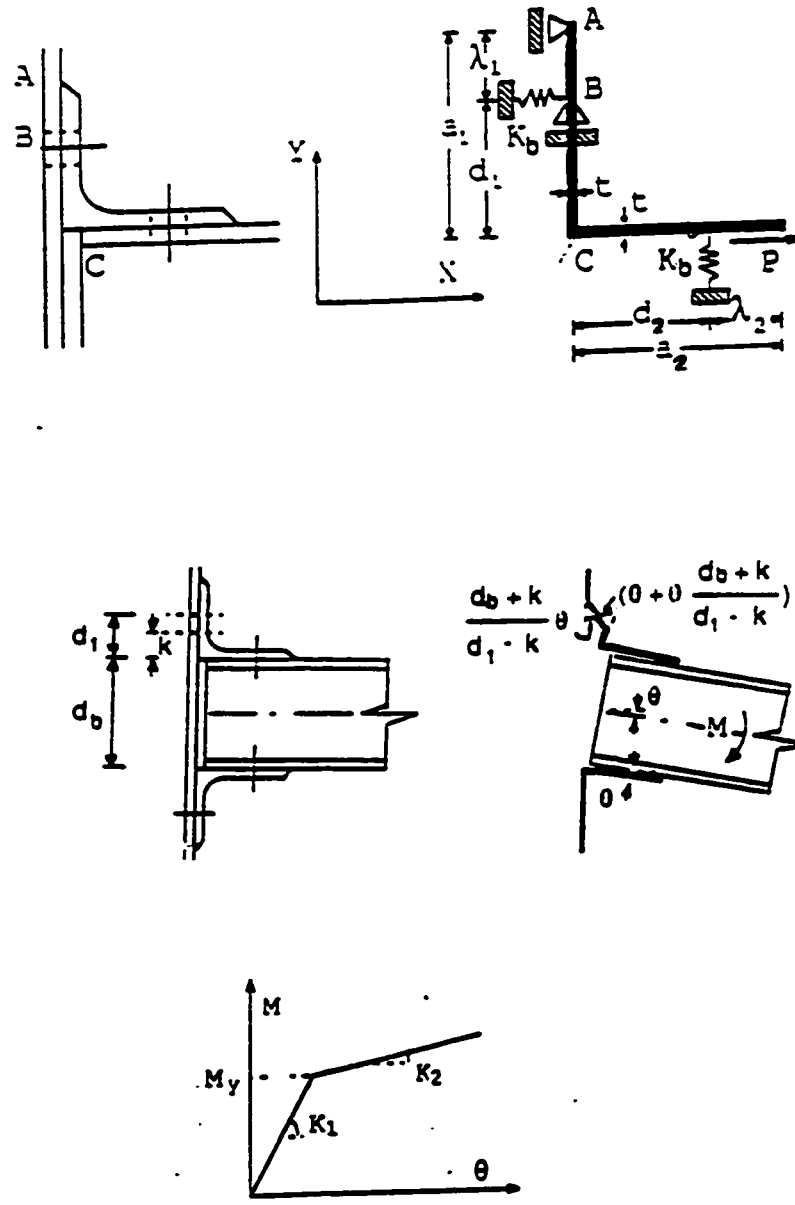

Figure 2.2 Physical models of top and seat angle connections for elastic and ultimate conditions with bi-linear M-θ relationship (Youssef-Agha et al., 1989)

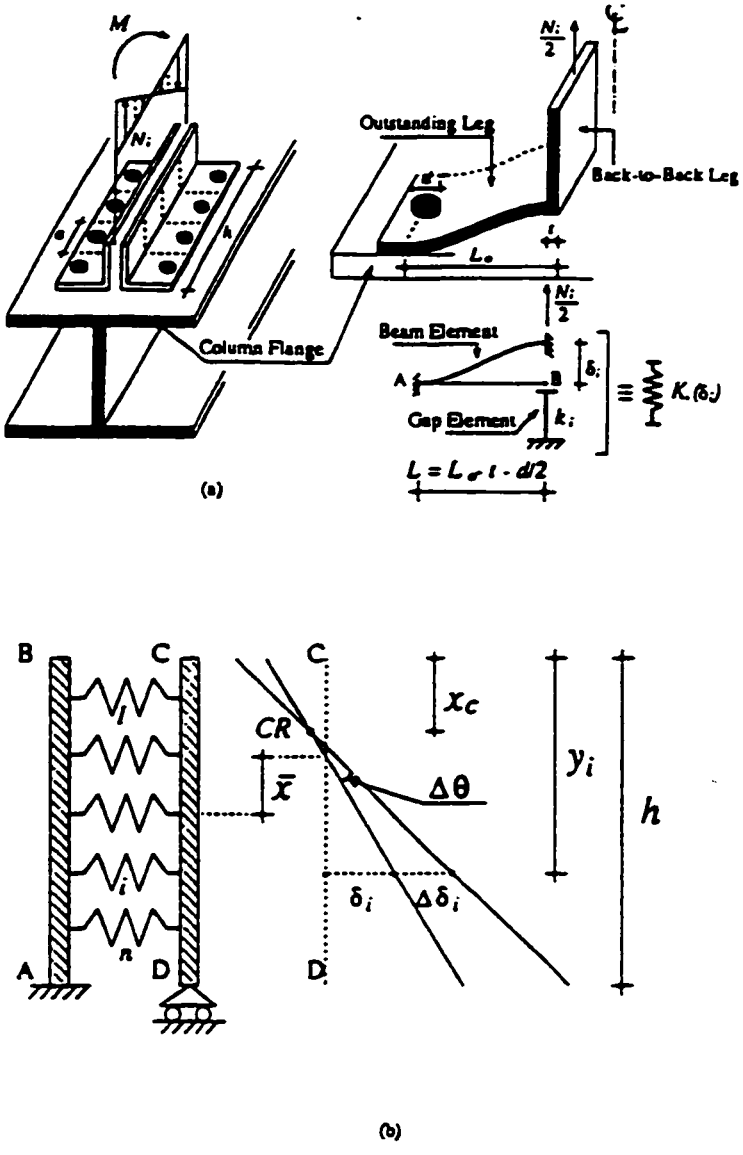

Figure 2.3 Web angle model developed by De Stephano et al., 1994
a)Definition of the geometrical properties of the model of web angle connection.
b)Model and numerical procedure for simulation of nonlinear response.

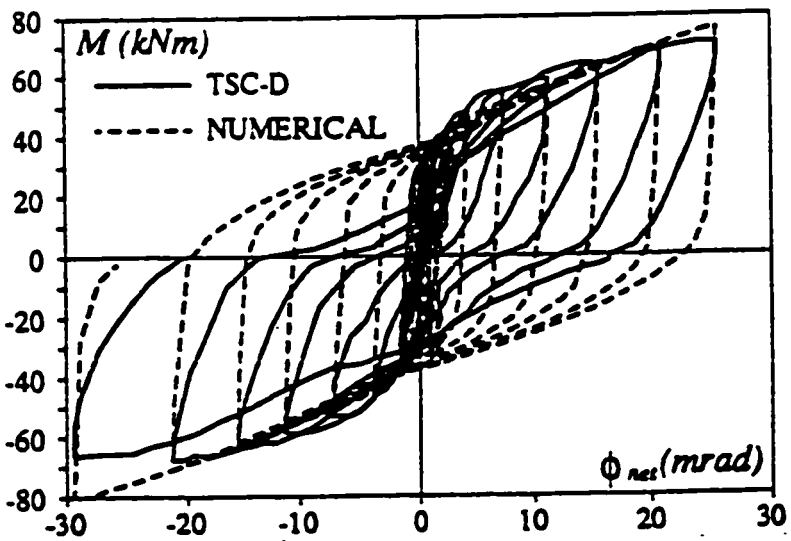

Figure 2.4 Comparison between experimental and numerical response of top and seat angle connection (De Luca, 1995)

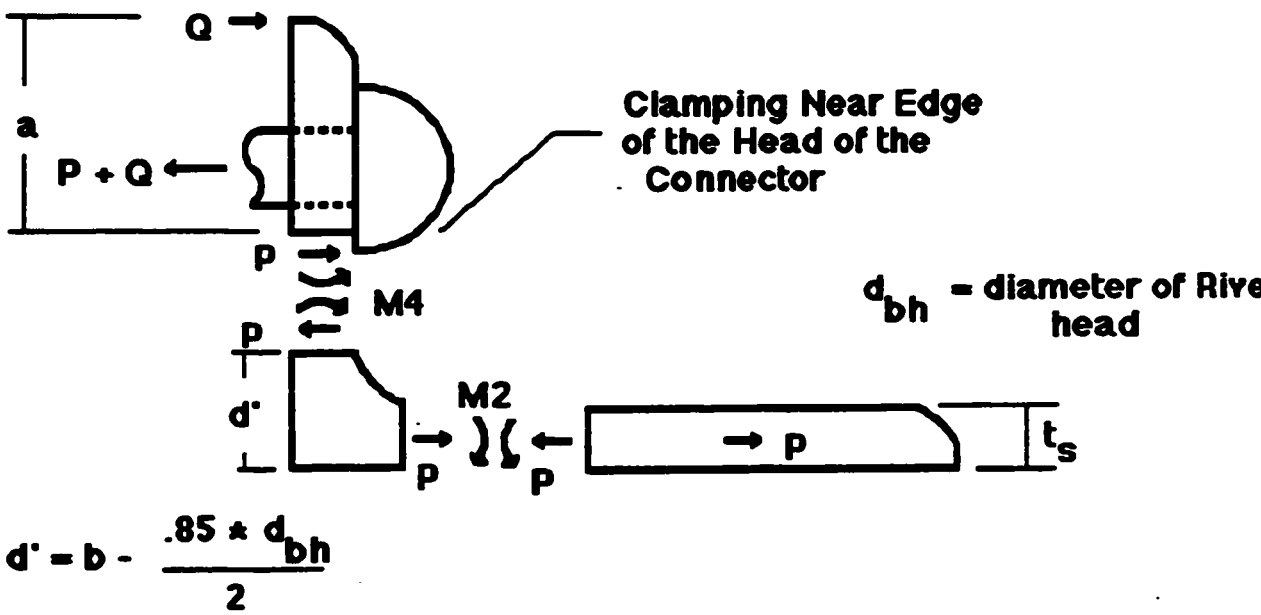

Figure 2.5 Local equilibrium for bending and prying in a clip angle connection (Roeder et al., 1994)

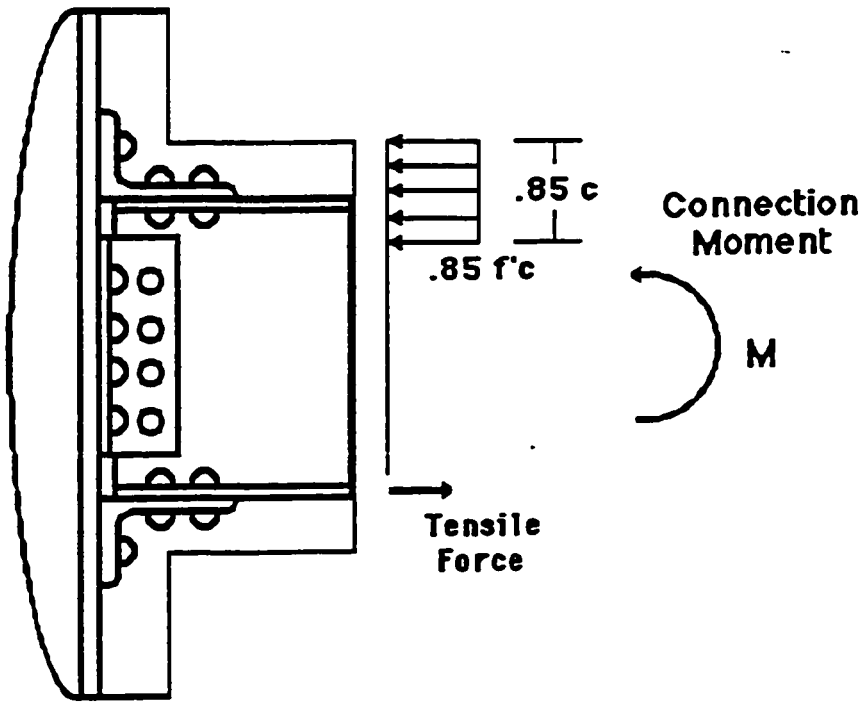

Figure 2.6 Effect of composite action on connection behaviour excluding web (Roeder et al. 1994)

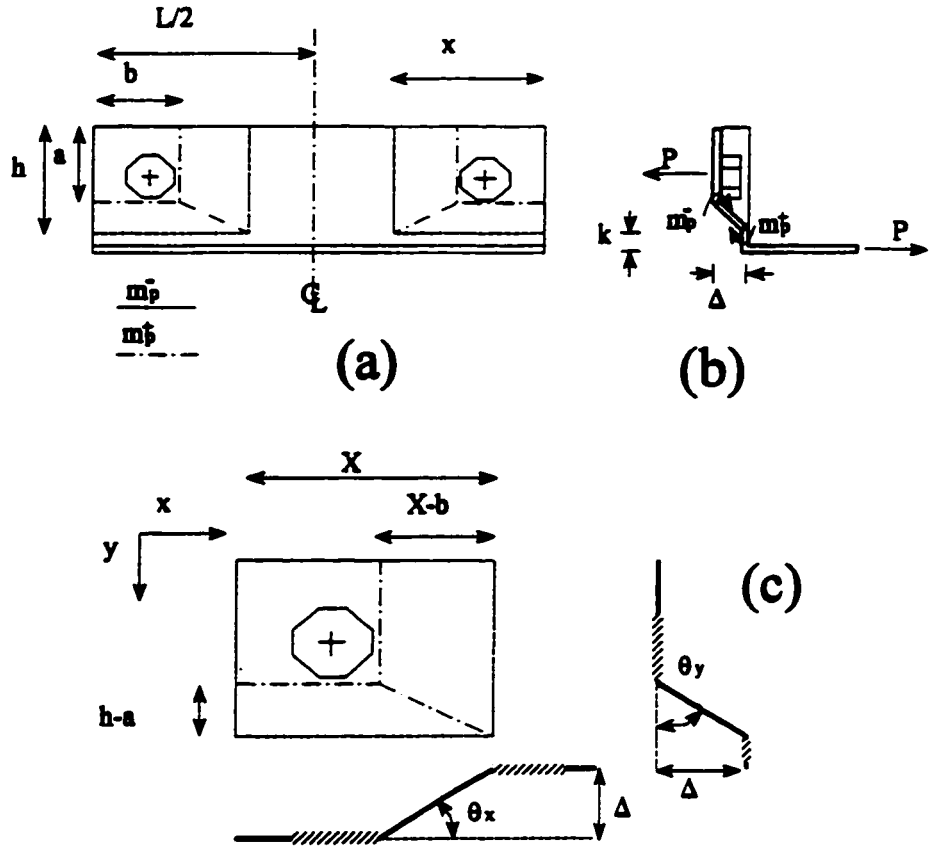

Figure 2.7 Plastic yield mechanism of top angle developed by Bruneau and Sarraf (1996)
a) Proposed yield-line pattern. b) Virtual displacement and external load P.
c) Definition for angles of rotations, θ_x and θ_y.

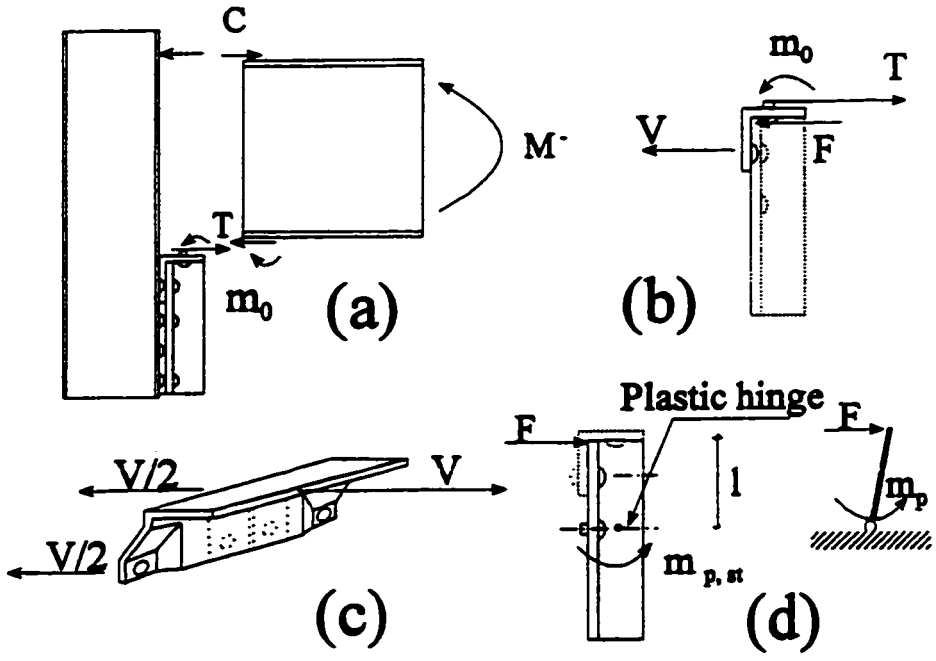

Figure 2.8 Analytical model of connection at ultimate developed by Bruneau and Sarraf (1996).
a) Free-body diagram of beam end under ultimate negative moment.
b) Free-body diagram of seat angle assembly. c) Seat angle plastic mechanism.
d) Free body diagram of stiffener angles assembly.

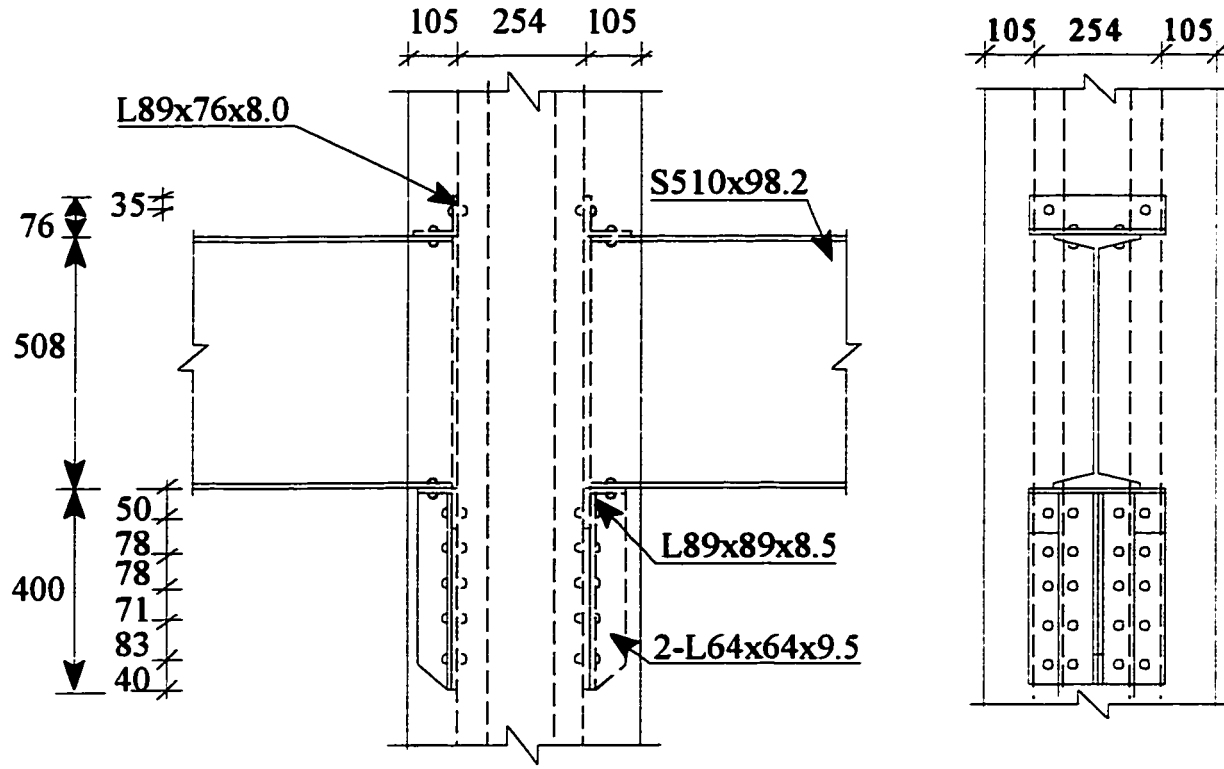

Figure 3.1 Typical connection detail

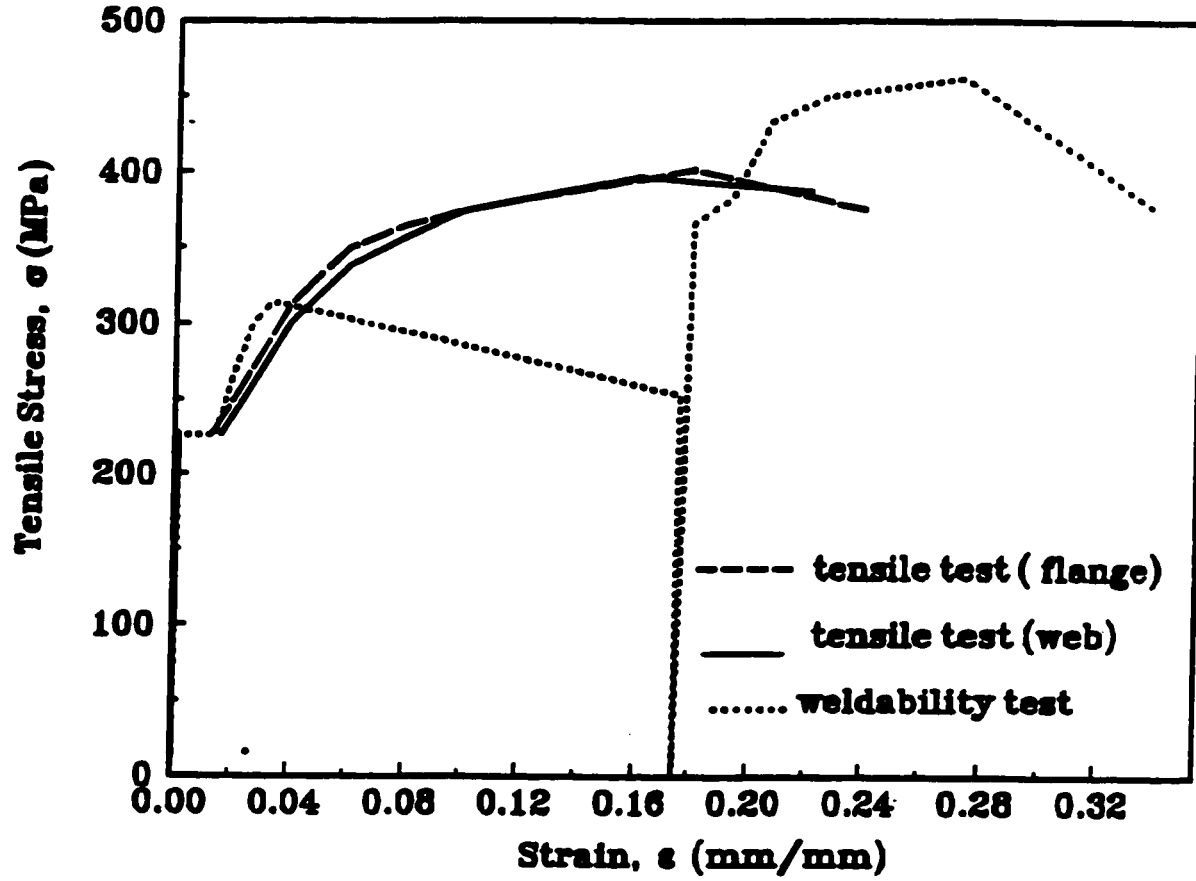

Figure 3.2 Stress-strain relationship for existing steel, as seen in Bruneau and Sarraf (1996)

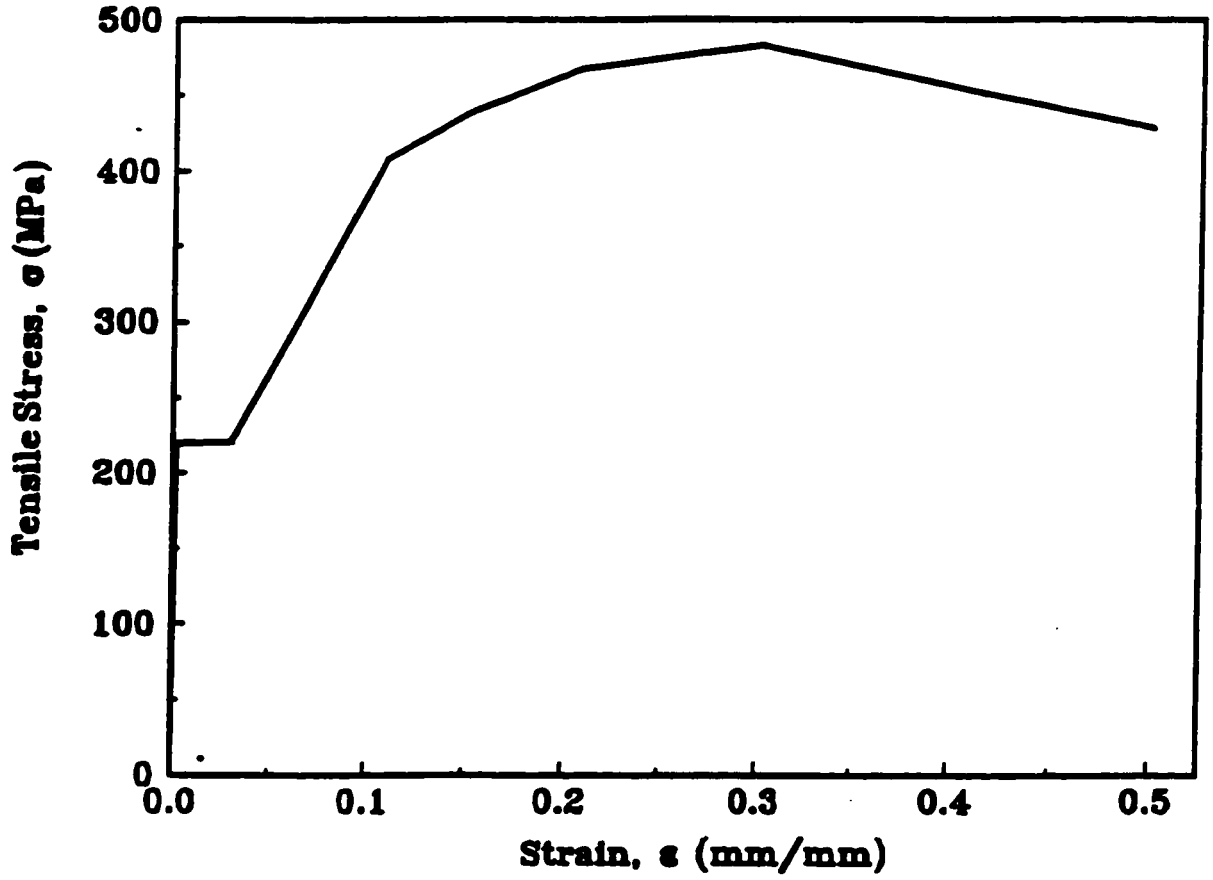

Figure 3.3 Stress-strain relationship obtained from tensile test of rivet of 3/4" diameter, as seen in Bruneau and Sarraf (1996).

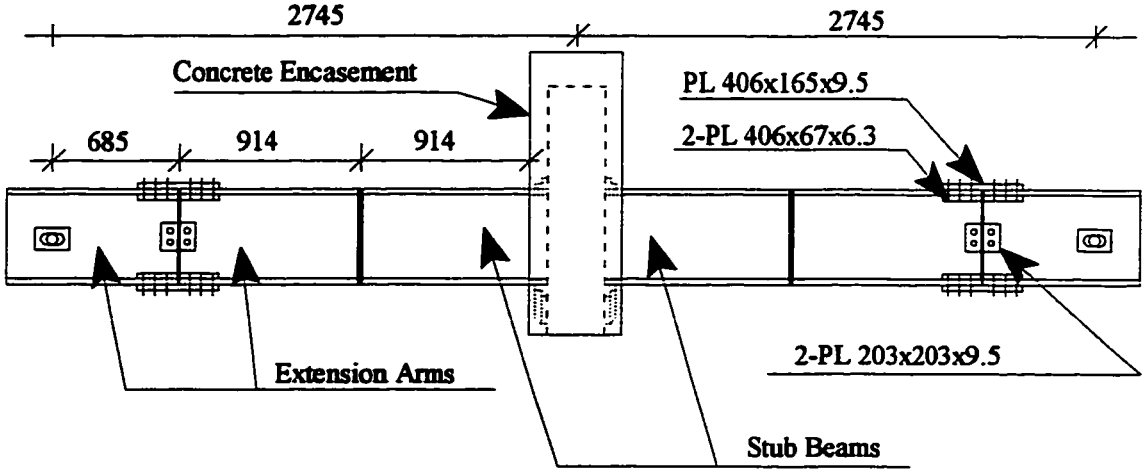

Figure 3.4 Typical specimen showing existing stub beams, additional extention arms and splice locations.

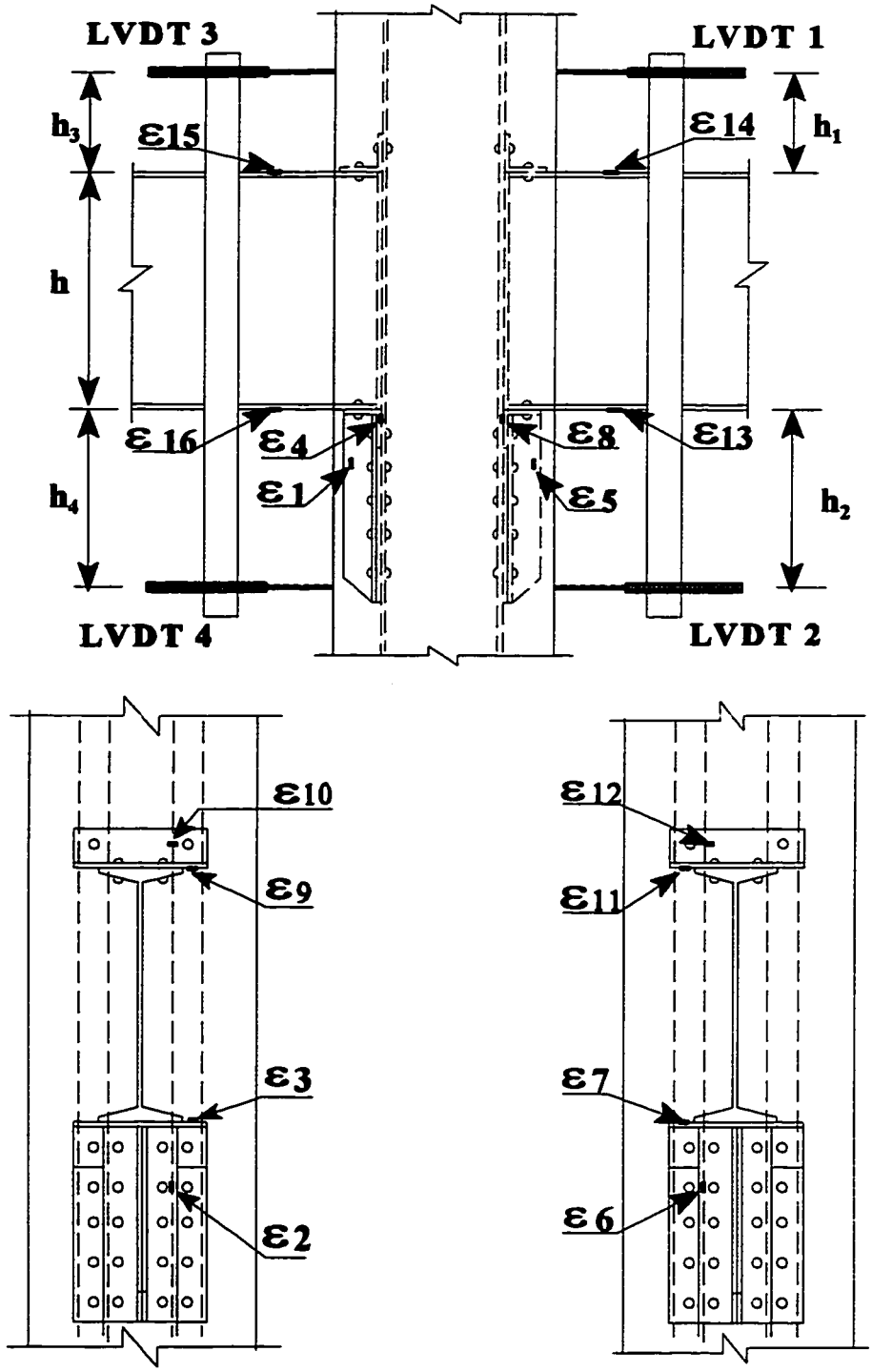

Figure 3.5 Instrumentations in specimen 1

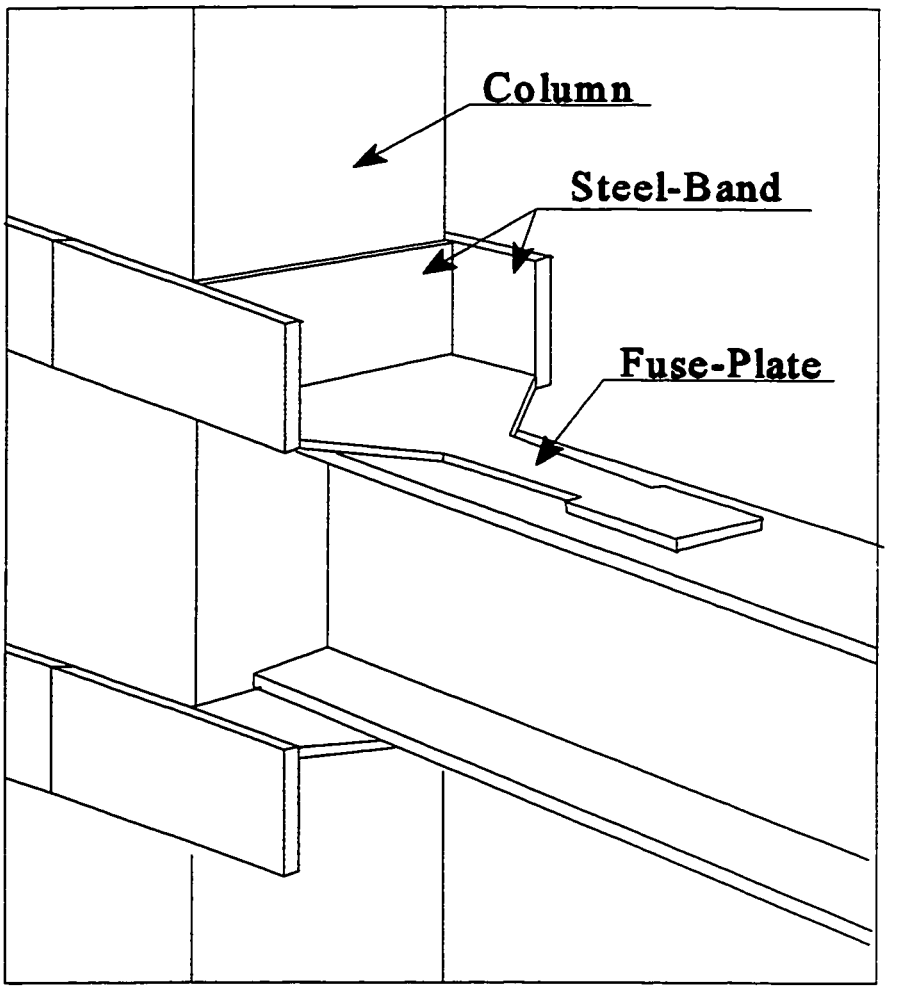

Figure 3.6 Steel-band fuse-plate retrofit tested for specimen 2

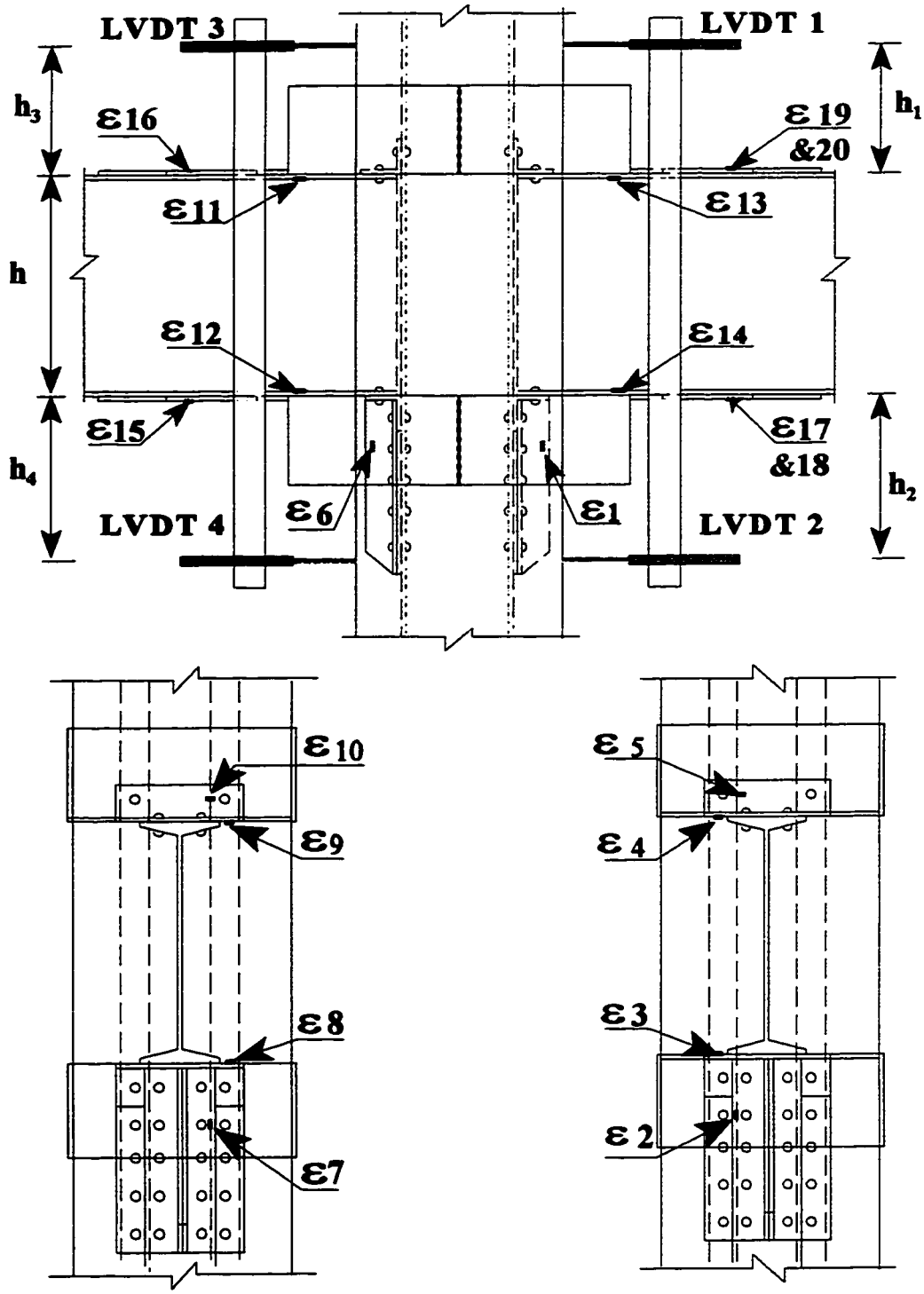

Figure 3.7 Instrumentations in specimen 2

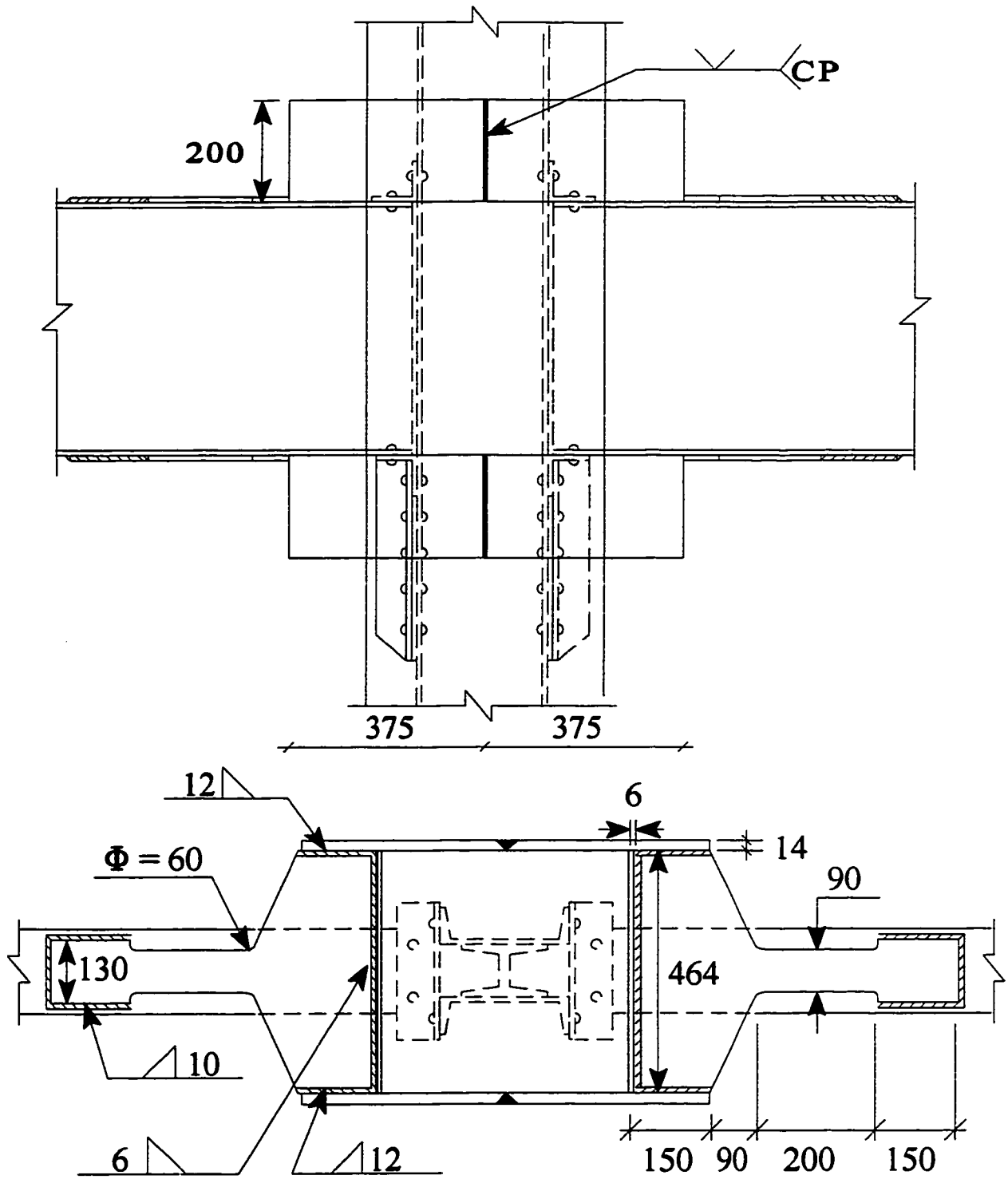

Figure 3.8 Steel band and fuse plate detail

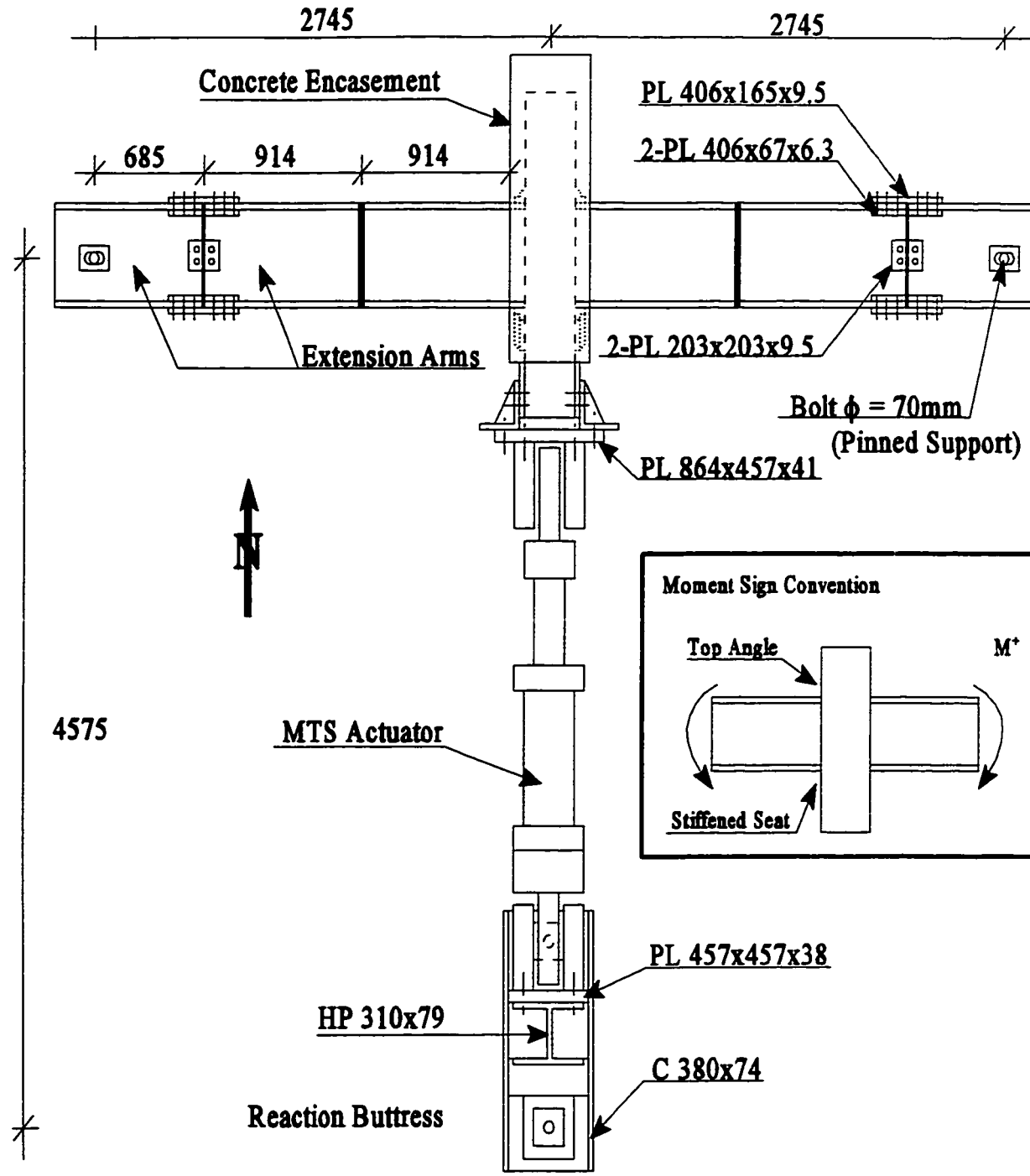

Figure 3.9 Test set-up (plan view)

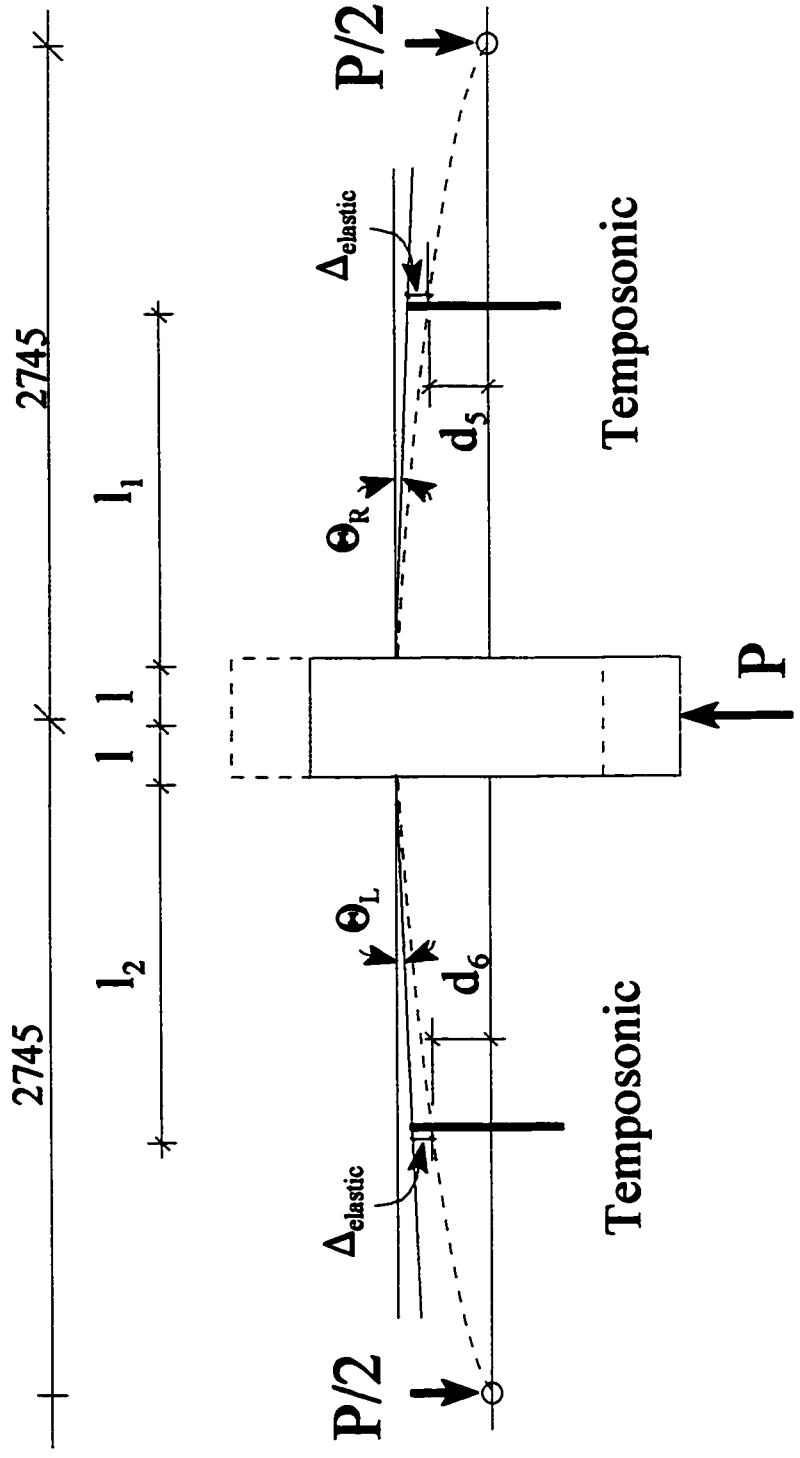

Figure 3.10 Temposonic locations and parameters used to calculate connection rotations as per equations 3.3 and 3.4.

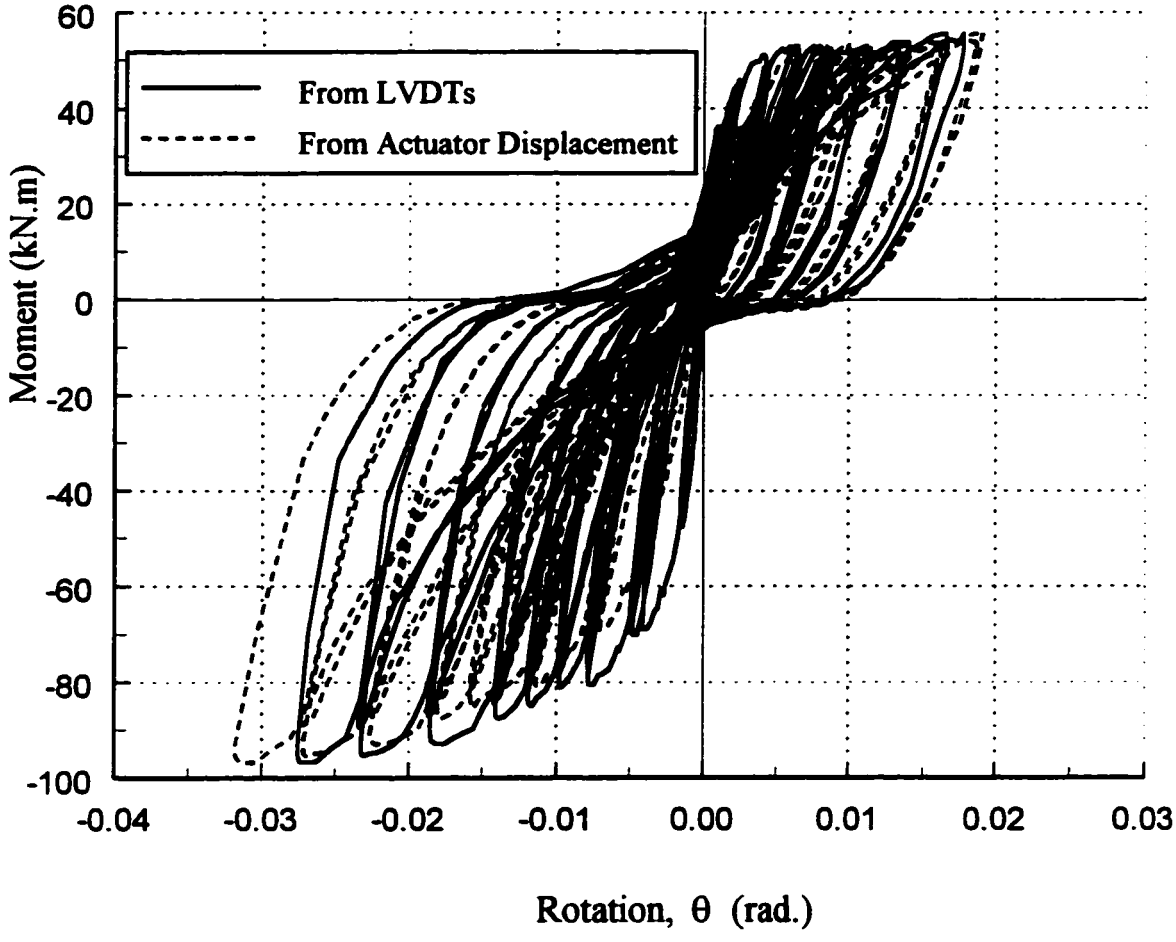

Figure 4.1 Comparison between rotations calculated using LVDTs and Actuator Displacement (to point where LVDTs were removed), specimen 1.

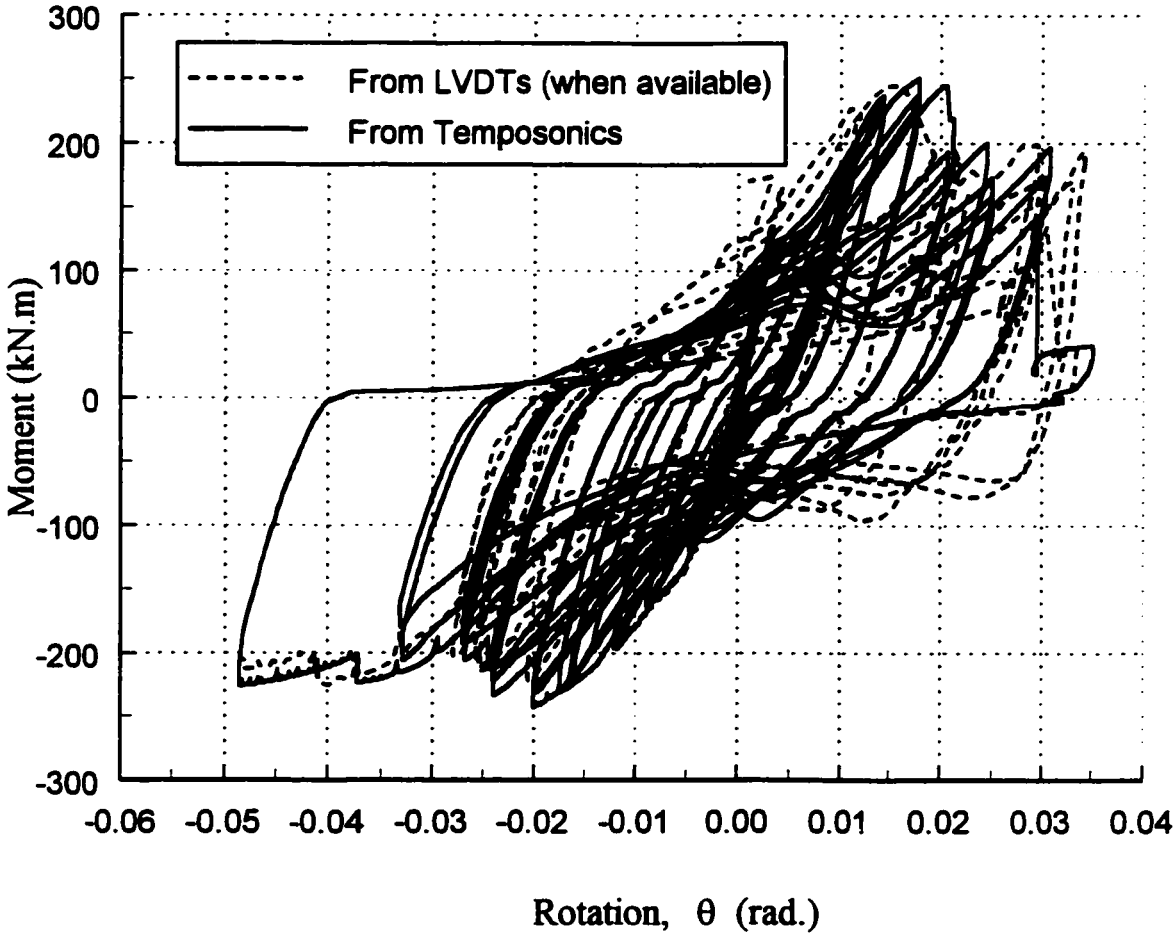

Figure 4.2 Comparison between LVDT and Temposonic data after correction, specimen 2.

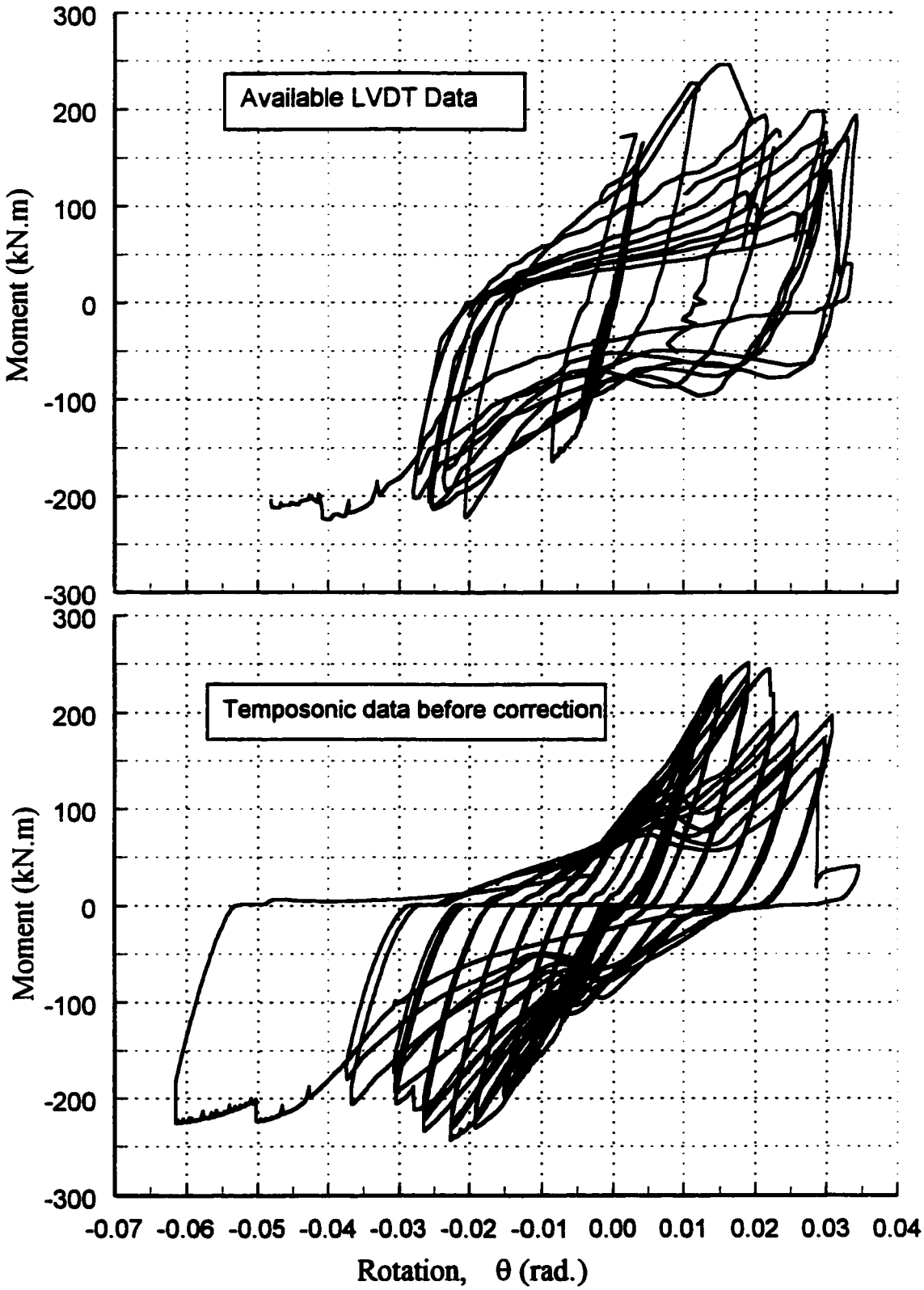

Figure 4.3 Comparison betwen LVDT & Temposonic data before slip removal, specimen 2.

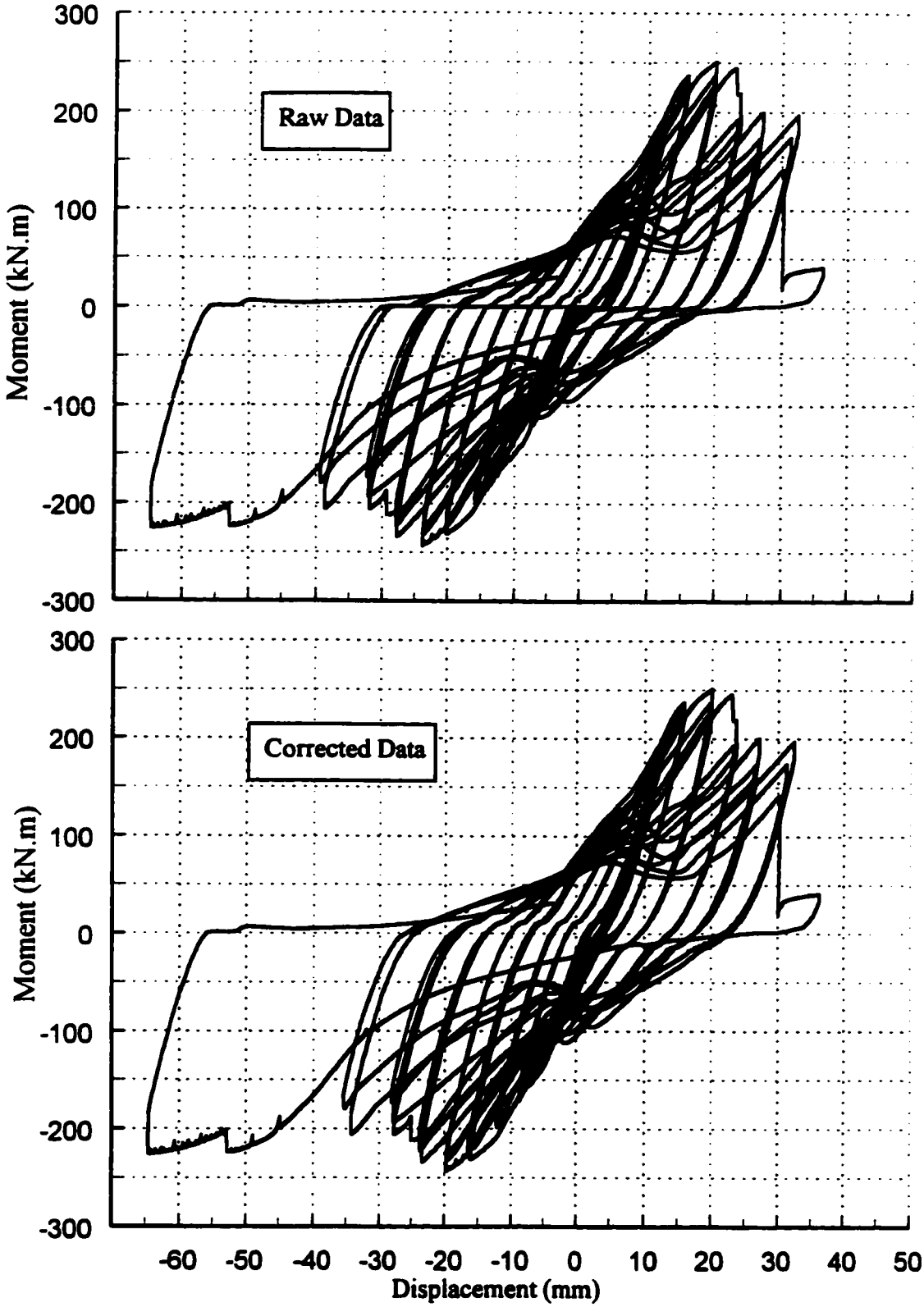

Figure 4.4 Comparison betwen raw dataset and corrected dataset

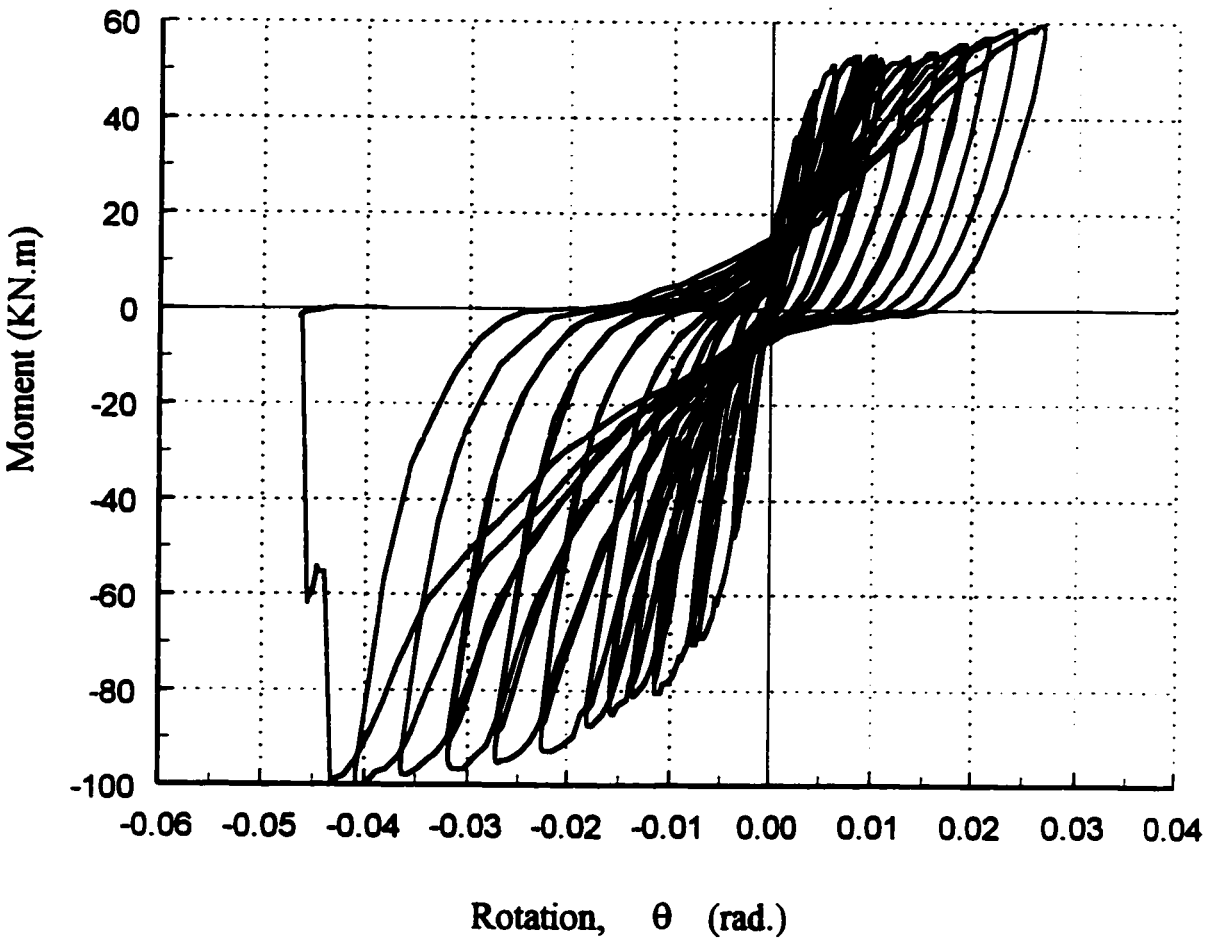

Figure 4.5 Moment-Rotation relationship for specimen 1, complete test (all cycles)

Figure 4.6 Hairline cracking of specimen 1.

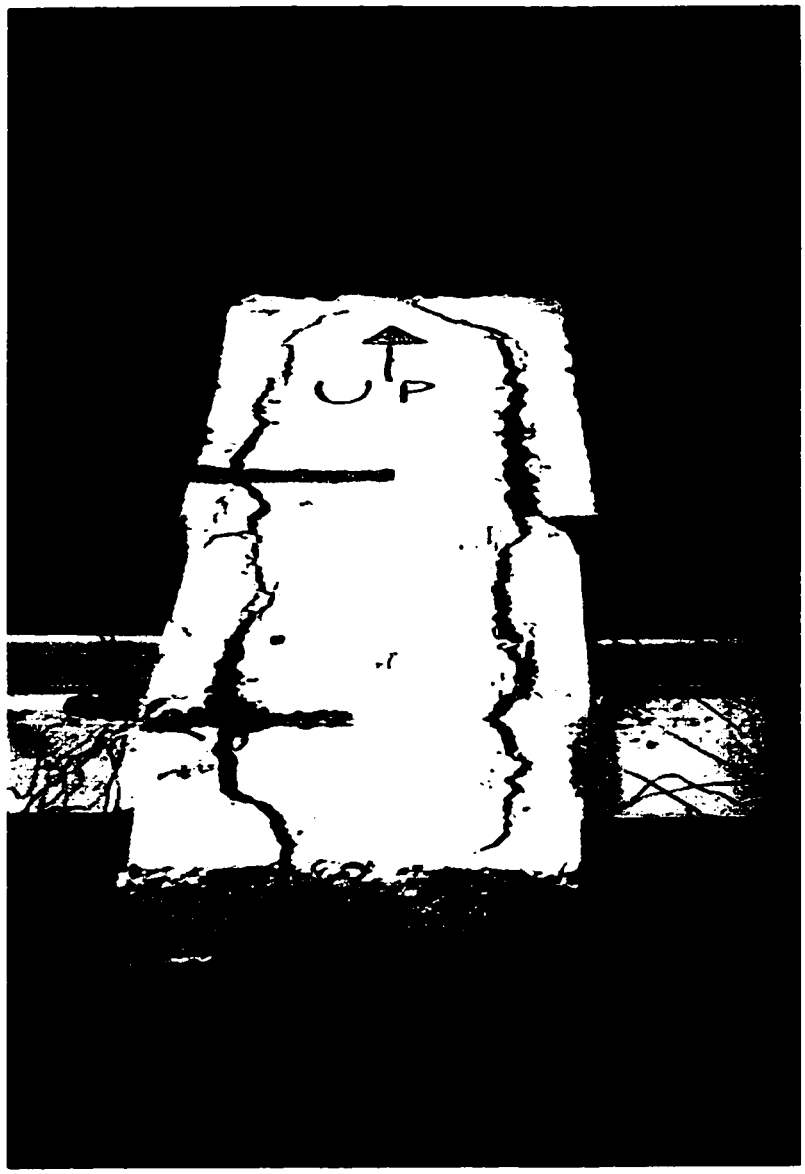

Figure 4.7 Severe concrete damage and large crack openings, specimen 1.

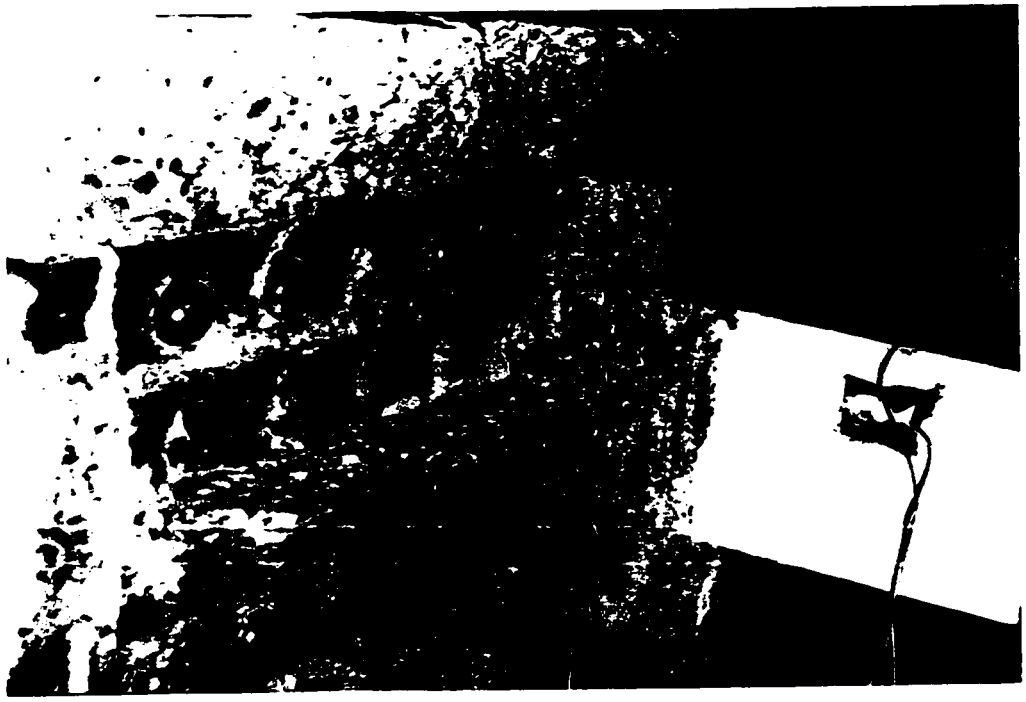

Figure 4.8 Shear failure of rivets connecting East beam to stiffened seat angle. View looking North at beam underside and South-East stiffened seat angle.

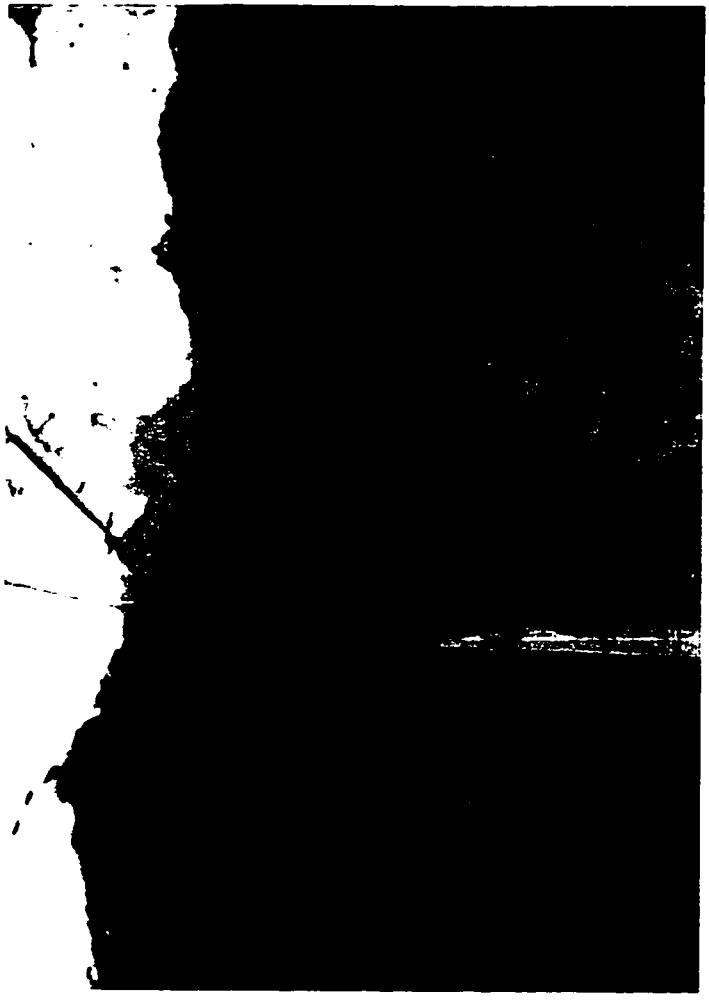

Figure 4.9 Shear failure of rivets connecting East beam to stiffened seat angle. View of South-East stiffened seat.

Figure 4.10 Separation of back of top angle from column face. View of North-West angle, looking North.

Figure 4.11 Separation of back of top angle from column face. View of North-East angle, looking North.

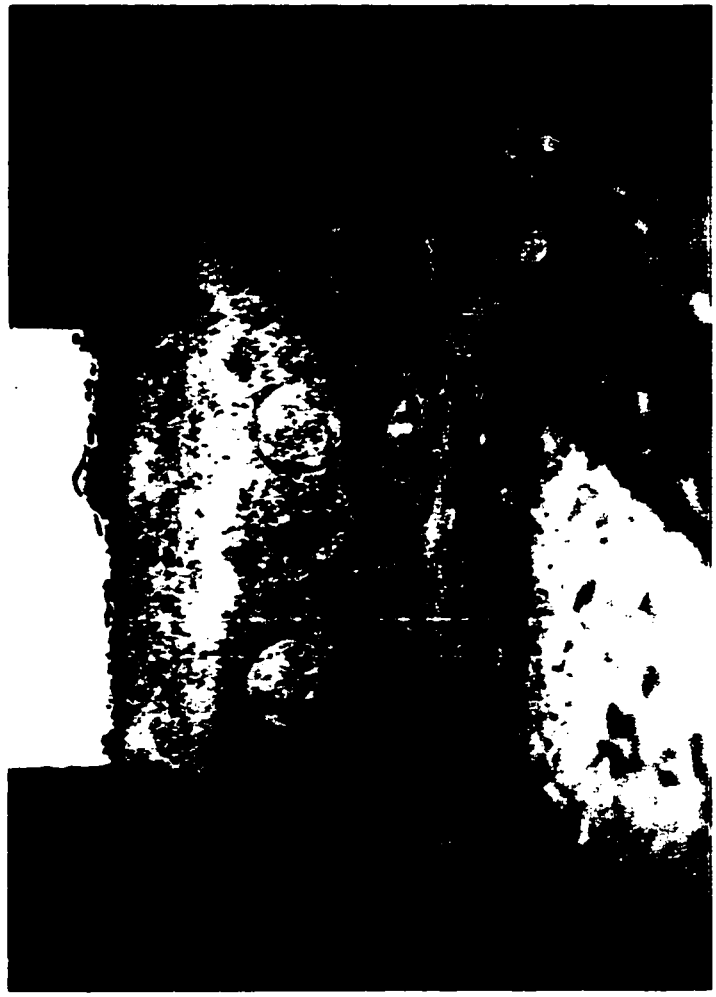

Figure 4.12 Yield lines of hinge mechanism in top angle. View of North-East angle, looking South.

Figure 4.13 Yield lines of hinge mechanism in top angle. View of North-West angle, looking South.

Figure 4.14 Elongation of rivets in vertical leg of North-East top angle.

Figure 4.15 Residual deformation of South-West seat angle and stiffeners.

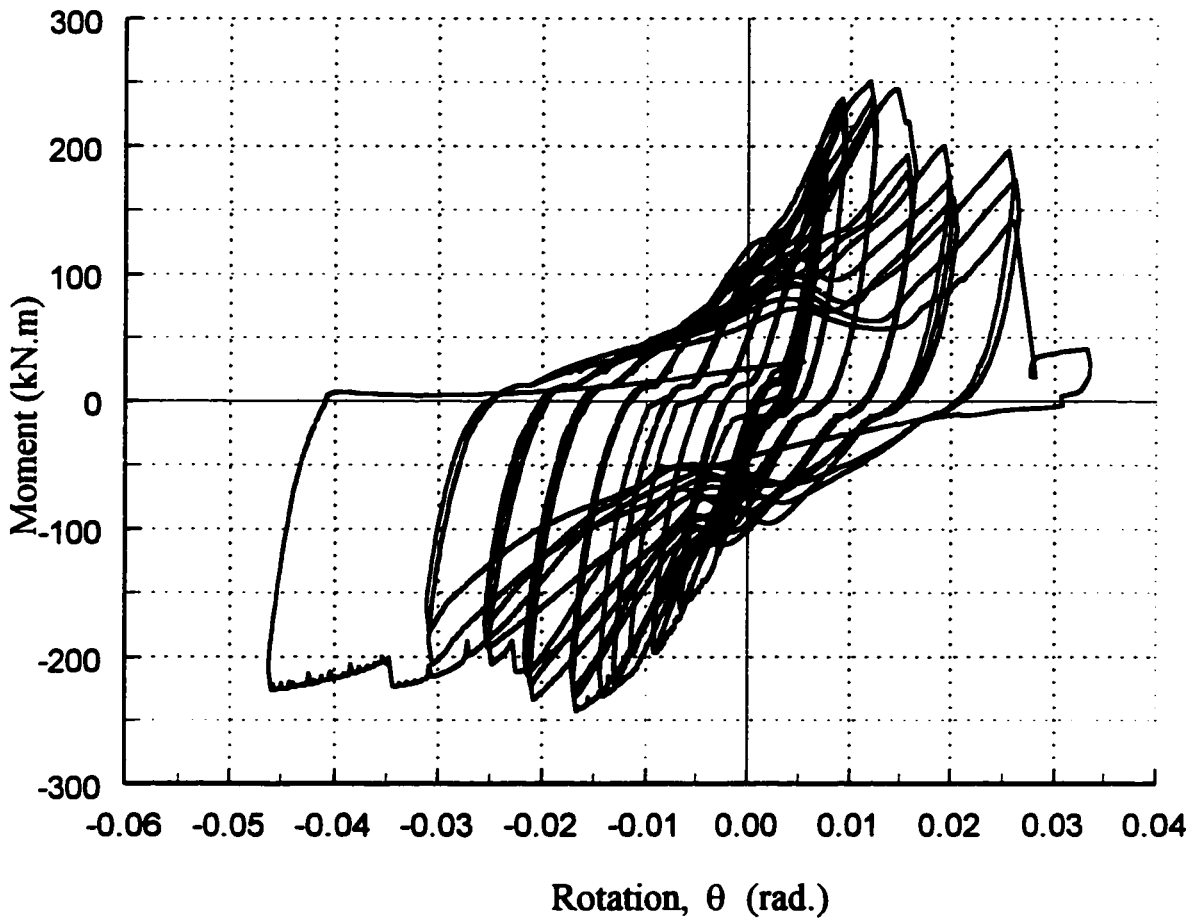

Figure 4.16 Moment-Rotation relationship based on results for the right side, specimen 2.

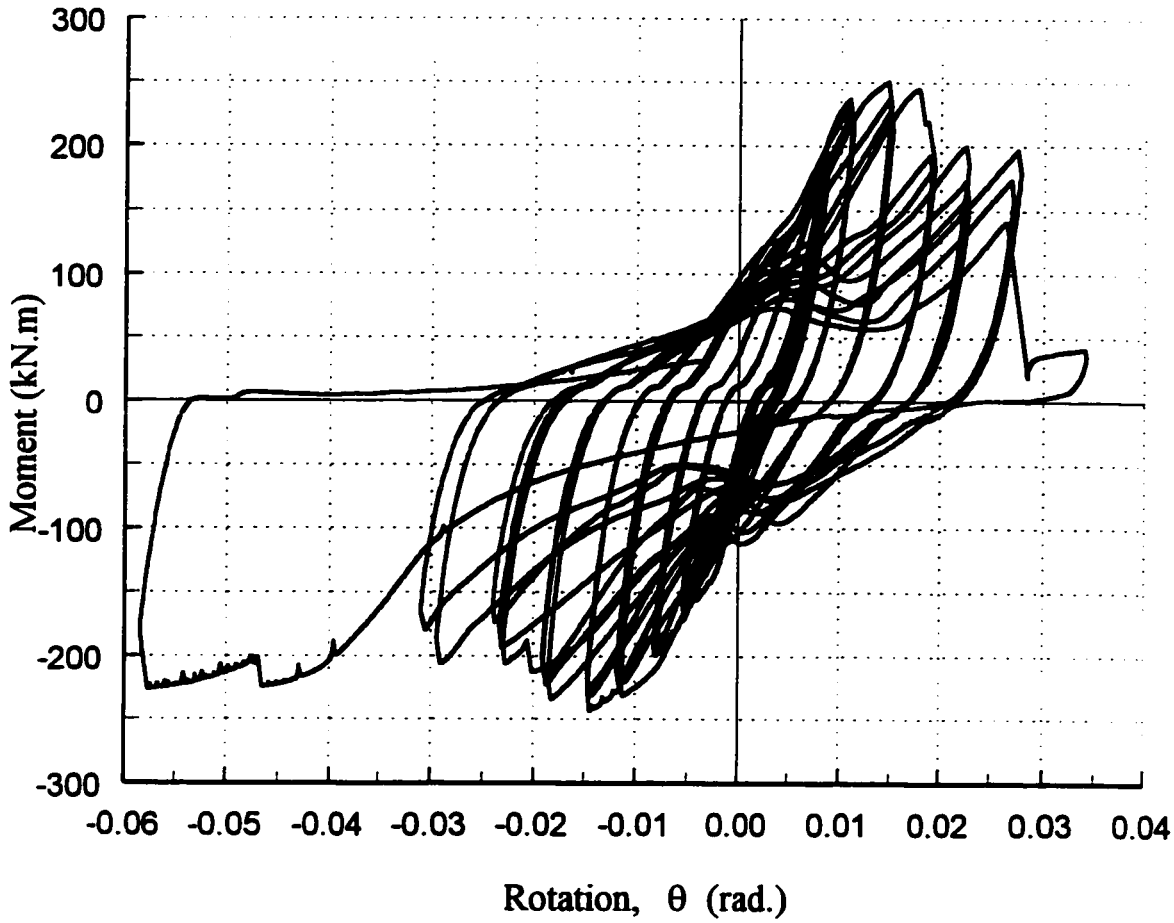

Figure 4.17 Moment-Rotation relationship based on results for the left side, specimen 2

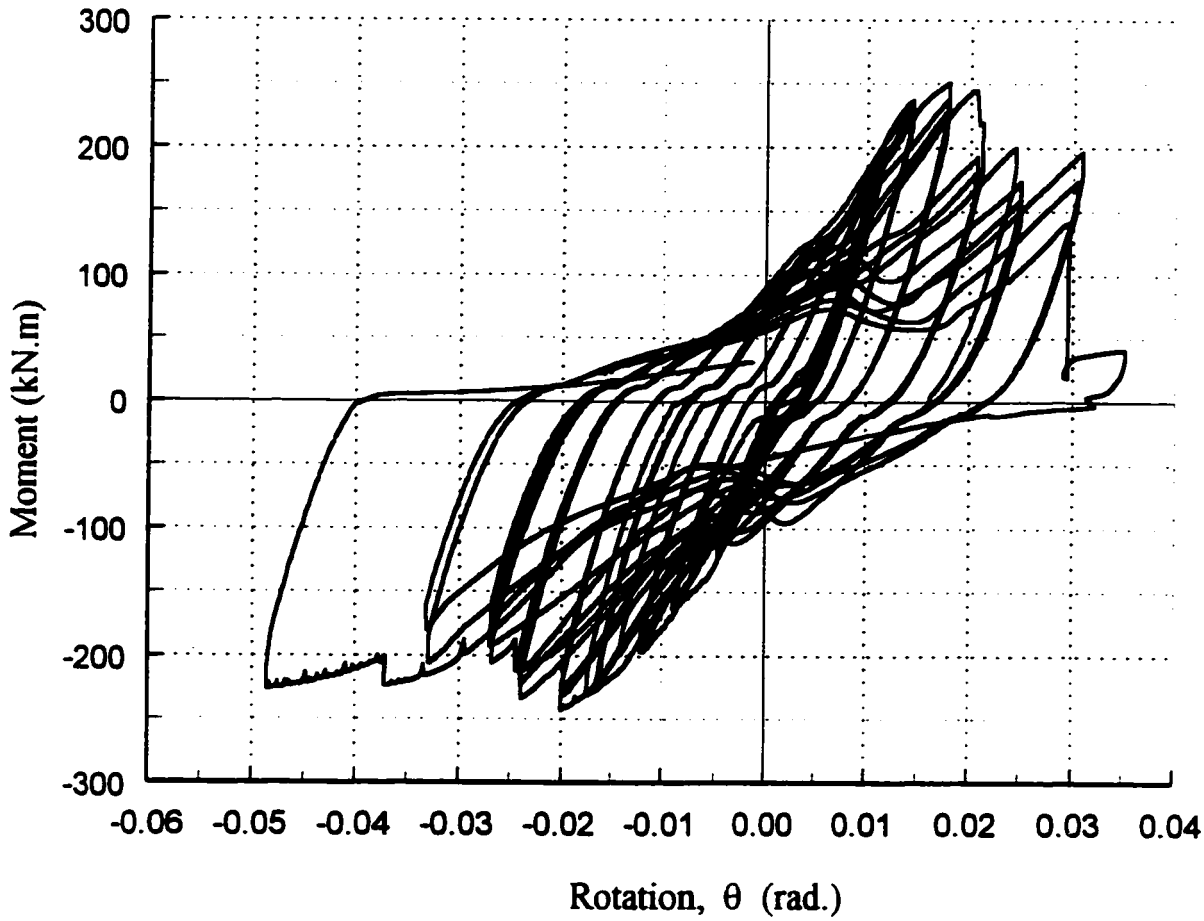

Figure 4.18 Moment-Rotation relationship based on average results for specimen 2

Cycle No.	Plate Uplift
31	2.0mm
37	3.5mm
42	5.0mm
46	7.0mm

Cycle No.	Plate Uplift
31	9.0mm
37	20.0mm
42	39.0mm
46	51.0mm

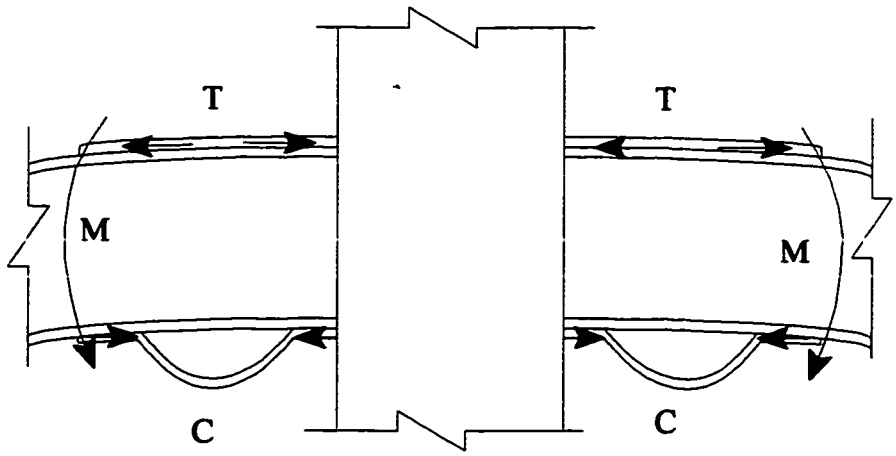

Cycle No.	Plate Uplift
31	4.0mm
37	13.0mm
42	24.0mm
46	36.0mm
48	49.0mm

Cycle No.	Plate Uplift
31	5.0mm
37	13.0mm
42	18.0mm
46	19.0mm
48	21.0mm

Figure 4.19 Uplift from the beam flange of the fuse-plates at different cycles.

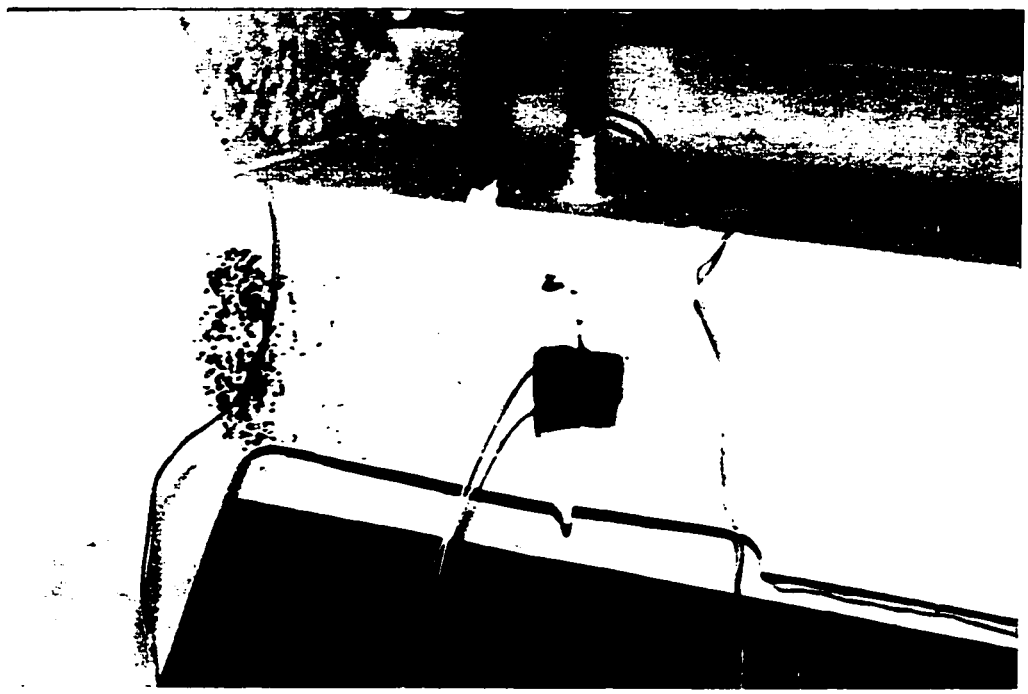

Figure 4.20 Yielding of fuse-plate shown by cracks in white paint of North-East fuse-plate.

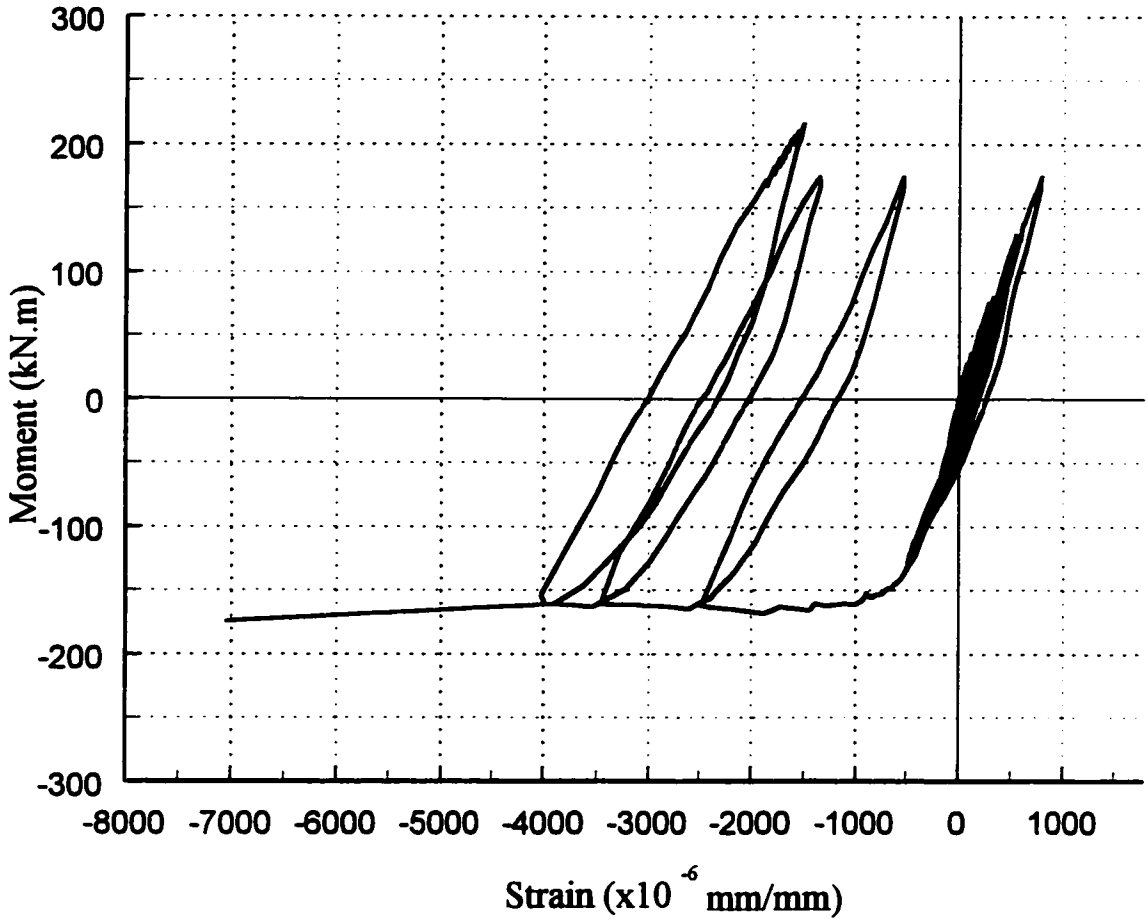

Figure 4.21 Moment-strain relationship for strain gage 17, specimen 2 (limited data recorded prior to gage failure)

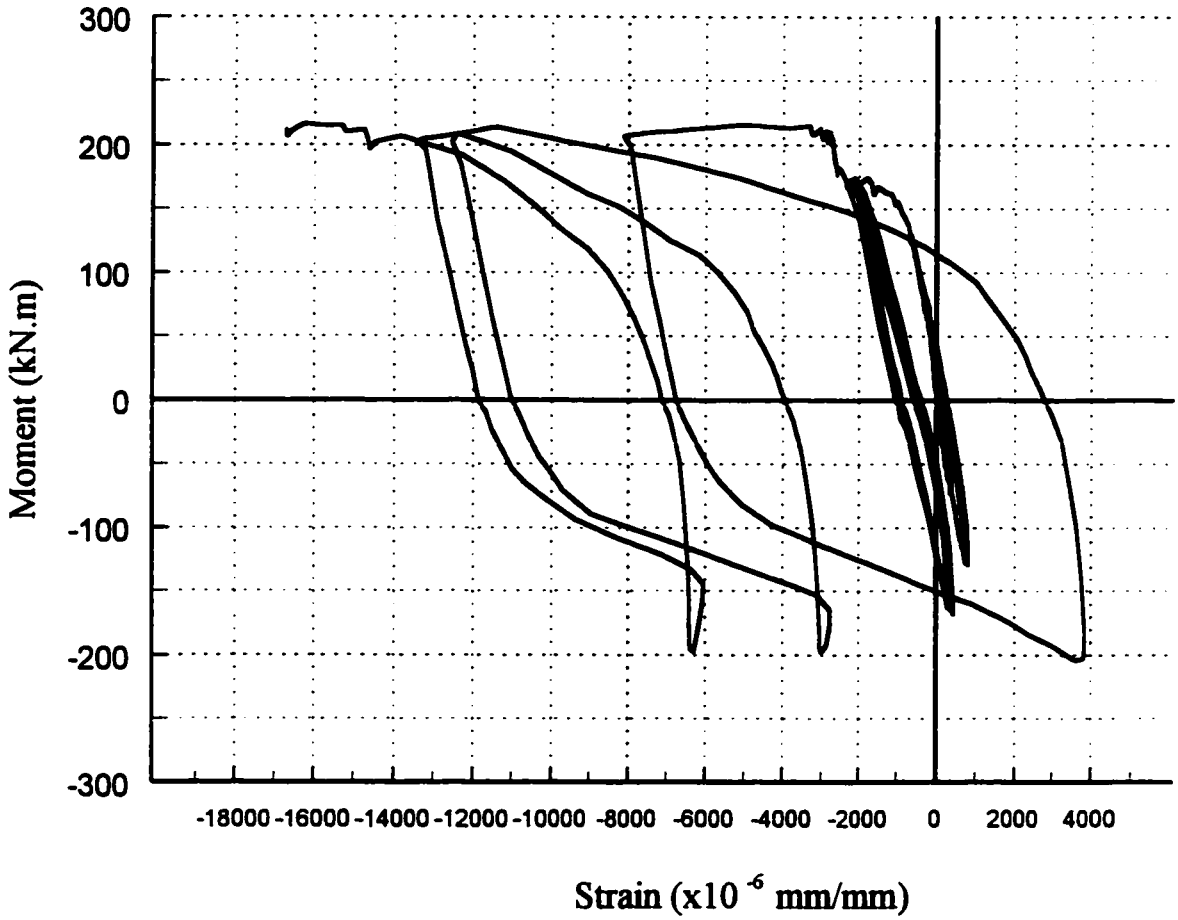

Figure 4.22 Moment-strain relationship for gage 20, specimen 2 (limited data recorded prior to gage failure)

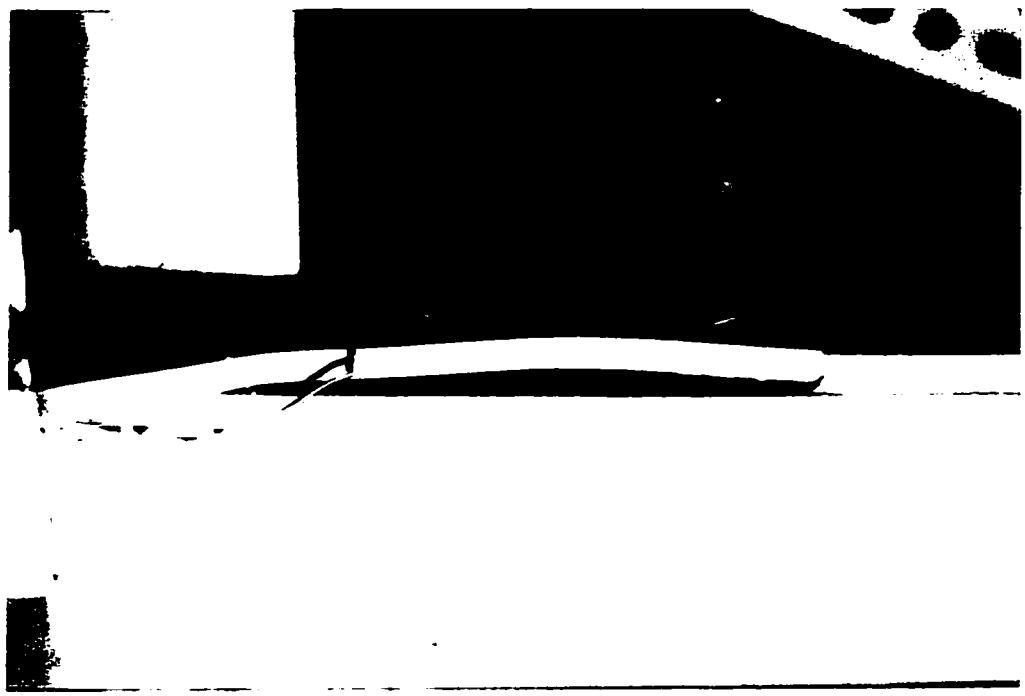

Figure 4.23 Typical buckling of South fuse-plate.

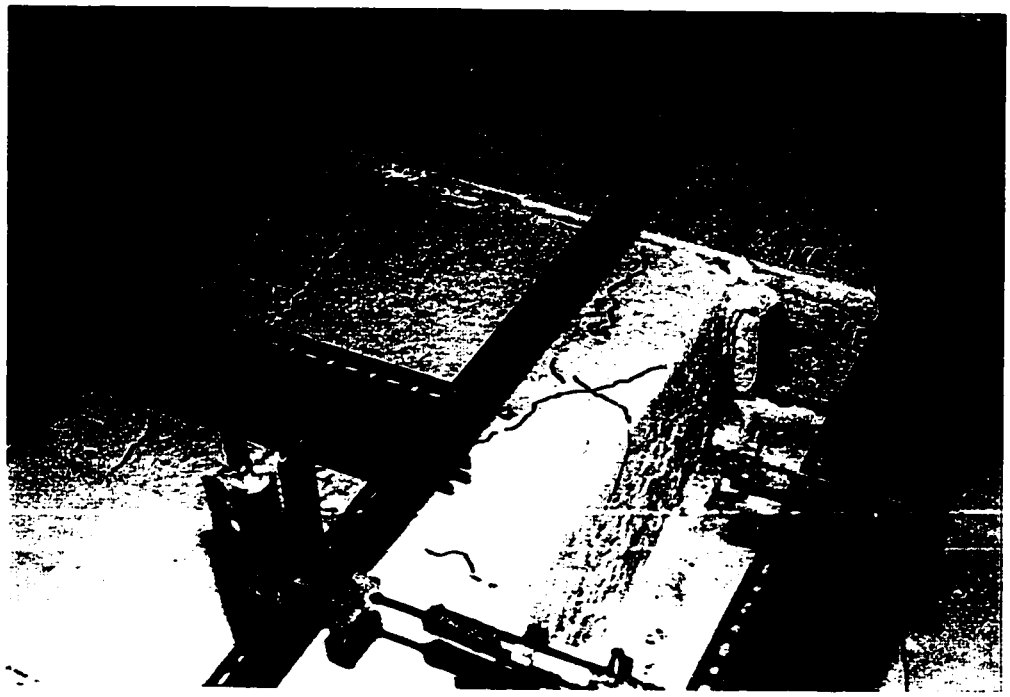

Figure 4.24 Formation of hairline cracks in specimen 2, highlighted by felt tip marker.

Figure 4.25 Buckling of North-East fuse-plate (approx. 20mm), specimen 2.

Figure 4.26 Sliding of East beam through concrete causing local spalling.

Figure 4.27 Sliding of East beam indicated by paint marks.

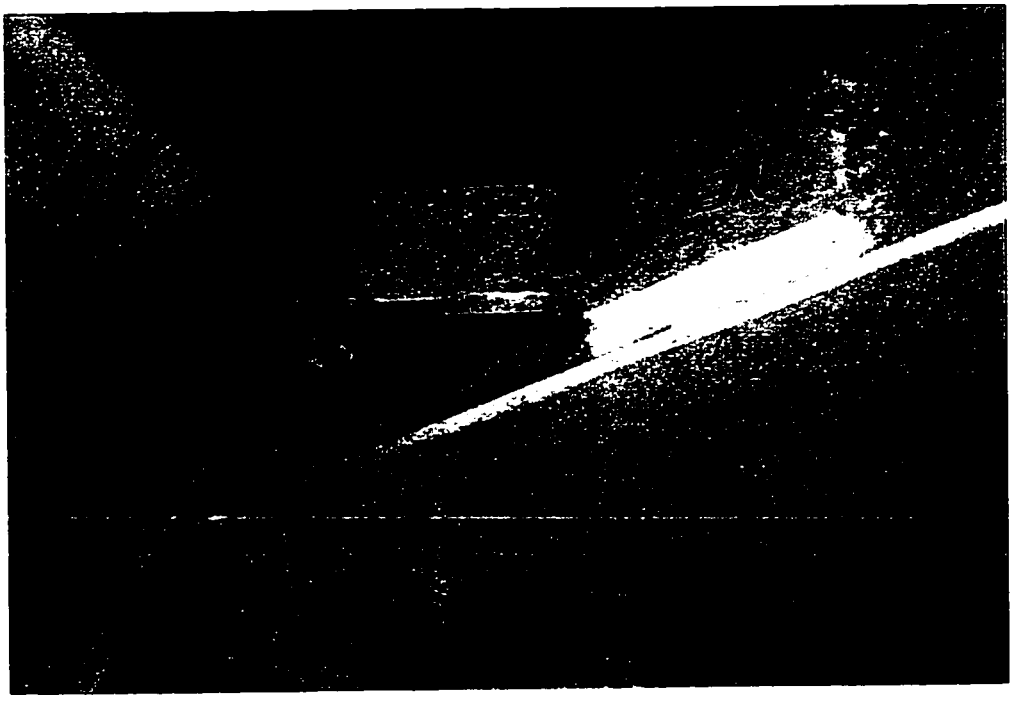

Figure 4.28 Maximum buckling deformation of North-East fuse-plate.

Figure 4.29 Maximum buckling deformation of South-West fuse-plate.

Figure 4.30 Gross area tensile failure of North-East fuse-plate.

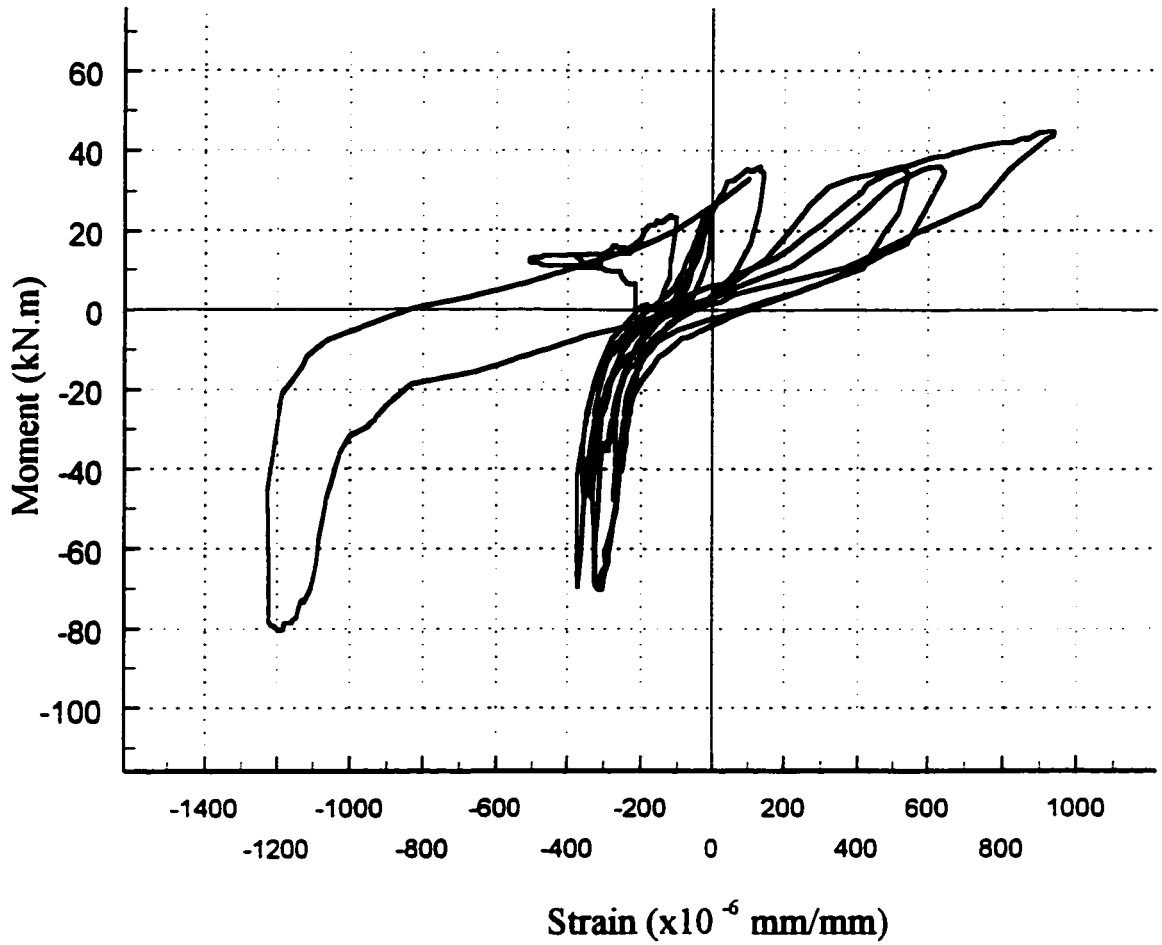

Figure 5.1 Moment-strain relationship for strain gage 9, specimen 1 (limited data recorded prior to gage failure)

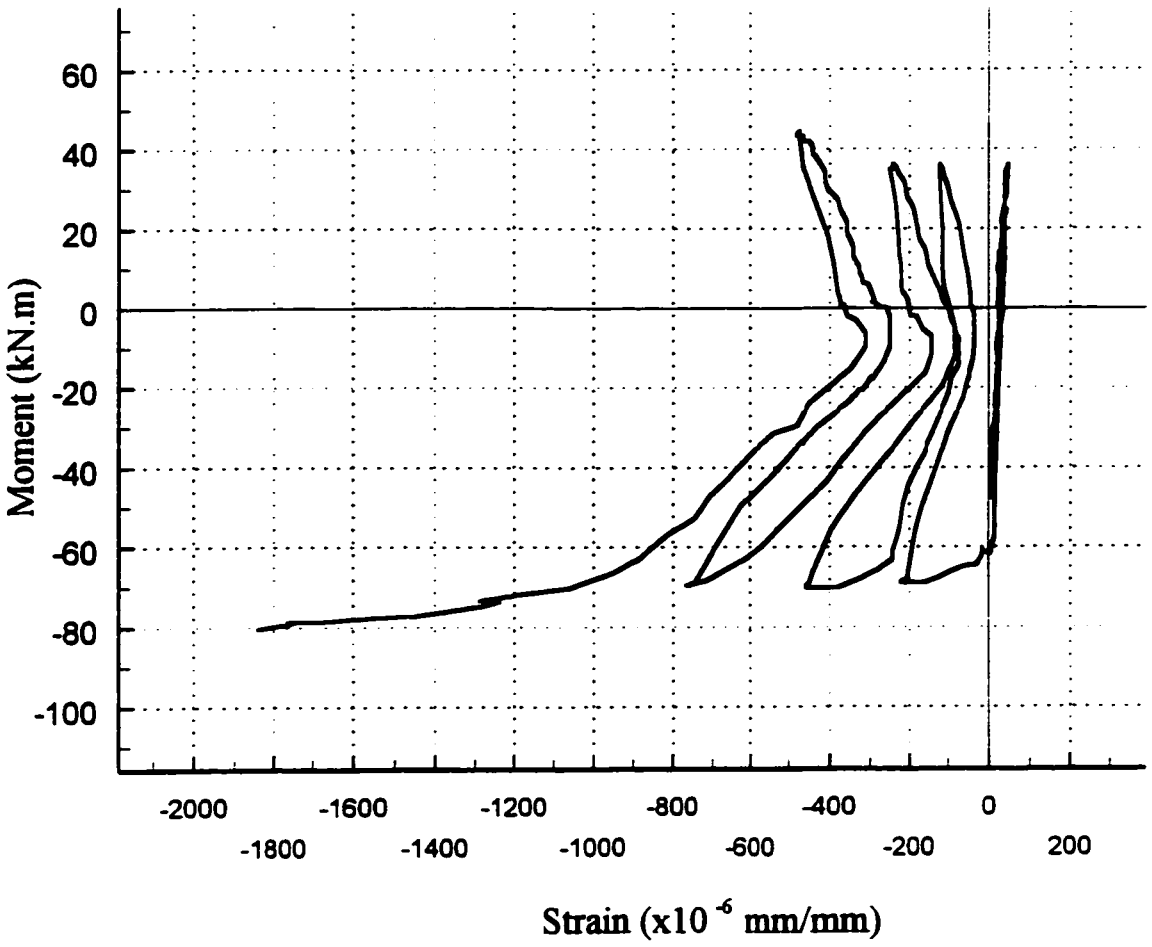

Figure 5.2 Moment-strain relationship for gage 2, specimen 1 (limited data recorded prior to gage failure)

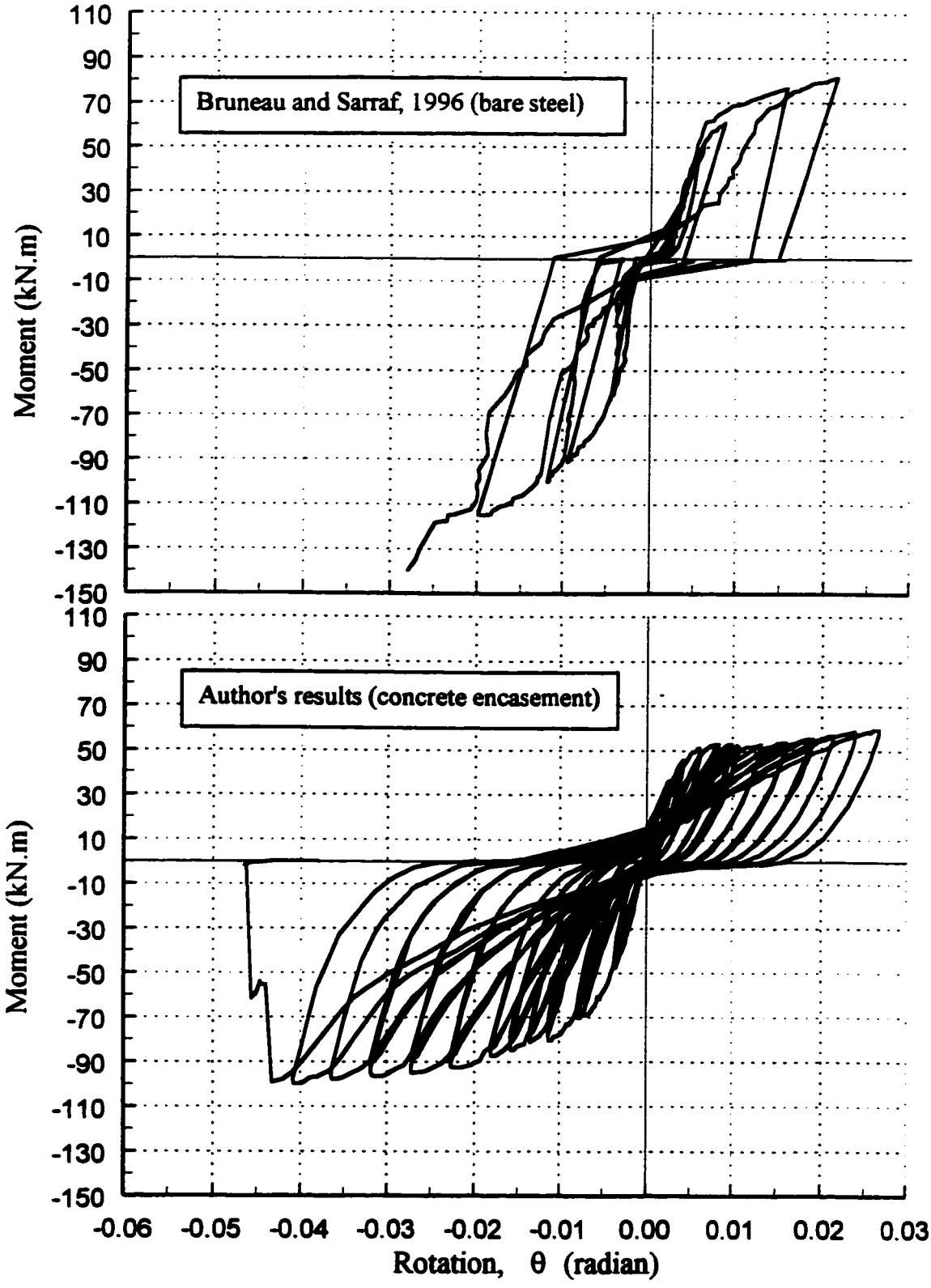

Figure 5.3 Comparison between results obtained by Bruneau and Sarraf (1996) for a bare steel specimen, and resutls obtained in this investigation for an encased specimen.

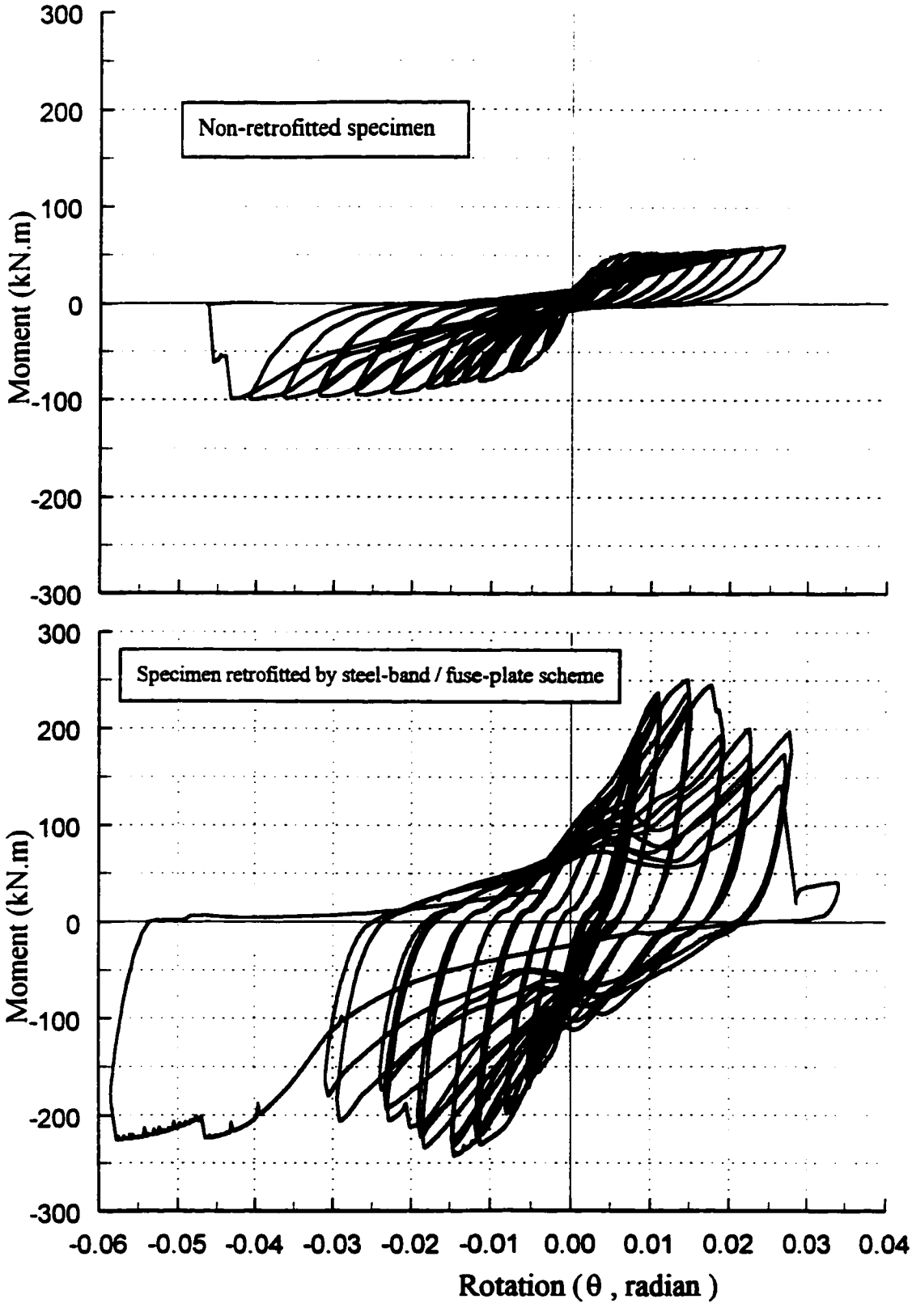

Figure 5.4 Comparison of non-retrofitted and retrofitted specimens

Appendix A

Prediction of Moment Capacities

A.1 Prediction of the positive moment capacity

A.1.1 Failure Mode 1: Top rivets tensile yielding

According to Kulak et al., the prying action in an angle can be evaluated according to Fig. a.1,

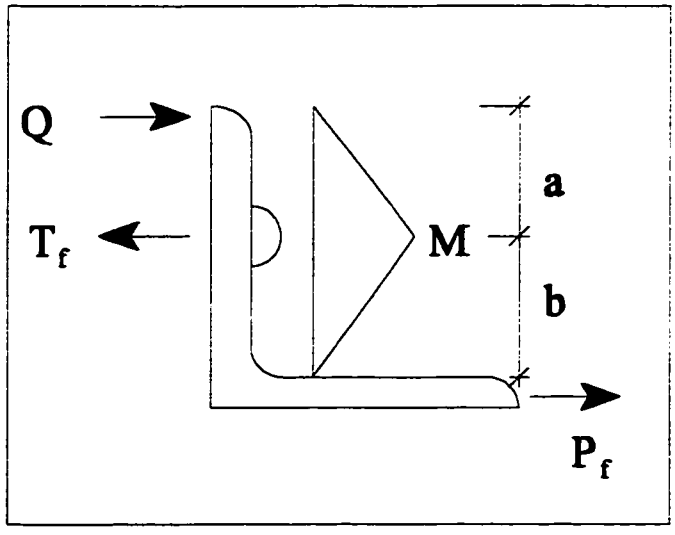

Figure a.1

Where:

$Q/P_f = b/a$, or $Q = P_f \times b/a$

and for this case,

a = 35mm

b = 30mm

Therefore, $Q = 0.857\ P_f$

Also, $T_f = Q + P_f$

or, $T_f = 1.857\ P_f$

T_f is the tensile resistance of 2 rivets,

$T_f = 2 \times A_{riv.} \times F_{y\ riv.}$ **(1)**

and, $F_{y\ riv.} = 258$ Mpa

Therefore, $T_f = 147.1$ kN and $P_f = 79.2$ kN

The moment applied to the connection becomes,

$M = 0.508 \times P_f = 40.2$ kN•m

A.1.2 Failure Mode 2: Formation of hinge mechanism in top angle

The model of a wide angle developed by Saraff and Bruneau (1996) is applied here.

$$x = b + \sqrt{h^2 - ha} \qquad \textbf{(2)}$$

Where:

b = 47.6mm, h = 63.0mm, and a = 50.8mm

Therefore, x = 75.3mm

Now,

$$P = t^2 F_y \times \left[\frac{h}{(x - b)} + \frac{x}{(h-a)}\right] \qquad \textbf{(3)}$$

Where t = 8.0mm, and $F_y = 225$ Mpa

Therefore, P = 121.6 kN

and, M = 61.8 kN•m

A.1.3 Failure Mode 3: Top rivets tensile failure

Using the same model shown in Fig. a.1, but substituting $F_{u\ riv.}$ for $F_{y\ riv.}$

Where $F_{u\ riv.}$ = 400 Mpa

Substitution into **(1)** gives T_f = 275 kN and P_f = 148 kN

Therefore, M = 75.3 kN•m

A.1.4 Failure Mode 4: Rivets shear failure

Since there are 2 rivets connecting the angle leg to the beam flange,

$V_r = 2 \times A_{riv.} \times F_{v\ riv.}$

Where $A_{riv.} = 334mm^2$

The shear to tension capacity of the rivet is taken as 0.75, therefore

$F_{v\ riv.} = F_{u\ riv.} \times 0.75$ = 362 Mpa and,

V_r = 242 kN

Therefore,

$M = V_r \times h$

M = 123 kN•m

A.1.5 Failure Mode 5: Bearing failure at rivet holes

According to CAN/CSA-S16.1-M89, clause 13.10.1(c) and omitting ϕ:

$Br = 3tdnF_u$ (a)

$Br = tneF_u$ (b)

In this case, t = 8.0mm, d = 19mm, n = 2, e = 25.4mm

and Fu = 483 for (a) and 400 for (b)

Keeping in mind there are 2 rivets connecting the angle leg to the beam flange,

using (a), Br = 881 kN and using (b), Br = 325 kN

Therefore Br = 325 kN governs and

M = 165 kN•m

A.1.6 Failure Mode 6: Outstanding angle leg net section yield

$Tr = A_n \times F_y$

The angle leg net area is the gross area minus 2 rivet hole diameters.

$A_n = A_g - 2dt$

$A_n = 8.0 \times 270 - 2 \times 19 \times 8.0$

$A_n = 1856\ mm^2$

$Tr = 1856 \times 225$

$Tr = 418$ kN and,

$M = 418 \times 0.508$

$M = 212$ kN•m

A.1.7 Failure Mode 7: Outstanding angle leg gross section yield

As above, but substituting A_g for A_n

$Tr = A_g \times F_y$

$Tr = 486$ kN and

$M = 247$ kN•m

A.1.8 Failure Mode 8: Gross shear failure of top angle leg

$Tr = A_g \times F_v$

Where $F_v = 0.6\ F_u = 0.6 \times 400 = 240$ MPa

Therefore,

$Tr = 518$ kN and,

$M = 263$ kN•m

A.2 Prediction of the negative moment capacity

A.2.1 Failure mode 1: Formation of hinge mechanism in seat angle stiffeners

The model developed by Saraff and Bruneau (1996) is applied here.

The same model applied to the wide angle in A.1.2 is used where:

a = 46mm, h = 75mm, b = 47.6mm and inserting these values into **(2)**,

x = 94.2mm

Now, inserting this value into **(3)** with t = 8.5mm

P = 79.0 kN

According to the model shown in Fig. a.2, a plastic hinge forms at the level of the second fastner and there is no contribution from the first row of fastners since they move as a subassembly with the angle.

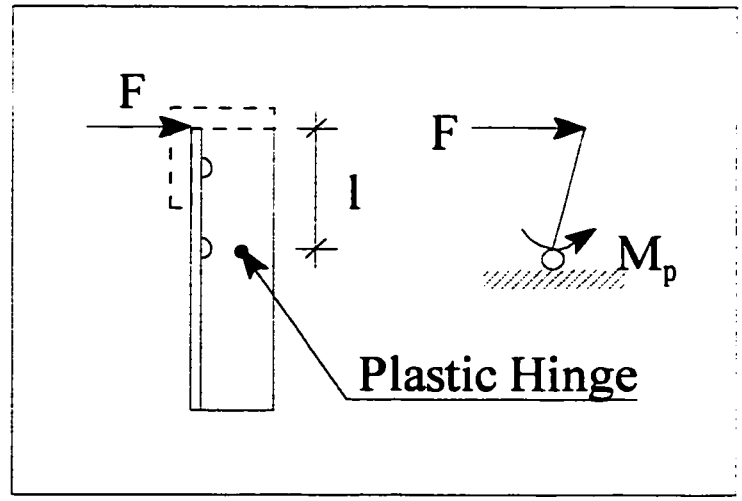

Figure a.2

In this case, l = 118mm

M_p = 8.4 kN•m for 2 angles,

and,

$M_p = F \times l$ or,

$F = M_p / l = 71.2$ kN

Therefore, the force required to cause this mechanism is

$T_r = P + F$

$T_r = 79.0 + 71.2 = 150.2$ kN

And the moment that will cause this mechanism is

M = 76.3 kN•m

A.2.2 Failure mode 2: Rivets shear failure

Since the top and bottom beam flanges are connected to the outstandings angle legs in the same manner, with two rivets, the failure mode is the same as **A.1.5** and,

M = 123 kN•m

A.2.3 Failure mode 3: Angle leg net section yield

$T_r = A_n \times F_y$

Where,

$A_n = 278 \times 8.0 - 2 \times 20.6 \times 8.0$

$A_n = 1894\ mm^2$

Therefore,

$T_r = 426$ kN and,

$M = 216$ kN•m

A.2.4 Failure mode 4: Angle leg gross section yield

Same as A.2.4, but substituting A_g for A_n

$A_g = 278 \times 8.0$

$A_g = 2224\ mm^2$

Therefore,

$T_r = A_g \times F_y$

$T_r = 500$ kN and,

$M = 254$ kN•m

A.2.5 Failure mode 5: Stiffener angles gross section shear failure

$F = A_g \times F_v$

For one angle, $A_g = 1350 mm^2$

Therefore,

$F = 2 \times 1350 \times 264$

$F = 712.8$ kN

And the moment is,

$M = 712.8 \times 0.508$

$M = 362$ kN•m

Appendix B

Design of Steel-Band Fuse-Plate Retrofit

The steel-band/fuse-plate retrofit is designed according to the loading and resulting forces shown in Fig. b.1. The moment in the beam induces tensile and compressive forces in the fuse plates.

For the design of the fuse-plate, many different combinations of plate width and thickness were considered, as well as the use of stiffeners to maximize the compression to tension capacity ratio (C_r/T_r) of the thinner plates. This preliminary design stage is not included here, but the optimal plate size was chosen for its C_r/T_r ratio, as well as for practical reasons, and the design checks follow.

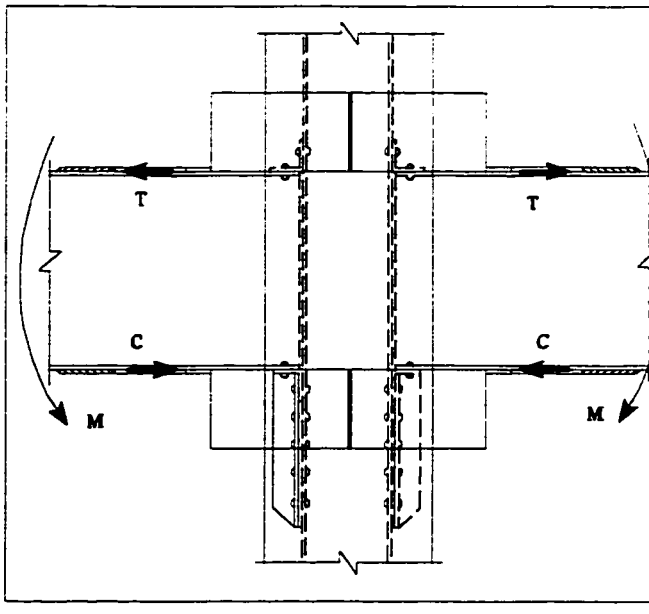

Figure b.1

The tensile and compressive forces can be equated to the applied moment (or desired moment capacity) in the following manner:

Assuming that the C_r/T_r ratio of the fuse-plates is close to 1.0 then,

$C = T = F$, and

$M = F \times h$

In this case, the desired moment capacity is 200 kN·m, and h = 508 mm therefore,

$F = 200/0.508 = 394$ kN

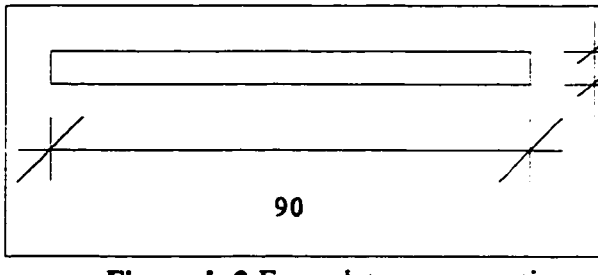

Figure b.2 Fuse plate cross-section

(Note that # refers to CAN/CSA S16.1-M89 clause number)

For the tapered region of the fuse-plate to yield in tension,

$T_r = A_s \times F_y \leq 394$ kN but $A_s \times F_u \geq 394$ kN

From the dimensions shown on Fig. b.2,

$A_s = 90 \times 14 = 1260$ mm^2

and, with $F_y = 300$ Mpa

$T_r = 1260 \times 300 = 378$ kN < 394 kN ✓

The expected yield moment is then,

$M_y = 378 \times 0.508 = 192$ kN·m

Check ultimate resistance, with $F_u = 450$ MPa:

$T_u = 1260 \times 450 = 567$ kN ✓

Check compressive resistance:

From # 13.3.1,

$$C_r = A_g \times F_y \times (1.035 - 0.202\lambda - 0.222\lambda^2)$$

and,

$$\lambda = \frac{KL}{r} \times \sqrt{\frac{F_y}{\Pi^2 E}}$$

with K = 0.5 (assuming fixity provided at one end by weld to beam flange and at other by rigidity of larger plate welded to steel band)

Refering to dimensions from Fig. 3.8, I = 20580 mm^4 , $A_g = 1260$ mm^2, r = 4.04 mm, L = 200 mm

$\therefore \lambda = 0.305$

and, $C_r = 360$ kN

$C_r / T_r = 0.95$ (close to 1.0) ✓

Check weld resistance:

From # 13.13.2,

$V_r = 0.67 \times \phi_w \times A_w \times X_u$, for weld metal

$V_r = 0.67 \times \phi_s \times A_s \times F_y$, for base metal

At connection to beam flange,

$V_r = 609$ kN > 394 kN for weld metal ✓

$V_r = 542$ kN > 394 kN for base metal ✓

At connection to steel-band,

$V_r = 511$ kN > 394 kN for weld metal ✓

$V_r = 607$ kN > 394 kN for base metal ✓

Appendix C

Additional Test Data

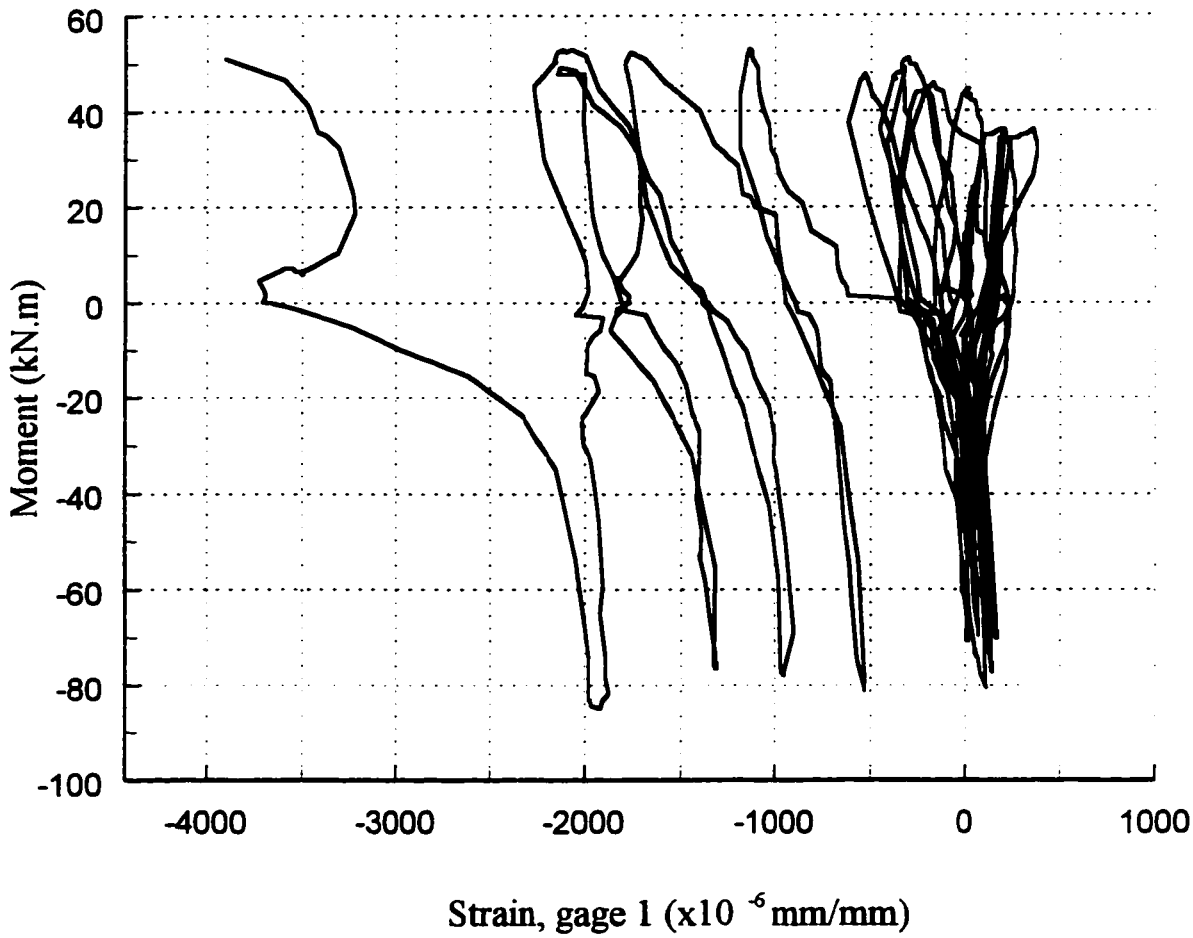
60
40
20
0
-20
-40
-60
-80
-100
Moment (kN.m)
-4000
-3000
-2000
-1000
0
1000
Strain, gage 1 (x10 -6 mm/mm)

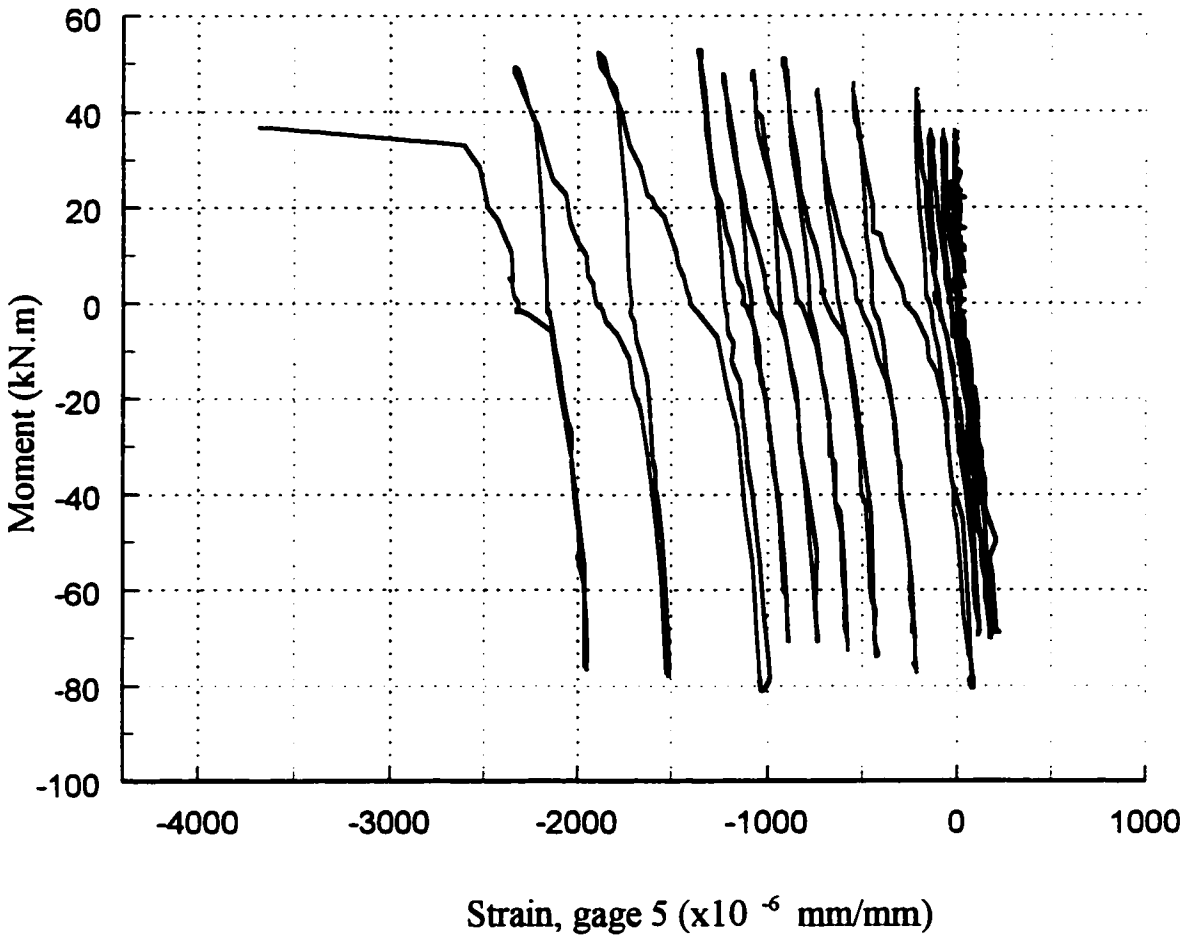
60
40
20
0
-20
-40
-60
-80
-100
Moment (kN.m)
-4000
-3000
-2000
-1000
0
1000
Strain, gage 5 (x10 -6 mm/mm)

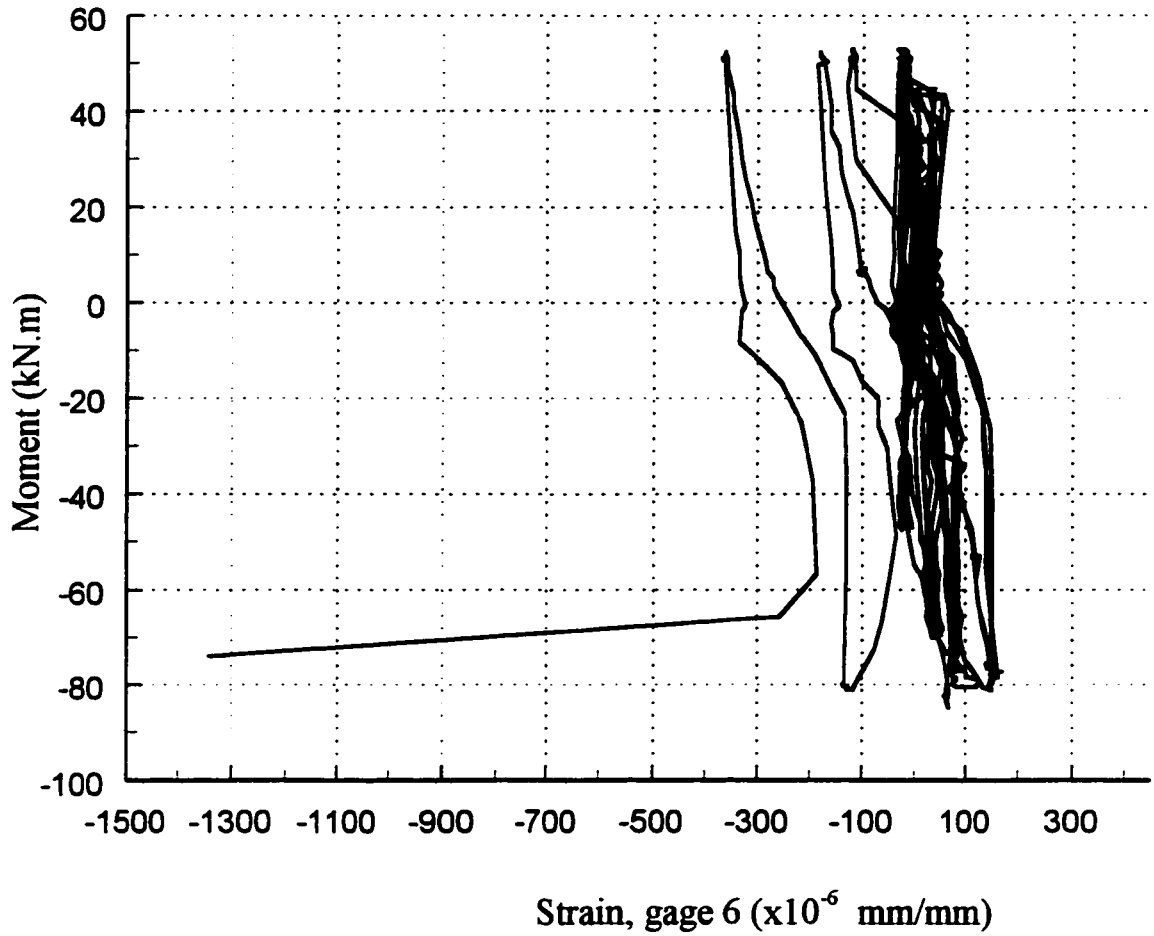
60
40
20
0
-20
-40
-60
-80
-100
Moment (kN.m)
-1500
-1300
-1100
-900
-700
-500
-300
-100
100
300
Strain, gage 6 (x10-6 mm/mm)

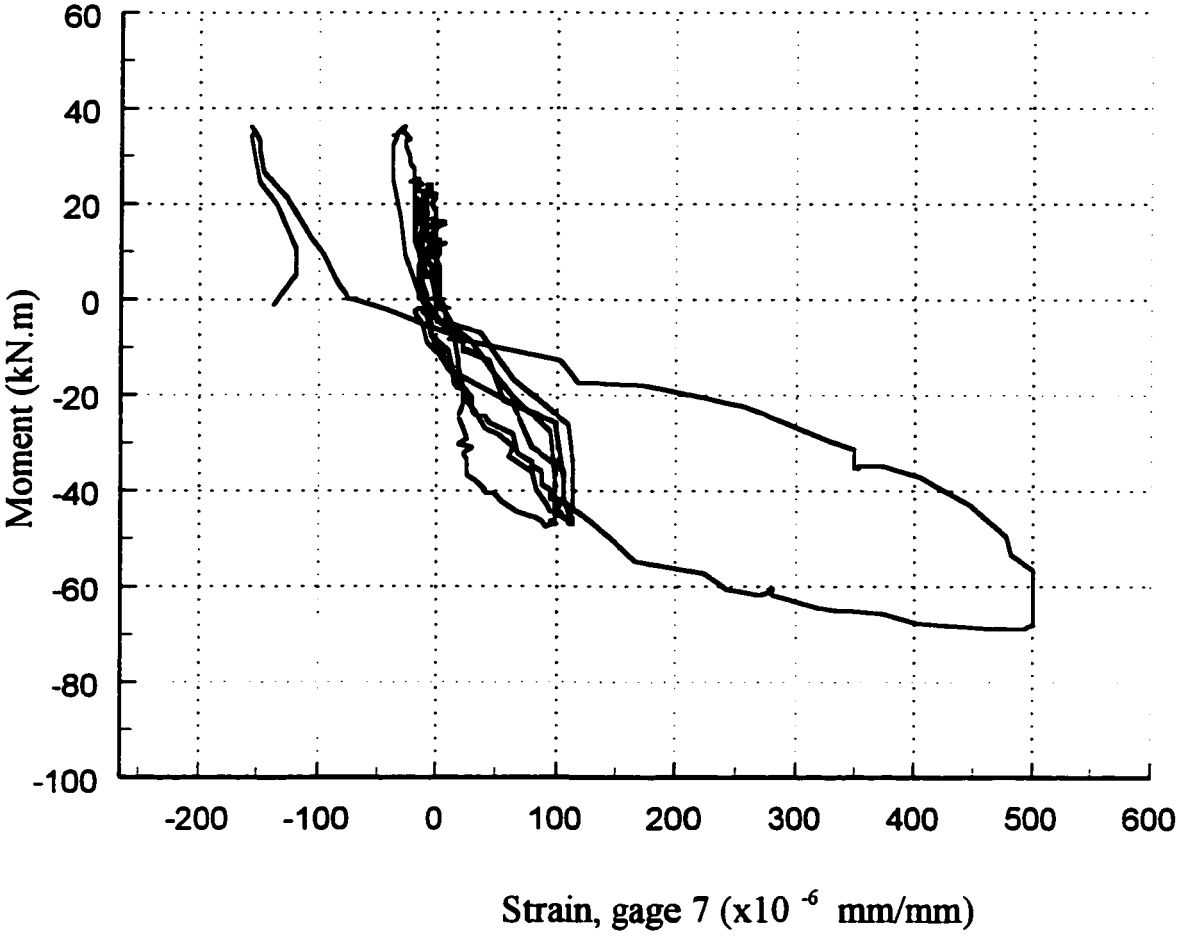
60
40
20
0
-20
-40
-60
-80
-100
Moment (kN.m)
-200
-100
0
100
200
300
400
500
600
Strain, gage 7 (x10 -6 mm/mm)

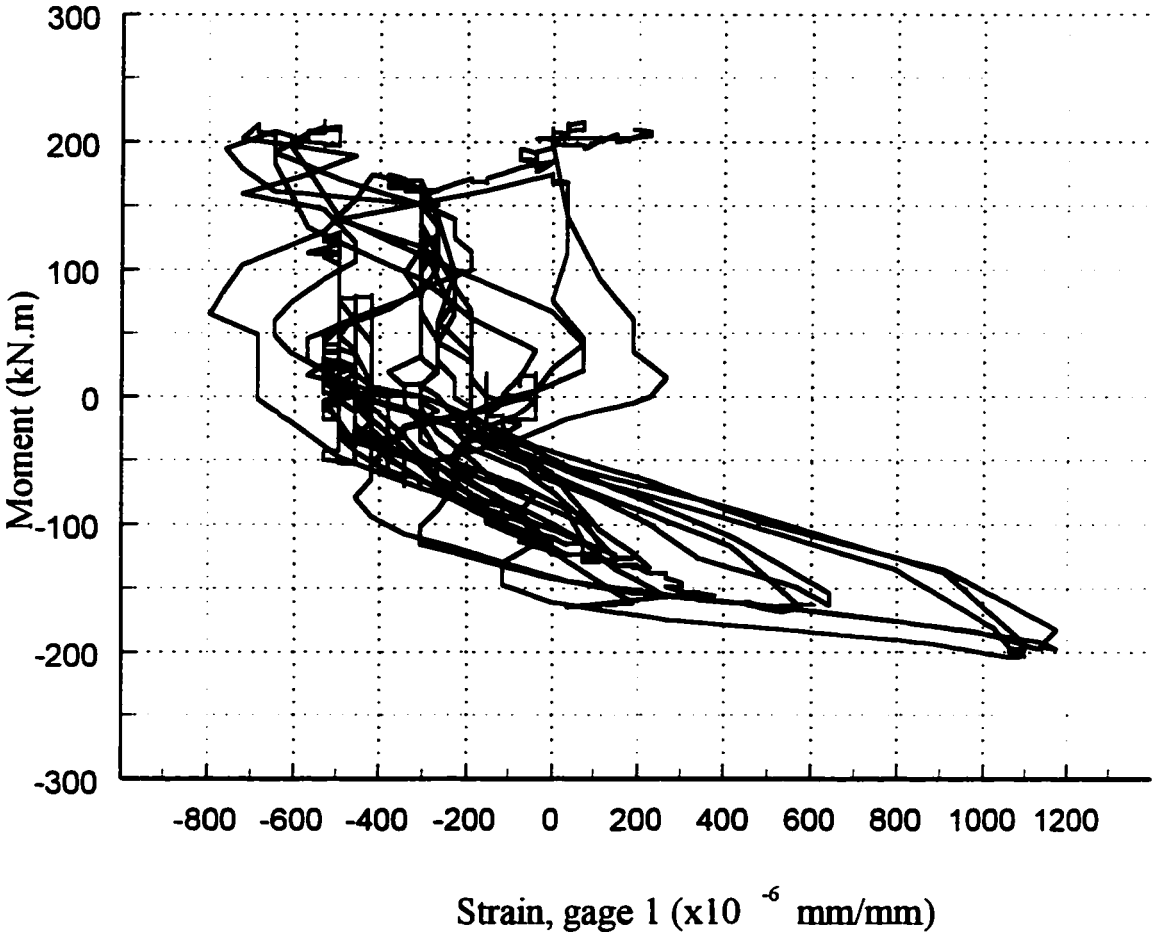
300
200
100
0
-100
-200
-300
Moment (kN.m)
-800 -600 -400 -200 0 200 400 600 800 1000 1200
Strain, gage 1 (x10 -6 mm/mm)

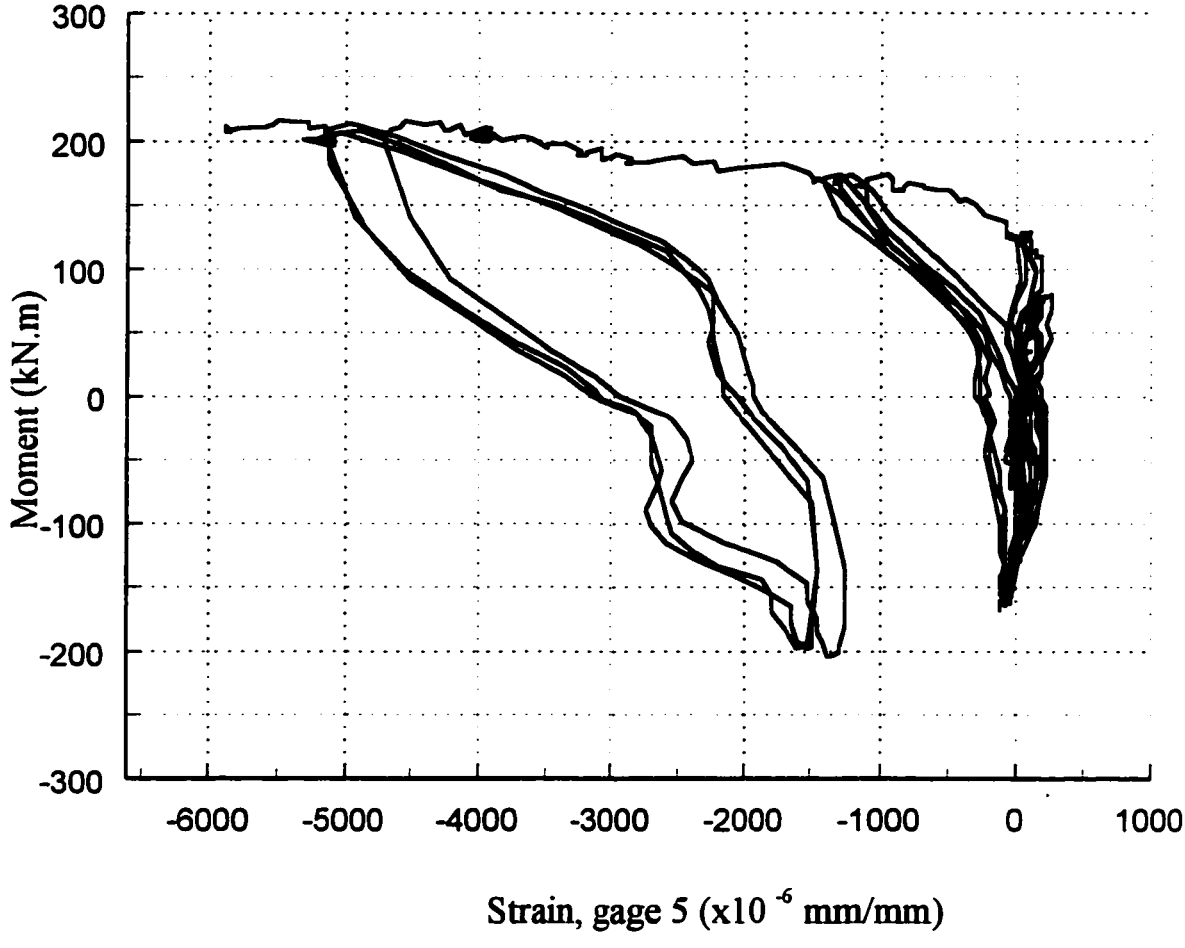
300
200
100
0
-100
-200
-300
Moment (kN.m)
-6000
-5000
-4000
-3000
-2000
-1000
0
1000
Strain, gage 5 (x10 -6 mm/mm)

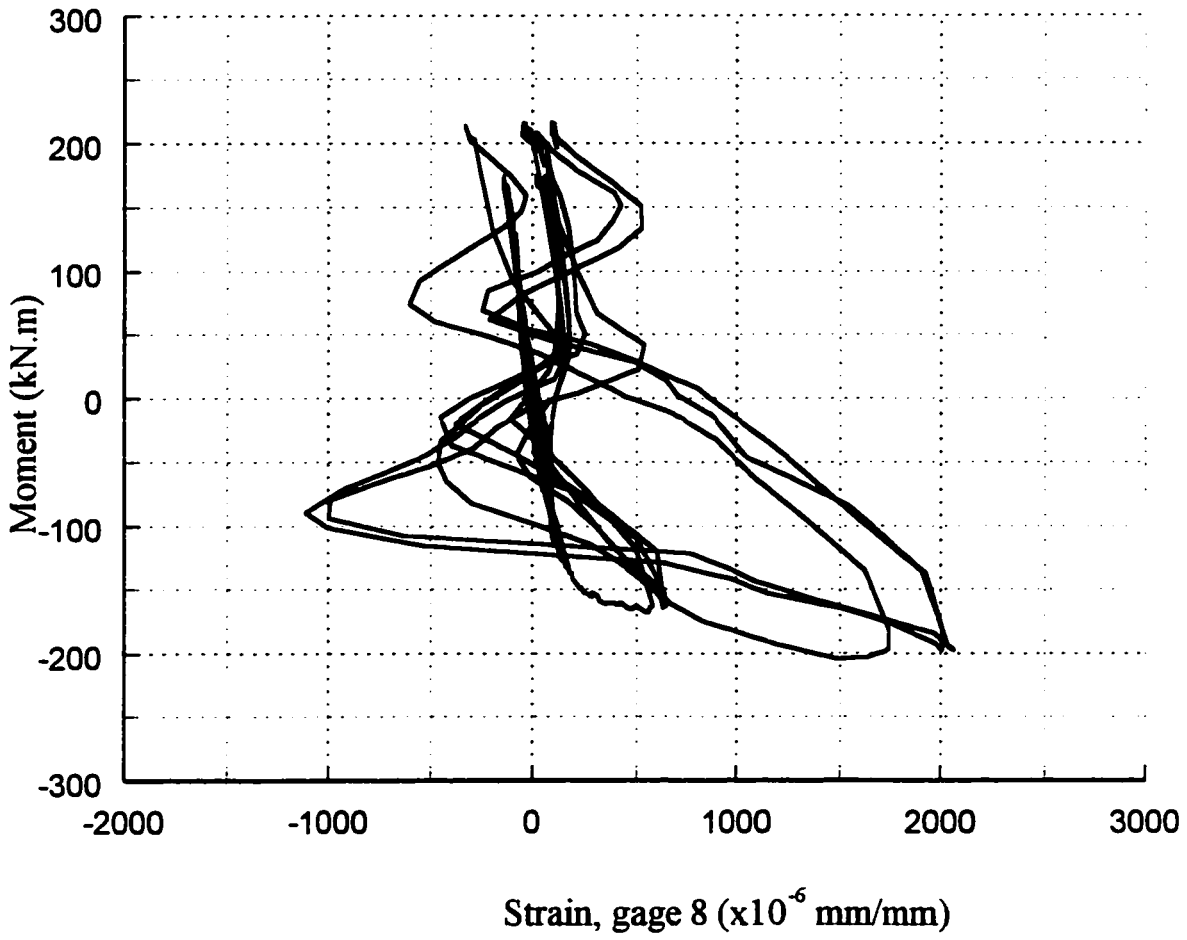
300
200
100
0
-100
-200
-300
Moment (kN.m)
-2000
-1000
0
1000
2000
3000
Strain, gage 8 (x10^-6 mm/mm)

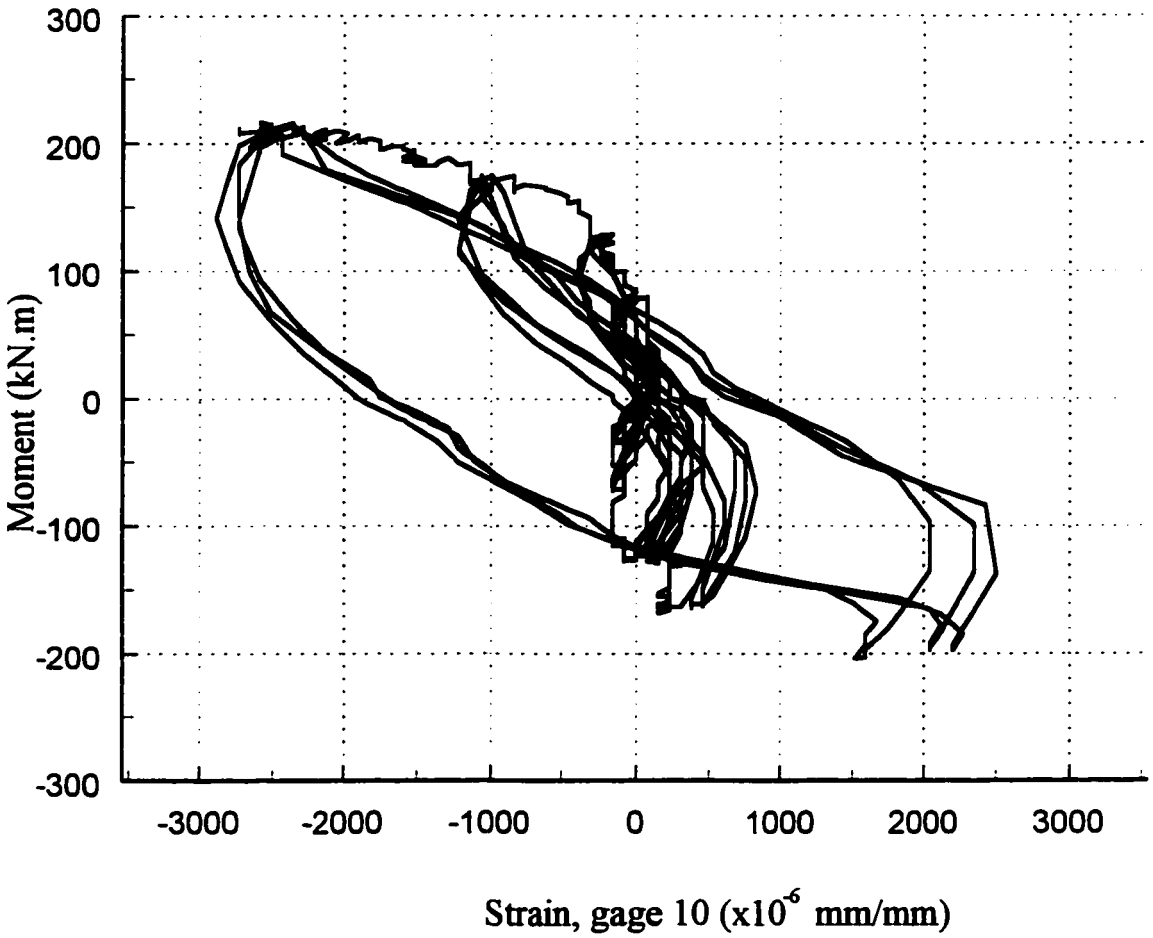
300
200
100
0
-100
-200
-300
Moment (kN.m)
-3000
-2000
-1000
0
1000
2000
3000
Strain, gage 10 (x10^-6 mm/mm)

Appendix D

Computer Program

```
      PROGRAM CUT
      REAL T2,MOM,PMARK,PMARK2,NMARK,NMARK2,NMARK3,TEMPT,TEMPM
      REAL MOM2,MOM3
      INTEGER FLAG
C
      NT1 = 10
      NT2 = 20
      NT3 = 30
      OPEN(NT1,FILE='C:\AXUMW\WORK\TEST2B\EXP2.DAT')
      OPEN(NT2,FILE='C:\AXUMW\WORK\TEST2B\NEWDAT.PRN')
      OPEN(NT3,FILE='C:\AXUMW\WORK\TEST2B\TEMP.DAT')
C
      TEMPT = 0.0
      TEMPM = 0.0
   50 FLAG = 0
      T2 = TEMPT
      MOM = TEMPM
      IF(.NOT.EOF(NT1)) THEN
      READ(NT1,1000) T2,MOM
      IF(MOM.GE.0) THEN
        CALL POS(T2,MOM,PMARK,PMARK2,NT1,NT2)
        GOTO 50
      ELSEIF(MOM.LT.0) THEN
     CALL NEG(T2,MOM,NMARK,NMARK2,NMARK3,MOM2,MOM3,NT1,NT3)
        COR1 = PMARK2 - NMARK
     COR2 = PMARK - NMARK2
     DELTM = ABS(MOM2 - MOM3)
     DELTD = ABS(NMARK2 - NMARK3)
     ANG = DELTM/DELTD
     SHCOR = 7/ANG
        IF(COR1.LE.COR2) THEN
          DELT = COR1
        ELSE
          DELT = COR2
     ENDIF
     DELT = ABS(DELT) - SHCOR
        TEMPT = T2
        TEMPM = MOM
        REWIND(NT3)
   60   IF(.NOT.EOF(NT3)) THEN
          READ(NT3,1000) T2,MOM
          T2 = T2 + ABS(DELT)
          WRITE(NT2,1100) T2,MOM
          GOTO 60
        ENDIF
        GOTO 50
      ENDIF
```

```
      GOTO 50
      ENDIF
C
 1000 FORMAT(2F8.0)
 1100 FORMAT(2F8.2)
      END
C-----------------------------------------------------------------------


      SUBROUTINE POS(T2,MOM,PMARK,PMARK2,NT1,NT2)
      REAL T2,MOM,PMARK,PMARK2
      INTEGER FLAG
C
      FLAG = 0
      PMARK = T2
   40 READ(NT1,1000) T2,MOM
      IF(MOM.LT.3.5) THEN
       PMARK = T2
       GOTO 40
      ENDIF
      WRITE(NT2,1100) T2,MOM
   60 READ(NT1,1000) T2,MOM
      IF(MOM.LT.3.5) THEN
        IF(FLAG.EQ.0) THEN
         PMARK2 = T2
         WRITE(NT2,1100) T2,MOM
         FLAG = 1
         GOTO 60
        ENDIF
        IF(MOM.LT.0) THEN
         GOTO 50
        ENDIF
        GOTO 60
      ENDIF
      WRITE(NT2,1100) T2,MOM
      GOTO 60
   50 RETURN
C
 1000 FORMAT(2F7.0)
 1100 FORMAT(2F8.2)
      END
C-----------------------------------------------------------------------
      SUBROUTINE NEG(T2,MOM,NMARK,NMARK2,NMARK3,MOM2,MOM3,NT1,NT3)
      REAL T2,MOM,NMARK,NMARK2,NMARK3,MOM2,MOM3
      INTEGER FLAG
C
      REWIND(NT3)
```

```
      FLAG = 0
      NMARK = T2
   40 READ(10,1000) T2,MOM
      IF(MOM.GT.-4.0) THEN
     NMARK = T2
        GOTO 40
      ENDIF
      WRITE(NT3,1100) T2,MOM
   60 READ(NT1,1000) T2,MOM
      IF(MOM.GT.-4.0) THEN
     IF(FLAG.EQ.0) THEN
      NMARK2 = T2
      MOM2 = MOM
         WRITE(20,1100) T2,MOM
         FLAG = 1
      GOTO 70
        ENDIF
        IF(MOM.GE.0) THEN
         GOTO 50
     ENDIF
   70       NMARK3 = T2
     MOM3 = MOM
        GOTO 60
      ENDIF
      WRITE(NT3,1100) T2,MOM
      GOTO 60
   50 IF(.NOT.EOF(NT3)) THEN
        WRITE(NT3,1200)
        GOTO 50
      ENDIF
      RETURN
C
 1000 FORMAT(2F8.0)
 1100 FORMAT(2F8.2)
 1200 FORMAT(' ')
C
      END
```

IMAGE EVALUATION
TEST TARGET (QA-3)

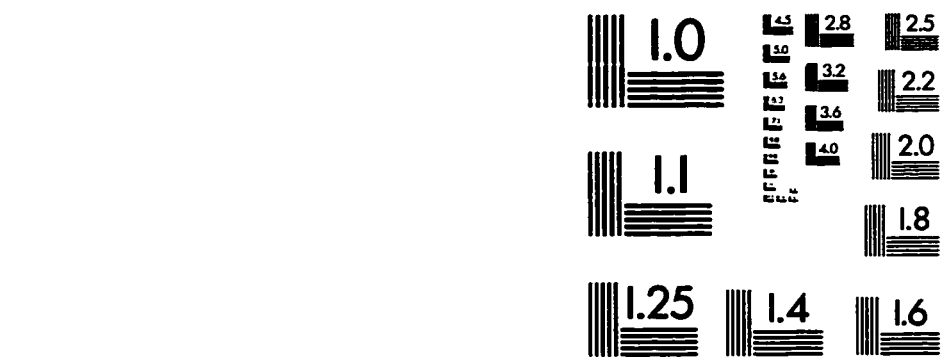

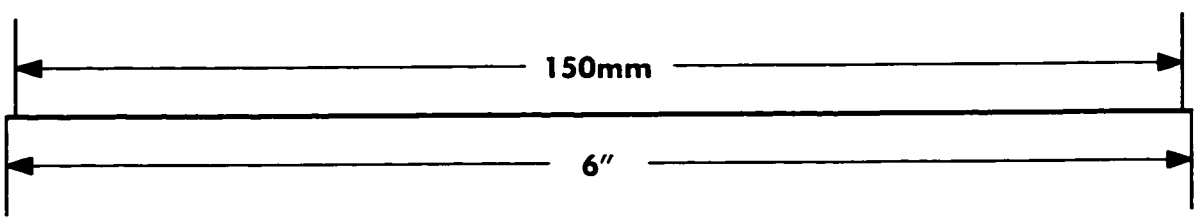

APPLIED IMAGE, Inc
1653 East Main Street
Rochester, NY 14609 USA
Phone: 716/482-0300
Fax: 716/288-5989